August 2018

Effects of High Pressure on Photochemical Reactivity of Organic Molecular Materials Probed by Vibrational Spectroscopy

Jiwen Guan
The University of Western Ontario

Supervisor
Yang, Song
The University of Western Ontario

Graduate Program in Physics

A thesis submitted in partial fulfillment of the requirements for the degree in Doctor of Philosophy

© Jiwen Guan 2018

Abstract

Chemical transformations of molecular materials induced by high pressure and light radiation exhibit novel and intriguing aspects that have attracted much attention in recent years. Particularly, under the two stimuli, entire transformations of molecular species can be realized in condensed phases without employing additional chemical constraints, e.g., the need of solvents, catalysts or radical initiators. This new synthetic approach in chemistry therefore satisfies the increasing need for production methods with reduced environmental impact. Motivated by these promises, my Ph. D thesis focuses on this state-of-the-art branch of high-pressure photochemistry. Specifically, high pressure is employed to create the necessary reaction conditions to transform molecular materials, whereas monochromatic light is applied to trigger and direct the chemical reaction according to selective paths. Systematic studies on selective molecular hydrocarbon materials provide new insights into the understanding of different effects that are achieved by the combined pressure-light tuning and demonstrate significant feasibility and controllability of the method in material synthesis.

Using optical microscopy and vibrational spectroscopy, I first studied pressure effects on the production of fuel materials from laser-induced decomposition of fluid ethylene glycol and a mixture of 2-butyne and water. The work demonstrated that the type of reaction and quantity of products as well as the associated kinetics were highly pressure dependent. Next, I examined pressure effects on photochemical phase transitions of fluid (Z)-stilbene. The study showed that increasing pressure not only tunes the photoisomerization type phase transitions but also opens a new reaction type, and thus allows the production of novel crystal and liquid. Finally, I explored polymeric transformations from three unsaturated hydrocarbon monomers under high pressure and/or UV radiation. In these studies, single reaction channel permits the quantitative analysis of polymerization kinetics and the pressure-dependence, so that correlations between rate

constant, activation volume and pressure can be obtained. Moreover, physical states of matter accessed by compression significantly influence the polymerization kinetics, selectivity and microstructures of products. Overall, these studies provide important contributions to discover and understand the high-pressure photochemistry of molecular materials and show profound implications of using the combined pressure-photon tunable power to produce controlled molecular materials of potential new applications.

Co-Authorship Statement

The following thesis contains materials from previously published manuscripts written by Jiwen Guan and co-authored, performed, or edited by others mentioned below. Prof. Yang Song is a co-author on all materials presented in this thesis and is responsible for the supervision of Jiwen Guan. Prof. Yang Song played a major role in the revision of the materials presented in all chapters. The materials used were either purchased from Alfa Aesar or Sigmal Aldrich Inc. Atactic polystyrene was purchased from Goodfellow Cambridge Ltd and syndiotactic polystyrene was kindly provided by Idemitsu Kosan Co. Ltd, Japan.

Jiwen Guan is responsible for most data collection. Part of high pressure IR and Raman measurements of dimethyl acetylene in Chapter 6 were performed by undergraduate students Roshan Daljeet and Arielle Kieran from the Department of Chemistry (Western). Also, group members, Pan Wang, Xuerui Cheng and volunteer student Xuetong Jin were participating part of data collections in Chapter 8. All the data analysis and *ab initio* calculations were done by Jiwen Guan.

Acknowledgments

I would like to first express my gratitude from the bottom of my heart to my supervisor Prof. Yang Song, for his exceptional supervision, encouragement, and unconditional support. Without his supervision, my graduate studies in Western would not have been possible. He is always there for help whenever I need him. In particular, I would like to express my gratitude to him because of his excellent supervision and extreme patience on improving my academic writing skills. From there, I learned how to be an exceptional scientist with high criteria towards the academic work, and how to express the complicated works to the public in a simple and rigorous way. His revisions on each of my publications are priceless treasure and I will absolutely keep them for future references. His rigorous attitude towards teaching and research wins my full respect.

I would like to thank people in my home department, e.g., Prof. Jeffrey L. Hutter, Prof. Lyudmila Goncharova, Prof. Martin Zinke-Allmang, Dr. Shailesh Nene, Clara Buma, Brian Davis, and Jodi Guthrie for their help and support during this study. I also would like to thank people in chemistry department, especially the supporting staff in the machine shop, ChemBioStores. All your excellent services made my research smoother.

I would also like to thank all the members in Song's group, especially Dr. Yue Hu, Fengping Xiao, Nilesh Shinde, Pan Wang, Dr. Xuerui Cheng, and Shan Jiang for their helpful discussions and constructive feedbacks. I would like to extend my thanks to my other friends in Western, in particular, Dr. Renjie Hou, Shoushun Cheng, Dr. Yan Liu, Jaewoo Park, Sivayini Kandeepan, Pubuditha Abeyasinghe, Nirosh Gatangama, Dr. Sebastine Ezugwu and Dr. Zahra Haghshenas. Without you guys, my life in Western cannot be such unforgettable.

Finally, I would like to give my special thanks to my parents, my mother-in-law and my wife, without their unconditional support and love, it is impossible for me to finish this

Ph.D. thesis. Many thanks to my wife Jiao Gao for bringing our adorable daughter, Eve to this world and making so much contributions to this family.

Jiwen Guan

Beaver Hall, March, 2018

Table of Contents

List of Tables

List of Figures

List of Abbreviations

DAC	diamond anvil cell
HOMO	highest energy occupied molecular orbital
LUMO	lowest energy unoccupied molecular orbital
UV	ultraviolet
PET	photoinduced electron transfer
IR	infrared
GLPC	gas-liquid partition chromatography
FTIR	Fourier-transform infrared spectroscopy
XRD	X-ray powder diffraction
PIPT	photoinduced phase transition
LC	liquid crystal
DMA	dimethyl acetylene
EDM	electric discharge machine
MCT	mercury cadmium telluride
DPSS	diode pumped solid state
BS	beam splitters
CCD	charge-coupled device
DFT	Density functional theory
B3LYP	Becke, 3-parameter, Lee-Yang-Parr
TPA	two-photon absorption
EG	ethylene glycol
GA	glycolaldehyde
GPa	gigapascals
FWHM	full width at half maximum
PES	potential energy surface
CI	conical intersection

DHP	4a,4b-dihydrophenanthrene
TSα, TSβ, TSγ	trans-stilbene α, β, γ phase
OBF	one-bond-flip
HT	Hula-twist
NMR	Nuclear magnetic resonance
APS	atactic polystyrene
IPS	isotactic polystyrene
SPS	syndiotactic polystyrene
PY	polymerization yield
ISC	intersystem crossing
PA	phenylacetylene
1D	one-dimensional

List of Schemes

Chapter 1

1 Introduction

1.1 High-pressure chemistry

Pressure is a thermodynamic variable that is as fundamental as temperature, but the full potential of the pressure in areas of physics, chemistry, and engineering far exceeds that of the temperature.[1-3] The realization of this potential relies on the advancement of high-pressure equipment. The gas containers or autoclave presses can generally create pressures up to 2×10^8 Pa, which is approximately 2000 higher than the atmospheric pressure at the Earth's surface. In industry, at this order of magnitude pressure, the running water (waterjet) becomes sharp enough to cut a wide variety of hard materials (Fig. 1.1). Pressures in this range are now widely used in chemical industry, biotechnology, and for crystal growth.[3] However, this pressure range is still too low to adequately meet the high-pressure technological requirements of today. In the last few decades, there have been revolutionary advances in high-pressure technology, where static pressures up to 400 GPa became achievable inside the diamond anvil cell (DAC) exceeding those available by any other means by a factor of ten.[1] This extremely high-pressure, which is equivalent to the pressure at the Earth's center, is the highest pressure obtained in the laboratory with presently available technology. With this degree of compression, the free-energy change (pressure-volume work) of materials can be more than 10 eV per molecule, which exceeds the strength of the strongest molecular bond.[2] This causes dramatic changes in the chemistry of materials.
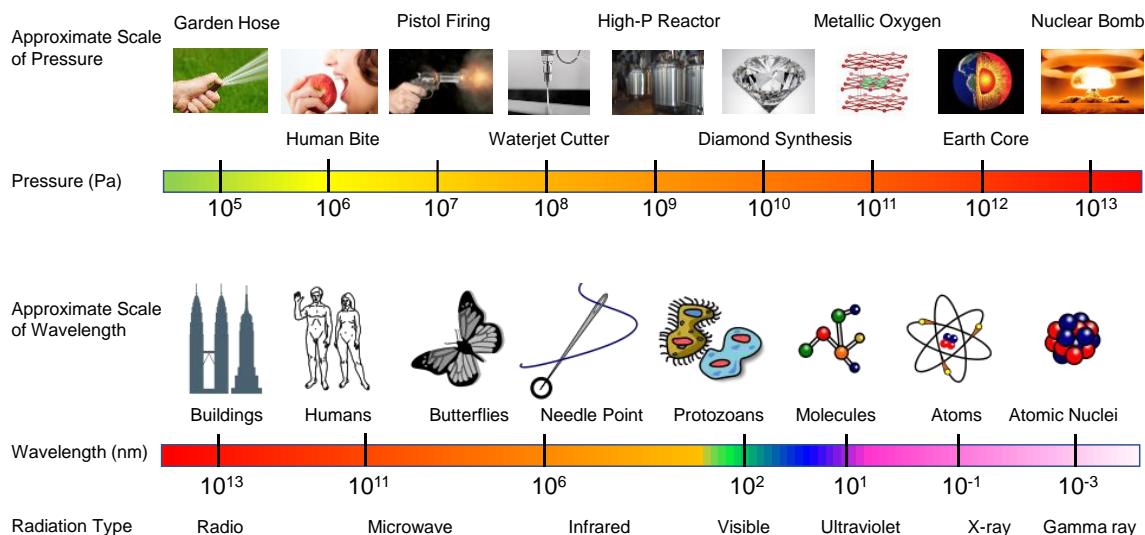
Figure 1.1: The magnitude of pressure and wavelength. The approximate scales of pressure and wavelength are illustrated. (Credit of electromagnetic spectrum: NASA via Wikipedia)

We must remember that most of our chemical knowledge has been gained from studies carried out at or near one-atmosphere pressure at the Earth's surface, while much of the matter in the Universe exists under much higher pressure conditions, deep inside planets and stars. In a basic chemical sense, we know that the effect of increasing pressure is to reduce the volume available of the matter. Using molecular materials as an example, the volume of molecular liquids and solids, in fact, can be compressed by one order of magnitude smaller, a size contraction corresponding to a shrinkage of intermolecular distances by a factor of two.[4] The reduced intermolecular distances increase weak intermolecular van der Waals interactions. The sufficient pressurization can enhance the van der Waals forces to such an extent that the van der Waals forces and covalent bonding forces are comparable in magnitude. In such conditions, the system becomes thermodynamically unstable, and the free energy must minimize through a full reorganization of molecules or the chemical bond connectivity. The responses of the

system to recover the new free energy minimization consequently lead to a number of structural reorganization phenomena such as condensation, phase transformations, polymerization, amorphization, ionization, dissociation and even metallization.[4] As these structural reorganizations are often accompanied by a change of the physical properties, e.g., optical, magnetic, and electric properties, etc. The high-pressure effects open broad opportunities to tune and change chemical equilibria and material properties and, on many occasions, allow access to a wide range of new compounds with exceptional properties.[1] The most spectacular examples of these aspects are the insulator-to-metal transition of very simple molecules such as oxygen and iodine under high pressure.[5,6]

Among the high-pressure phenomena, the pressure-induced chemical transformations of molecular materials are particularly interesting as the pressurization profoundly alters the electronic structure of molecules compared with that at ambient conditions. Specifically, the pressurization increases overlapping among adjacent electronic orbitals that scales up the electronic delocalization, and also causes a relative displacement of the molecular orbitals. These effects are much pronounced when the materials contain unsaturated chemical bonds. For the unsaturated molecules, the energy gap between the LUMO and HOMO are reduced or canceled, the electronic energy levels are drastically shifted, broadened, and overlapped at high pressure (the example ethylene is shown in Fig. 1.2). The overall effect of these processes can significantly lower the thermal barrier, and mix the ground and the excited states.[7] These changes of the electronic distribution and molecular geometry can possibly trigger a chemical reaction with neighboring molecules. The reactions lead to products that can often have extraordinary structural and physical properties. As shown in Fig. 1.3, the colorless diiodobutadiyne crystal is partially polymerized at 2.5 GPa, which produces poly(diiododiacetylene) with a blue color. At higher pressures > 6 GPa, the samples turn to black and contain primarily the polymer.[8] The produced polymer has an ordered and one-dimensional conjugated structure. The peculiarities of chemical reactions from other molecular systems occurring in the high-

pressure regime have been recently reviewed,[4,9] and as a whole, these results show that high-pressure activation of chemical reactions offers elevated possibilities for fundamental studies of reaction mechanisms and for many applications to obtain novel products.
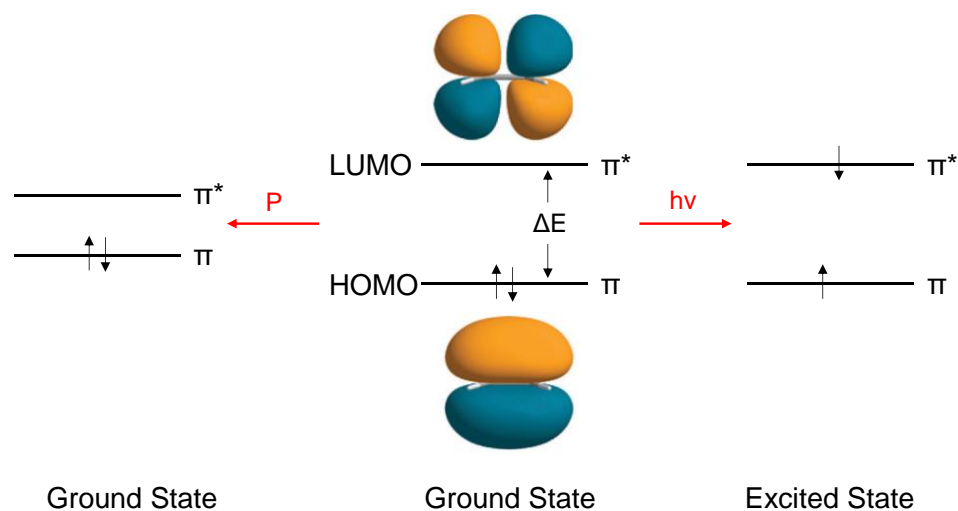
Figure 1.2: Selected molecular orbitals and molecular geometries of ethylene upon compression or photoexcitation.

Figure 1.3: Powdered samples of diiodobutadiyne in an oxalamide host, before pressing (left), after pressing to 2.5 GPa (center), and after pressing to 6 GPa (right). (ref. 8) (Reproduced with the permission of American Chemical Society)

1.2 High-pressure photochemistry

The high-pressure effect on creating excited species becomes extremely relevant to photochemical effects on molecular materials because at ambient conditions photoradiation is the most common method to produce excited species from the ground state (Fig. 1.2). By photoexcitation, specific chemical reactions may be induced, which has long been pursued and practiced in the synthesis of materials.[10] Specifically, when compared to chemical reactions at the ground electronic state induced by pressure or temperature, photochemical reactions are characterized by the fact that they involve electronic excitation in the wavelengths of ultraviolet (UV) or visible light. At these wavelengths, the photon energies are comparable to the bond energies of molecules (Fig. 1.1). Thus, by selected light absorption, the electron configuration of a molecule changes, which leads to an increase in the reactivity of a compound. It is obvious that the photochemical reactions considerably augment the number of transformations of a compound induced by other means. Often, photochemical reactivity is even complementary to ground state chemistry as molecules in electronic excited states sometimes act as new molecules.[10,11] Moreover, according to the specific photoabsorption means such as direct excitation, photosensitization, photocatalysis, photoinduced electron transfer (PET), and photoredox catalysis, the photo-induced effects on compounds vary from elimination, cleavage, rearrangement, isomerization, cyclization, addition, and electron transfer, etc. These basic photoreactions have nowadays played remarkable roles in the portfolio of synthetic chemistry at the ambient pressure.

Despite the respective importance of high pressure or photo-radiation in synthetic chemistry, the chemical activation and transformation of materials induced by the synergy of the two had not yet been properly explored and developed. This is in part due to the low mechanical strength of high-pressure optical windows,[12] hence, the maximum pressure was limited to 0-0.2 GPa in the photochemical research sector.[13,14] Thankfully, the picture

began to change when the DAC was introduced as the photochemical reaction vessel. The DAC contains two diamonds, the advantages of which are the low absorption of short wavelength X-rays and transparency to UV, visible and IR radiation as well as the extreme hardness of diamond, allowing the DAC to reach considerable pressures. In the 1980s, high-pressure chemists found that the visible excitation light used in Raman measurements can influence the chemical stability of samples under pressures.[15,16] The first example is that the visible excitation laser was found to cause photopolymerization of solid CO at room temperature and above 4.6 GPa.[15] Under high pressure, another compound, crystalline N_2O_4 was reported to be photolyzed upon irradiation by 488 nm laser radiation,[16] which led to first the formation of N_2O_3, and then a new N_2O_4 crystalline phase at prolonged radiation times. The exhibited results were very distinct and not observed under pure high pressures. After 2000, systematic studies of chemical transformations of molecular materials induced by the combined pressure and light radiation have attracted increasing interest (see Fig. 1.4(A)) as the exhibited novel and intriguing aspects brought by this novel and physical approach. Under the two stimuli, the entire transformations of molecular species in condensed phases can be easily realized and is free from additional chemical constraints, e.g., the need of solvents, catalysts or radical initiators.[7] This new synthetic approach in chemistry, therefore, satisfies the increasing need for alternative production methods with reduced environmental impacts and offers opportunities for green chemistry.
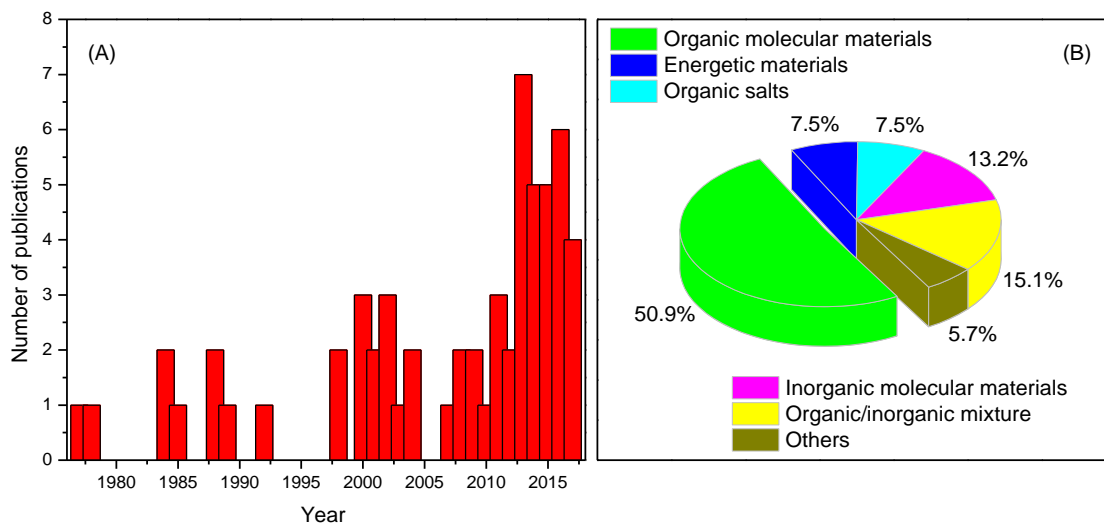
Figure 1.4: (a) The number of papers published in high-pressure photochemistry from 1977-2017. (b) The studied materials and their percentages in the time period.

To date, upon the two stimuli, various kinds of materials have been investigated such as organic molecular materials,[12-14,17-39] inorganic molecular materials,[15,16,40-44] organic and (or) inorganic mixtures,[45-52] organic salts,[53-56] molecules in porous materials,[57] energetic explosives[58-61] and so on[62,63] (see Fig. 1.4(B)). However, the studies in the early years on few organic and inorganic molecular materials partially explored either pressure effects on materials' photochemical responses or laser effects on materials' chemical reactivity under high pressure. Until recent years, systematic studies that comprehensively evaluate the roles of pressure and light are exclusively carried out by few groups. The developments particularly benefit from customized *in situ* high-pressure photochemical equipment, which is not the usual establishment of the chemistry laboratories and has been so far an almost exclusive privilege for those highly specialized laboratories discussed below. Despite the lack of accessibility of such experimental equipment, the progress that has been made on high-pressure photochemistry so far demonstrates great promises of using this approach on material synthesis and reaction kinetics analysis. For instance, this approach was employed to efficiently trigger reactivity in water-containing mixtures at room temperature and a few tenths of a GPa.[45,48] Using optical microscopy and Raman

spectroscopy, a large amount of molecular hydrogen (H_2) and other relevant products have been clearly identified (Fig. 1.5). As the reactions occurred in the total absence of solvents, catalysts, and radical initiators, the production of H_2 from water (H_2O) is extremely relevant to the current goal of environmentally friendly synthetic methods based on renewable sources to produce the energy vector of the future. Furthermore, the applications have been extended to mixtures of fluid hydrocarbon and porous materials.[57] Specifically, when fluid ethylene was confined in the channels of silicalite (a pure SiO_2 zeolite), under mild pressure and ultraviolet irradiation conditions, Santoro et al., has obtained a unique nano-composite material, where single polyethylene chains adapt very well to the confining channels (Fig. 1.6). The formation of this nano-composite resulted in significant increases in bulk modulus and density with respect to silicalite. Mechanical properties were modified correspondingly. This finding further demonstrates a potential of high-pressure photochemistry in material synthesis, e.g., producing a unique generation of technological, functional materials based on simple hydrocarbons polymerized in confining meso/micro-porous solids.
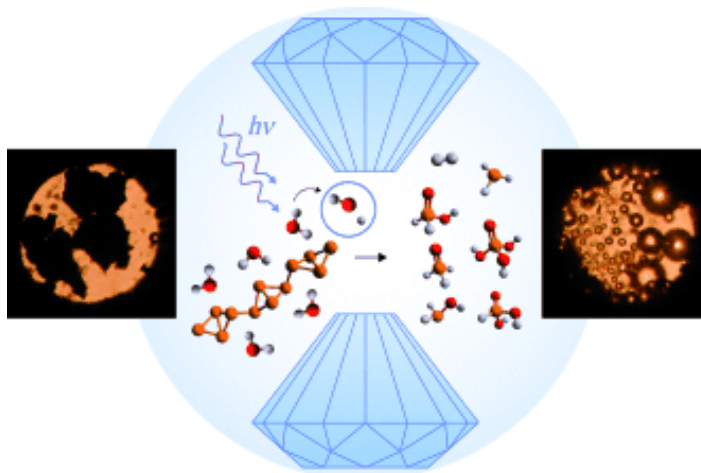
Figure 1.5: Microphotographs of red phosphorous and water before and after UV radiation under pressures. The reaction produces molecular hydrogen and other chemicals. The H₂ is mainly contained in the bubble area of the right photograph. (ref. 45) (Reproduced with the permission of John Wiley and Sons)
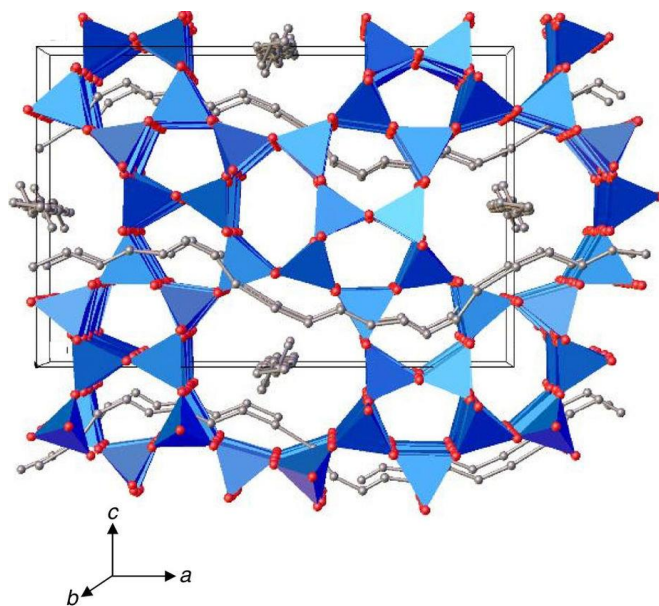
Figure 1.6: The structure of the nano-composite, where single polyethylene chains adapt very well to the confining channels of silicalite, synthesized by high-pressure chemistry. (ref. 57) (Reproduced with the permission of Springer Nature)

1.3 Applications to organic molecular materials

Aside from the inorganic mixtures, fluid-porous materials mixtures, up to the present, organic molecular materials were increasingly and vigorously studied in the field, which accounts for nearly half of the total publications in the last 40 years (see Fig. 1.4(B)). As seen in Table 1.1 and 1.2, the application of pressure on organic photochemical synthesis in the first few works performed were carried out in solution. This results in a pressure limit due to the low freezing pressures of solvents, although that can be partially extended by increasing the temperature (typically the melting point increases by 10–20 °C per 0.1 GPa). Nevertheless, for these studies in solution, the pressures were increased only up to 0.4 GPa, and the changes of the electronic structure were not dramatic.[4] Thus, the pressure was mainly exploited to control the kinetics of photochemical reactions.[14]

On this aspect, the basic information of the pressure effects on reaction kinetics has been obtained, which serves as the first principle of high-pressure photochemistry. It turns out that reaction rate and pressure are associated with the volume profile of the reaction that encompasses the activation and the reaction volumes.[4,64-66] The studies have demonstrated that the fundamental effects of pressure in a chemical reaction are described by the thermodynamic and kinetic equations:

$$\left(\frac{\partial lnK}{\partial P}\right)_T = -\frac{\Delta V}{RT}\,, \qquad \left(\frac{\partial lnk}{\partial P}\right)_T = -\frac{\Delta V^{\neq}}{RT}\,, \qquad (1.1)$$

where K, k, ΔV, and $\Delta V^{\neq}$ are the equilibrium constant, the rate constant, the reaction volume, and the activation volume, respectively. The activation volume $\Delta V^{\neq}$ is the volume change of the reaction system from reactant to transition state, and the reaction volume ΔV is the corresponding volume change from reactant to product. Figure 1.7 illustrates the $\Delta V^{\neq}$ and ΔV concepts schematically in a bond formation process. From these equations, it can be seen that an increase of pressure will favor chemical reactions occurring with a negative ΔV and will accelerate reaction pathways with negative $\Delta V^{\neq}$. For the same reason, reactions

with positive ΔV can be completely ineffective at high pressures. Consequently, compression can alter the overall outcome of the certain types of reactions in solution.

reactant
V_r

transition state
V_{TS}

product
V_p

reaction volume: $\Delta V = V_p - V_r$
activation volume: $\Delta V^{\neq} = V_{TS} - V_r$
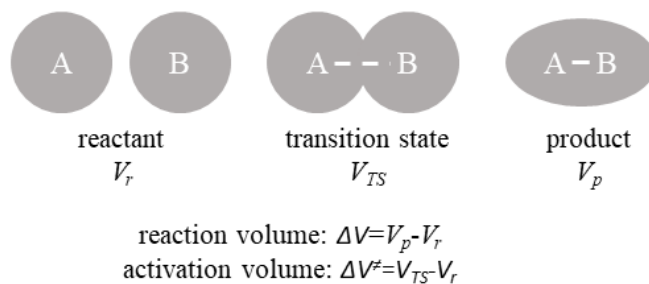
Figure 1.7: Schematic representation of activation volume ($\Delta V^{\neq}$) and reaction volume (ΔV) in a bond formation reaction between two neutral species. In this reaction, both $\Delta V^{\neq}$ and ΔV are negative.

Table 1.1: Summary of organic materials and systems investigated at high pressures and light radiations.

Reactants	Medium	Pressure (GPa)	λ (nm)	Methods	Refs
Acrylonitrile, naphthalene	Solutions	0-0.15	NA	GPC	17
Phenyl alkyl ketones	Solutions	0-0.18	200-400	GLPC	13
Norbornadiene, Benzophenone	Solution	0-0.15	313, 366	GLPC	12
2-adamantanone, Trans-dicyanoethylene	Solution	0-0.2	313	Fluorescence, GC/MS	14
2,3-dihydropyran, benzene or naphthalene	Solution	0-0.1	254	GC/MS	20
Z-Cyclooctene, chiral aromatic esters	Solution	0-0.4	UV	GC	22
Acetylene	Crystal	4	647	FTIR	21,23
Butadiene	Liquid	0-0.8	458, 488, 514	FTIR	25
Benzene	Crystal	16	407, 458, 514, 550, 647	UV-vis, FTIR	24,28
Ethylene	Liquid	< 1	≤ 460	FTIR, Raman, XRD	26,36
Isoprene	Liquid	0.5, 1.1	458	FTIR	27
Thiophene	Liquid	< 8	514.5	Raman	18

Table 1.2: Continued.

Reactants	Medium	Pressure (GPa)	λ (nm)	Methods	Refs
Ethanol	Liquid	0-1.5	350	FTIR, Raman	29,30
Methanol	Liquid	0.1-1.8	350	FTIR, Raman	31
Dinitroanthracene	Crystal	0-2	405	Raman	32
Furylfulgide	Crystal	0-8.2	375,513	Optical absorption	34
Non-biaryl atropisomers	Solution	0-0.1	300	HPLC, UV/Vis, fluorescence, circular dichroism	33
2-tert-butylphenylphenylmethanone	Crystal	0.1-1.5	≥ 350	XRD	35
2,6-difluorocinnamic acid	Crystal	0.1-2.1	≥ 350	XRD	39
2-benzyl-5-benzylidenecyclopentanone	Crystal	0.1-0.7	≥ 350	XRD	38
2-(hydroxyethyl)methacrylate	Liquid	0.1-1.6	355,488	Raman	37

The recent interests of high-pressure photochemistry have greatly shifted from reactions in solution to the reactivity of organic molecules in condensed phases. These developments are based on the unique advantages of the customized high-pressure photochemical apparatus. In the apparatus, the pressure and light irradiation parameters became more controllable and tunable in broad scales, and more importantly, optical probes such as UV-Vis, FTIR, Raman, and XRD are adapted to characterize the microscale reactions in the DAC *in situ*. Over the years, particular efforts were made on mainly two categories of organic materials (see Table 1.1 and 1.2). The first ones are the polymerization of unsaturated hydrocarbons, e.g., acetylene,[23] butadiene,[25] ethylene,[26] etc. The method sometimes showed high selectivity on the reaction pathways and products in comparison with high-pressure synthesis and conventional chemical synthesis methods. For instance, in case of butadiene, a variety of reaction products were produced via conventional chemical methods (Fig. 1.8).[25] Under high pressure alone, vinylcyclohexene was produced above 0.7 GPa, according to a cyclo-addiction reaction and only a trace amount of polybutadiene was found. In contrast, when the compressed sample is irradiated by a few milliwatts of the 488-nm Ar^+ laser line, the production of vinylcyclohexene was completely inhibited, and the rapid formation of pure trans-polybutadiene was observed. While the chemical catalytic method produces polybutadiene with a mixture of the trans and cis isomers, the high-pressure photochemical method produces a highly stereoregular polymer (trans-polybutadiene). Therefore, the work shows that the high-pressure photochemical method can have a high selectivity in transforming organic materials. In addition, as butadiene is transparent at 488 nm, the successful triggering of the reactions at this wavelength further suggested that photoactivation of the sample might be achieved by a two-photon absorption process, as the very first step of the photochemical reactions.
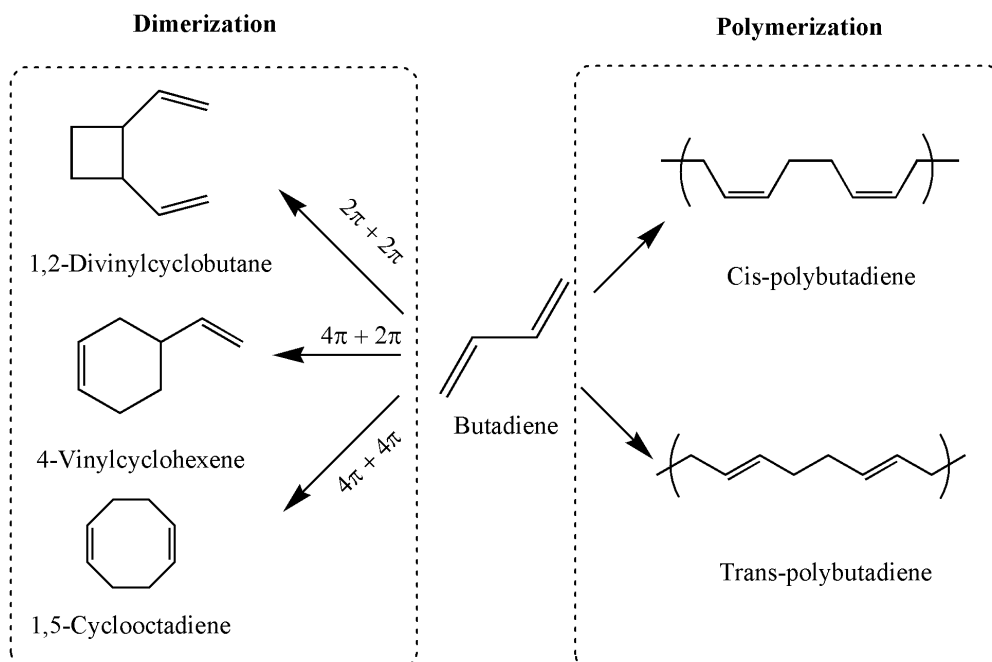
Figure 1.8: The various reaction products synthesized from butadiene via chemical catalytic methods. In contrast, vinylclohexene is mainly produced via the high-pressure method whereas trans-polybutadiene is selectively produced when high pressure and laser radiation are simultaneously applied. (ref. 25)

The last scientific issue became extremely relevant in studies of the second category of organic materials where the two-photon absorption was used to induce reactions from liquid alcohols such as ethanol (C_2H_5OH) and methanol (CH_3OH).[29,31] These kinds of species normally possess much higher-lying electronic excited and dissociative states. For instance, at ambient conditions, the onset of the lowest singlet excited state (S_1) corresponding to the n→σ* Rydberg transition of ethanol was measured to be 6.9 eV (180 nm),[67] and the S_1 state has a dissociative character along the C_2H_5O-H coordinate. As shown in Fig. 1.9, upon the near-UV 350 nm (~3.5 eV) radiations, the photoreactions of liquid ethanol are effectively triggered at different pressures. The initiation of reactions can only be explained by the consequences of the two-photon absorption. More importantly, the selectivity of reaction products by tuning pressures is again pronounced. By varying

the loading pressures, the authors obtained completely different photoproducts as shown in the microphotographs. This work is of great importance as liquid alcohols are successfully dissociated by two-photon absorption of near-UV photons. A complex reactivity, depending on pressure and on the reactant amount, leads to the formation of a few specific products among which H_2 is remarkable, especially at the mild pressure conditions required for its synthesis.
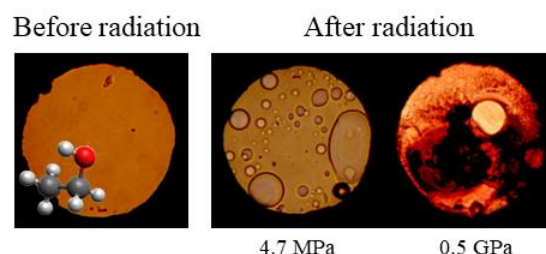
Figure 1.9: The microphotographs of liquid ethanol before and after UV radiation at different pressures at room temperature. (ref. 29) (Reproduced with the permission of the American Chemical Society)

1.4 Objectives and structure of the thesis

From all these examples above, we can expect several important consequences from the combined tuning of the pressure and light radiation on organic molecular materials: (1) modified photoreaction kinetics at high pressures, (2) highly selectivity of products caused either by pressure or light, (3) efficient reactions in condensed phases induced by the two-photon absorption. However, the generalization and expansion of these concepts or principles would require extensive investigations on numerous molecular systems. Motivated by these promises, in this Ph.D. thesis, I apply the method to more organic molecular materials with specific characters of molecular structures. The overall objects are to discover and enhance the understanding of the combined pressure-photon effects on the transformation of organic molecular materials. Correspondingly, I will particularly

focus on the following aspects: (1) the detailed pressure correlation and dependency of various photo-induced reactions (e.g., dissociation, isomerization, cyclization, and polymerization reactions), (2) the compressibility behavior of the electronic states as function of pressure, which is mandatory to understand the reactivity of sample and the selectivity of the products, (3) effects of the compressed medium (e.g., physical states) on the photochemical reactions, (4) synthesis and characterization of innovative technological materials by the high-pressure photochemical approach. In the thesis, most of the experimental information is gained from optical microscopy, FTIR, and Raman spectroscopy, the advantages of which will be discussed in Chapter 2.

The contents of the thesis are organized as follows: Chapter 1 provides an introduction of high-pressure photochemistry method, its applications on organic synthesis, and the motivations of the thesis work. Chapter 2 describes the experimental apparatuses used in this thesis. Chapters 3 to 8 constitute the body of the thesis and are further grouped into three themes (I-III) as described below. Finally, chapter 9 summarizes the general conclusions of the thesis and outlines the future work.

Theme I. Laser-induced decomposition of molecular (energetic) materials at static high-pressure (Chapter 3-4).

In the spectrum of electromagnetic radiation, ultraviolet (UV) photons with energies comparable to the dissociation energy of many chemical bonds, typically in the multiple electronvolt (eV) range, provide enhanced access to a wide range of photochemical reactions. Despite the interesting findings from studies of alcohols and water containing mixtures, photochemistry in the UV range varies on specific molecular systems at ambient pressures, and not to mention at high-pressures such that many detailed reaction processes are poorly understood. Therefore, investigation of analogous molecular systems with specific structural characteristics under the combined pressure-photon condition is of fundamental importance. In this part, fluid ethylene glycol is firstly studied (Chapter 3)

because the molecule is a model system known as a triple rotor about the C−H, C−C, and C−O bonds allowing the photodecomposition study along these coordinates.[68] Moreover, the two hydroxyl groups that enable intra- and intermolecular hydrogen bonding in addition to the intrinsic molecular conformations (e.g., trans versus gauche) provide another structural parameter in understanding the chemical stability and reactivity. In Chapter 4, photochemistry in mixtures of 2-butyne ($H_3CC{\equiv}CCH_3$) and a trace amount of H_2O were investigated as a function of pressure at room temperature. The two compounds under the combined extreme conditions allow the examination of pressure and laser effects on competitive photodissociation vs. photopolymerization reactions from H_2O, 2-butyne, respectively.

Theme II. Effects of Pressure on Photochemical Phase Transitions (Chapter 5).

Apart from the photo-induced decomposition of molecular materials, we extend our study to photoisomerization of organic molecules at high pressures. The studied photoisomerization in condensed phase is further associated with photoinduced phase transitions (PIPT). This phenomenon is important as PIPT at ambient pressures have been established in various materials, and it is now developing into a method for exploring hidden nature of materials and realizing the new phase that is not formed in thermal equilibrium.[69,70] A prominent example is the photoinduced phase transition from the equilibrium nematic to the non-equilibrium isotropic phase in liquid crystals (LCs).[70] In the systems, stilbene or azobenzene moiety is doped in LCs, and the trans-cis isomerization transformation is the key for the isothermal photochemical nematic-isotropic phase transition and the change of which can have large impacts on the properties of LCs.

As mentioned above, studies of high-pressure effects on photochemical reactions in recent years were primarily focused on dissociation and polymerization type reactions, therefore, have not yet extended to other types of chemical transformations such as the PIPT via photoisomerization reaction. In this part, for the first time, we put effort into

investigating high-pressure effects on PIPT of cis-stilbene in the condensed phase. The study shows that increasing pressure not only tunes the photoisomerization type phase transitions but also opens a new reaction type, and thus obtains novel crystal and liquid material, respectively. Moreover, mechanism studies via reaction kinetics allow us to clearly demonstrate the correlation between the behavior of the electronic states as a function of pressure and the selectivity of products. The details are presented in chapter 5.

Theme III. Effects of Pressure on Polymerization of Unsaturated Hydrocarbons (Chapter 6-8).

In the frame of polymerization of molecules with unsaturated bonds, molecules with triple bonds are of enormous interest as the molecules can be used as a precursor to produce important technological materials, e.g., conducting polymers and high-density extended solids. In Chapter 6, we explore the transformations from crystalline dimethyl acetylene (DMA) to amorphous poly(DMA) under high pressure for the first time. We find that the pressure required for the amorphization and polymerization is as high as 12 GPa. The high threshold pressure was also found in the pressure-induced polymerization of its analogs, e.g., styrene, phenylacetylene. In order to reduce the reaction pressures of these species, in Chapter 7 and 8, polymeric transformations of styrene and phenylacetylene are studied under combined high pressure and UV radiation conditions. In these two cases, firstly, UV radiation was found to significantly reduce the large pressure threshold to a few tenths of a GPa. Secondly, single reaction channel in polymerization reaction permits us to quantitatively analyze photochemical reaction kinetics and its pressure-dependency. Therefore, correlations between rate constant, activation volume and pressure are obtained. Finally, effects of physical states, accessed by varying compression rate, on the polymerization kinetics, selectivity, and microstructure of products are also investigated.

1.5 References

(1)   Badding, J. V. *Annual Review of Materials Science* **1998**, *28*, 631.

(2)   Hemley, R. J. *Annual Review of Physical Chemistry* **2000**, *51*, 763.

(3)   Brazhkin, V. V. *High Pressure Research* **2007**, *27*, 333.

(4)   Schettino, V.; Bini, R. *Chemical Society Reviews* **2007**, *36*, 869.

(5)   Riggleman, B.; Drickamer, H. *The Journal of Chemical Physics* **1963**, *38*, 2721.

(6)   Akahama, Y.; Kawamura, H.; Hausermann, D.; Hanfland, M.; Shimomura, O. *Physical Review Letters* **1995**, *74*, 4690.

(7)   Bini, R. *Accounts of Chemical Research* **2004**, *37*, 95.

(8)   Wilhelm, C.; Boyd, S. A.; Chawda, S.; Fowler, F. W.; Goroff, N. S.; Halada, G. P.; Grey, C. P.; Lauher, J. W.; Luo, L.; Martin, C. D.; Parise, J. B.; Tarabrella, C.; Webb, J. A. *Journal of the American Chemical Society* **2008**, *130*, 4415.

(9)   Schettino, V.; Bini, R. *Physical Chemistry Chemical Physics* **2003**, *5*, 1951.

(10)   Kagan, J. *Organic photochemistry: principles and applications*; Academic Press, 2012.

(11)   Oelgemoller, M. *Chemical Reviews* **2016**, *116*, 9664.

(12)   Tamura, K.; Sugiyama, S.; Lenoble, W. J. *Journal of Organic Chemistry* **1984**, *49*, 3836.

(13)   Neuman, R. C.; Berge, C. T. *Tetrahedron Letters* **1978**, 1709.

(14)   Turro, N. J.; Chung, W.-S.; Okamoto, M. *Journal of Photochemistry and Photobiology A: Chemistry* **1988**, *45*, 17.

(15)   Katz, A. I.; Schiferl, D.; Mills, R. L. *Journal of Physical Chemistry* **1984**, *88*, 3176.

(16)   Agnew, S. F.; Swanson, B. I.; Jones, L. H.; Mills, R. L. *Journal of Physical Chemistry* **1985**, *89*, 1678.

(17)   Lenoble, W. J.; Tamura, K. *Tetrahedron Letters* **1977**, 495.

(18)   Shimizu, H.; Matsunami, N. *Journal of Raman Spectroscopy* **1988**, *19*, 199.

(19)   Tamura, K.; Abe, M.; Terai, M. *Journal of the Chemical Society, Faraday Transactions 1: Physical Chemistry in Condensed Phases* **1989**, *85*, 1493.

(20)   Gilbert, A.; Heritage, T. W.; Isaacs, N. S. *Journal of the Chemical Society-Perkin Transactions 2* **1992**, 1141.

(21)   Bernasconi, M.; Chiarotti, G. L.; Focher, P.; Parrinello, M.; Tosatti, E. *Physical Review Letters* **1997**, *78*, 2008.

(22)   Inoue, Y.; Matsushima, E.; Wada, T. *Journal of the American Chemical Society* **1998**, *120*, 10687.

(23)   Ceppatelli, M.; Santoro, M.; Bini, R.; Schettino, V. *Journal of Chemical Physics* **2000**, *113*, 5991.

(24)   Ciabini, L.; Santoro, M.; Bini, R.; Schettino, V. *Physical Review Letters* **2002**, *88*.

(25)   Citroni, M.; Ceppatelli, M.; Bini, R.; Schettino, V. *Science* **2002**, *295*, 2058.

(26)   Chelazzi, D.; Ceppatelli, M.; Santoro, M.; Bini, R.; Schettino, V. *Nature Materials* **2004**, *3*, 470.

(27)   Citroni, M.; Ceppatelli, M.; Bini, R.; Schettino, V. *Journal of Physical Chemistry B* **2007**, *111*, 3910.

(28)   Citroni, M.; Bini, R.; Foggi, P.; Schettino, V. *Proceedings of the National Academy of Sciences of the United States of America* **2008**, *105*, 7658.

(29)   Ceppatelli, M.; Fanetti, S.; Citroni, M.; Bini, R. *Journal of Physical Chemistry B* **2010**, *114*, 15437.

(30)   Fanetti, S.; Ceppatelli, M.; Citroni, M.; Bini, R. *Journal of Physical Chemistry B* **2011**, *115*, 15236.

(31)   Fanetti, S.; Ceppatelli, M.; Citroni, M.; Bini, R. *Journal of Physical Chemistry C* **2012**, *116*, 2108.

(32)   Salzillo, T.; Bilotti, I.; Della Valle, R. G.; Venuti, E.; Brillante, A. *Journal of the American Chemical Society* **2012**, *134*, 17671.

(33)   Ayitou, A. J. L.; Fukuhara, G.; Kumarasamy, E.; Inoue, Y.; Sivaguru, J. *Chemistry-a European Journal* **2013**, *19*, 4327.

(34)   Tomotsune, S.; Sekiya, T. *European Physical Journal B* **2013**, *86*.

(35)   Bakowicz, J.; Turowska-Tyrk, I. *Crystengcomm* **2014**, *16*, 6039.

(36)   Ceppatelli, M.; Bini, R. *Macromolecular Rapid Communications* **2014**, *35*, 787.

(37)   Evlyukhin, E.; Museur, L.; Traore, M.; Nikitin, S. M.; Zerr, A.; Kanaev, A. *Journal of Physical Chemistry B* **2015**, *119*, 3577.

(38)   Bakowicz, J.; Turowska-Tyrk, I. *Crystengcomm* **2016**, *18*, 8898.

(39)   Galica, T.; Bakowicz, J.; Konieczny, K.; Turowska-Tyrk, I. *Crystengcomm* **2016**, *18*, 8871.

(40)   Eckert, B.; Schumacher, R.; Jodl, H. J.; Foggi, P. *High Pressure Research* **2000**, *17*, 113.

(41)   Liu, X. J.; Moritomo, Y.; Ichida, M.; Nakamura, A.; Kojima, N. *Journal of Luminescence* **2000**, *87-9*, 649.

(42)   Liu, X. J.; Moritomo, Y.; Nakamura, A.; Kojima, N. *Phase Transitions* **2001**, *74*, 51.

(43)   Deng, Y. H.; Sui, Z. L.; Gong, J. B.; Dai, R. C.; Wang, Z. P.; Zhang, Z. M.; Ding, Z. J. *Journal of Physical Chemistry C* **2013**, *117*, 25012.

(44)   Sui, Z. L.; Hu, S. H.; Chen, H.; Gao, C.; Su, H.; Rahman, A.; Dai, R. C.; Wang, Z. P.; Zheng, X. X.; Zhang, Z. M. *Journal of Materials Chemistry C* **2017**, *5*, 5451.

(45)   Ceppatelli, M.; Bini, R.; Schettino, V. *Proceedings of the National Academy of Sciences of the United States of America* **2009**, *106*, 11454.

(46)   Ceppatelli, M.; Bini, R.; Schettino, V. *Journal of Physical Chemistry B* **2009**, *113*, 14640.

(47)   Ceppatelli, M.; Bini, R.; Schettino, V. *Physical Chemistry Chemical Physics* **2011**, *13*, 1264.

(48)   Ceppatelli, M.; Bini, R.; Caporali, M.; Peruzzini, M. *Angewandte Chemie-International Edition* **2013**, *52*, 2313.

(49) Ceppatelli, M.; Fanetti, S.; Bini, R. *Journal of Physical Chemistry C* **2013**, *117*, 13129.

(50) Ceppatelli, M.; Pagliai, M.; Bini, R.; Jodl, H. J. *Journal of Physical Chemistry C* **2015**, *119*, 130.

(51) Ceppatelli, M.; Scelta, D.; Tuci, G.; Giambastiani, G.; Hanfland, M.; Bini, R. *Journal of Physical Chemistry C* **2016**, *120*, 5174.

(52) Duwal, S.; Yoo, C. S. *Journal of Physical Chemistry C* **2017**, *121*, 12863.

(53) Iwai, S.; Yamamoto, K.; Hiramatsu, F.; Nakaya, H.; Kawakami, Y.; Yakushi, K. *Physical Review B* **2008**, *77*.

(54) Bakowicz, J.; Turowska-Tyrk, I. *Journal of Photochemistry and Photobiology a-Chemistry* **2012**, *232*, 41.

(55) Konieczny, K.; Bakowicz, J.; Turowska-Tyrk, I. *Crystengcomm* **2015**, *17*, 7693.

(56) Konieczny, K.; Bakowicz, J.; Turowska-Tyrk, I. *Journal of Photochemistry and Photobiology a-Chemistry* **2016**, *325*, 111.

(57) Santoro, M.; Gorelli, F. A.; Bini, R.; Haines, J.; van der Lee, A. *Nature Communications* **2013**, *4*.

(58) Citroni, M.; Fanetti, S.; Bini, R. *Journal of Physical Chemistry C* **2014**, *118*, 10284.

(59) Hebert, P.; Saint-Amans, C. *18th Aps-Sccm and 24th Airapt, Pts 1-19* **2014**, *500*.

(60) Holtgrewe, N.; Lobanov, S. S.; Mahmood, M. F.; Goncharov, A. F. *Journal of Physical Chemistry C* **2016**, *120*, 28176.

(61) Fanetti, S.; Citroni, M.; Falsini, N.; Bini, R. *The Journal of Physical Chemistry C* **2018**.

(62) Prasad, S. K.; Rao, D. S. S.; Jeyagopal, P. *Physical Review E* **2001**, *64*.

(63) Pinkowicz, D.; Rams, M.; Misek, M.; Kamenev, K. V.; Tomkowiak, H.; Katrusiak, A.; Sieklucka, B. *Journal of the American Chemical Society* **2015**, *137*, 8795.

(64) Chen, B.; Hoffmann, R.; Cammi, R. *Angewandte Chemie-International Edition* **2017**, *56*, 11126.

(65) Klarner, F. G.; Wurche, F. *Journal Fur Praktische Chemie-Practical Applications and Applied Chemistry* **2000**, *342*, 609.

(66) Lenoble, W. J. *Chemie in Unserer Zeit* **1983**, *17*, 152.

(67) Bonang, C. C.; Anderson, D. J.; Cameron, S. M.; Kelly, P. B.; Getty, J. D. *Journal of Chemical Physics* **1993**, *99*, 6245.

(68) Murli, C.; Lu, N.; Dong, Z. H.; Song, Y. *Journal of Physical Chemistry B* **2012**, *116*, 12574.

(69) Tokura, Y. *Journal of the Physical Society of Japan* **2006**, *75*.

(70) Prasad, S. K.; Nair, G. G.; Rao, D. S. S. *Liquid Crystals* **2009**, *36*, 705.

Chapter 2

2 Instrumentation

2.1 High-pressure apparatus

2.1.1 Diamond anvil cell (DAC)

High pressure chemistry is an expanding area of interest, due in large part to the accessibility of pressures on the order of hundreds of GPa provided by a modernized high-pressure cell. The first inventor of high-pressure cells was physicist Percy Bridgman,[1] who produced high pressure by using an opposing anvil system initially of chrome steel, and subsequently tungsten carbide cemented in cobalt when the original system proved too brittle. The development to opposed diamond anvil cells (DAC) was not made until 1959 by Jamieson.[2] The advantages of DACs are firstly the extreme hardness of diamond, allowing the DAC to reach considerable pressures, secondly, the low absorption of short wavelength X-rays and transparency to UV, visible and IR radiation of diamonds allowing in situ optical and spectroscopic measurements of the micrometric sample in the DAC. A general set-up of the DAC is shown in Fig. 2.1. The DAC has two parts: piston and cylinder. A pair of diamonds are held in place on two tungsten carbide seats, which are aligned to the piston and cylinder. A gasket between the two diamonds is used to immobilize the sample under investigation. To be used in the experiment, the gasket must be first pre-indented to a thickness of tens of microns from an initial thickness of 280 µm. Next, a hole, the size of which is about one third of the diamond culet, is drilled at the center of the pre-indented mark using an electric discharge machine (EDM) and used as the sample chamber. Once all these components are well assembled, the pressure can be produced through by manual tightening the four bolts with spring washers. The operation provides mechanical forces perpendicularly to the surface of the diamonds. The tip sizes

of the diamond anvils can be customized varying from tens to hundreds of microns in diameter, thus, enormous pressure can be easily generated (e.g., 1 N can generate 8×10^6 Pa on a 400 µm culet.).[3] The smaller the culet size is, the higher the maximum pressure can be achieved. In the sample holder there is also a ruby (5-10 mm), which allows the pressure inside the cell to be precisely measured (discussed below).
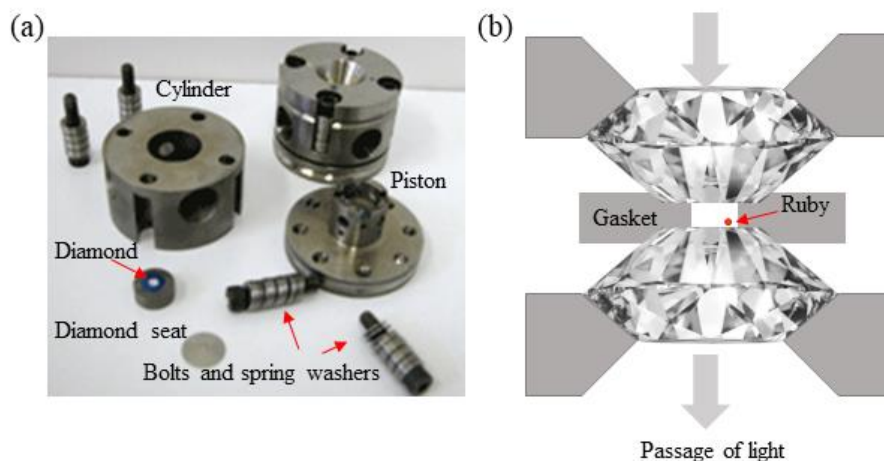
Figure 2.1: Photo (a) and schematic (b) of a symmetric DAC. Red dot is a ruby ball loaded in a sample hole in the DAC.

Several parameters should be considered when selecting or constructing a diamond anvil cell for use, e.g., optical transparency, diamond shape and size, gasket hardness, sample hole diameter, etc. As vibrational spectroscopy is used as the major probe in this thesis (as described later), the optical transparency is the prime factor in selecting diamond anvils. There are basically two types of diamonds used for different spectroscopic probes, namely types I and II, which can be further classified to types Ia, Ib, IIa and IIb according to the level and type of their chemical impurities.[3] All diamonds have an intense first order Raman line at 1332 cm^{-1} (F$_{2g}$ mode), but with different infrared absorption ranges. Type I stones (with more nitrogen impurities) have two strong absorption regions, which are around 2000 cm^{-1} and 1000-1350 cm^{-1}, respectively. In contrast, type II stones (low levels of nitrogen impurities) have a clean window below 2000 cm^{-1} allowing IR measurements

in the DAC. Due to their different optical transparencies, type I diamonds are only suitable for Raman spectroscopy, while type II diamonds are mainly used for IR spectroscopy.

2.1.2 Pressure gauge

While the sample is loaded, a ruby (Al_2O_3 doped with Cr^{3+}) is also loaded into the sample holder, which allows the pressure inside the cell to be measured via the ruby fluorescence method initially developed by Forman et al. in 1972.[4] When excited by a 532-nm laser, the ruby has two intense luminescent peaks R_1 and R_2 (Fig. 2.2). The positions of the R_1 and R_2 peaks are sensitive to pressure and shift to a longer wavelength upon compression. Using pressure values indirectly obtained from the isothermal equations of state of metals (e.g., Au, Cu, Pt, Mo,) derived from shock wave data as a standard, the correlation between pressure and R_1 peak shift can be calibrated up to 80 GPa.[3] With these references, an equation (eq. 2.1) was established to describe the relationship.

$$P = \frac{1904}{B}\left[\left(1 + \frac{\Delta\lambda}{694.24}\right)^{B} - 1\right] \qquad (2.1)$$

where P is the in-situ pressure in GPa, and $\Delta\lambda$ is the wavelength shift of R_1 in nm. The parameter B equals 7.665 under quasi-hydrostatic condition. Using this method, the resolution of the pressure can be achieved to $\pm$ 0.05 GPa.
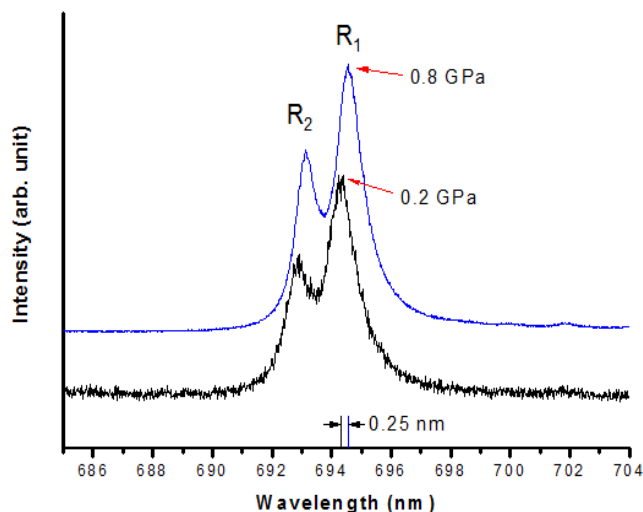
Figure 2.2: Ruby fluorescence measured at different pressures with the two luminescent peaks labeled (R_1 and R_2). The pressure condition for each spectrum is labeled beside.

2.1.3 Setup of high-pressure photochemistry

Increasing chemical instability following laser irradiation was first noticed in high pressure experiments of unsaturated molecule acetylene.[5] Specifically, pressure-induced polymerization of solid acetylene was experimentally found to occur at 4.2 GPa at room temperature,[6] where 532 nm laser was used in Raman measurement. However, *ab initio* simulations performed by Bernasconi et al. found the polymerization to occur around at 25 GPa, thus at a much higher pressure than the experimental value.[7] Nevertheless, the transformation pressure felt down to 9 GPa by inserting in the cell a molecule of acetylene in the first triplet state locating at 3.78 eV. This result suggests that the laser used in Raman experiments is not non-invasive and can strongly affect the threshold pressure of the polymerization. Influences of laser radiation were observed in more molecular systems, e.g., CO,[8] N_2O_4,[9] and S_8.[10] The spectroscopic investigations of these substances at high pressure and laser irradiation showed that the chemical reactions induced are different from

those induced by pressure alone. These results further showed that light absorption strongly affects chemical reactivity of molecules at high pressures, but in none of these studies was a careful characterization of the photochemical reaction pursued.
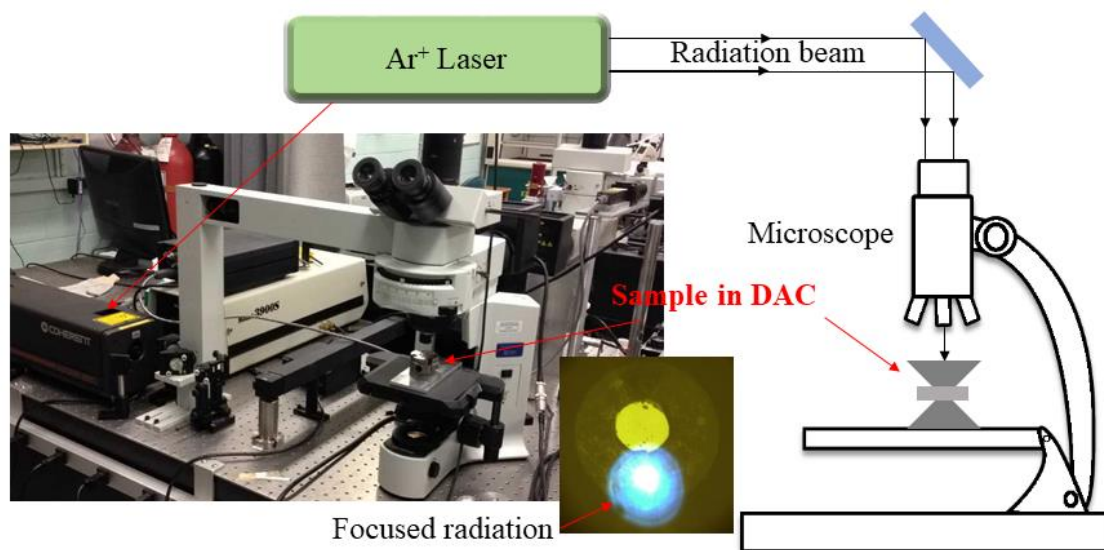
Figure 2.3: Photo and schematics of the high-pressure photochemistry setup. The microphotograph shows a sample hole and the focused laser beam.

More controllable laser irradiation, including tunable beam size, power density, and incident wavelength, is therefore introduced into high-pressure DAC to investigate the role of irradiation and pressure on the chemical reactivity of molecular species. In the Song's laboratory, the setup can be briefly described as follows. First, the sample loaded in a DAC with a measured pressure is placed on the sample stage of the microscope (Fig. 2.3). Next, laser radiation from an argon ion laser (Innova 90C, Coherent) is focused on the sample in the DAC via the microscope. The argon ion laser provides three standard output wavelengths (e.g., multiline visible 457.9-514.5 nm, 488 nm, 514.5 nm) and several optional output wavelengths. In this thesis, the multi-line UV emission with a peak wavelength at ~ 350 nm is mainly used. The beam size and laser power are adjustable, which will be clarified in the specific projects.

2.2 *In situ* structural characterization via vibrational spectroscopy

To investigate structural transformation and physical properties of materials in situ under high pressure, powerful penetrating micro-sampling probes are required to reach the micro-size samples through the wall of the pressure vessel. Up to the present, various analytical techniques including synchrotron-based probes and other analytical probes (see Fig. 2.4) have been successfully adapted to the studies of micrometric samples contained in the DAC, taking advantage of the diamond transparency from the X-ray to the infrared region, and of laser or synchrotron beams that can be focused on the samples inside the DAC. Among all these available in situ structural characterization probes, vibrational spectroscopy, including Raman and Infrared (IR) spectroscopy, has demonstrated strong sensitivity and accuracy as well as efficiency in monitoring the physical or chemical transformations.[11] The two spectroscopic methods, complementary to each other, provide reliable and valuable information on molecular structures, the nature of bonding, lattice dynamics as well as quantity of materials in the tiny DAC sample chamber. Therefore, in this thesis, state-of-the-art, highly-customized high-pressure spectroscopic and optical microscopic systems in the Song laboratory are used, which allow structural transformation and chemical reaction processes to be probed *in situ*.
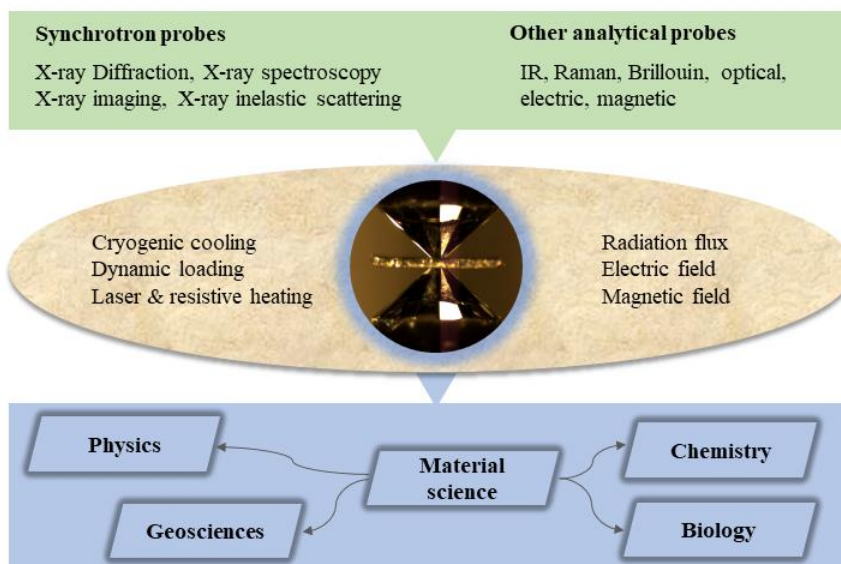
Figure 2.4: Various characteristics probes have been developed to study samples under extreme environments and their applications to multidisciplinary sciences.

2.2.1 *In situ* high-pressure FTIR system

The *in situ* high-pressure IR measurements were carried out using a customized Fourier-transform infrared (FTIR) micro-spectroscopy system. Fig. 2.5 shows the schematic diagram of the system.[3] A commercial Fourier transform infrared (FTIR) spectrometer from Bruker Optics Inc. (model Vertex 80v) equipped with a Globar IR light source constitutes the main component of the system, which is operated under a vacuum of < 5 mbar such that interference from H_2O and CO_2 is efficiently removed. A collimated IR beam of varying diameters set with apertures ranging from 0.25 mm to 8 mm is directed into a relay box through a KBr window on the spectrometer. The beam is then focused onto the sample in the DAC by IRIS optics and a $15\times$ reflective objective lens with a numerical aperture of 0.4. The size of the IR beam is set to be identical to the size of sample (e.g., ~ 200 µm) by a series of IRIS apertures. The transmitted IR beam is collected using another identical reflective objective as the condenser and is directed to a mid-band mercury

cadmium telluride (MCT) detector equipped with a ZnSe window allowing measurements in the spectral range of 600 cm^{-1} to 12000 cm^{-1}.
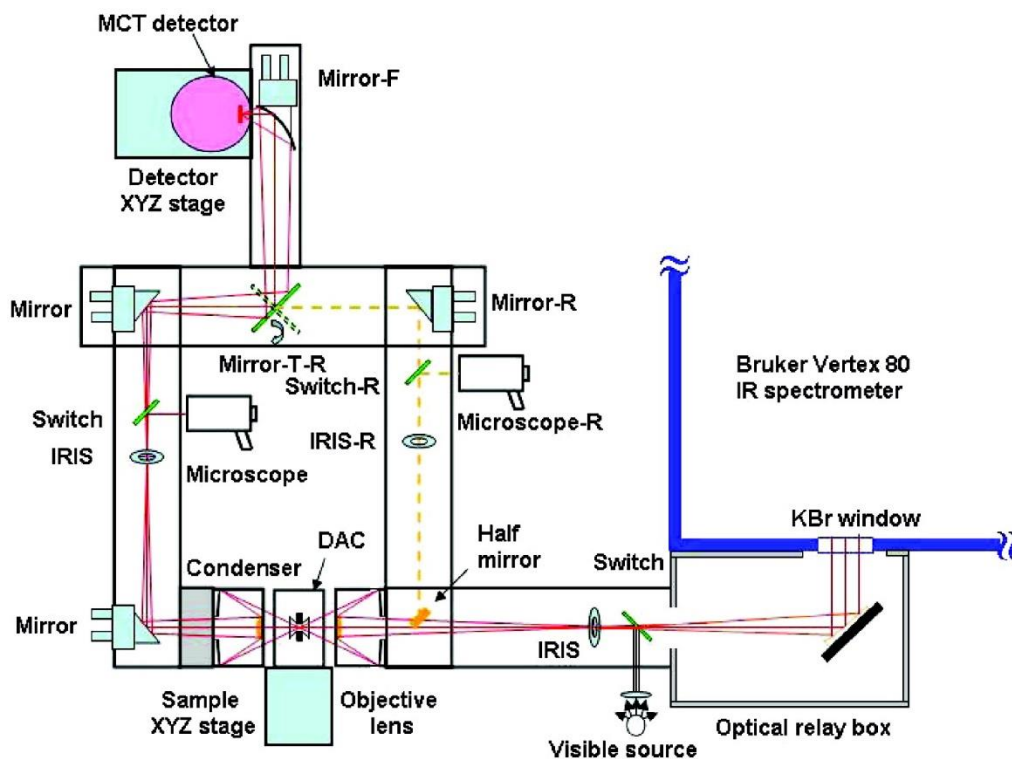
Figure 2.5: Schematic diagram of the IR microspectroscopy system. The IR spectrometer (model Vertex 80) from Bruker is operated under vacuum. The collimated IR beam comes out through a KBr window. The rest of the optics is purged using CO$_2$-free dry air in closed boxes or frames. All major optical components are labeled. Those with "-R" and half mirror are for reflection measurements, whereas the rest are for transmission/absorption measurements. "Switch" refers to switchable mirrors for illumination purposes. "Mirror-TR" is a mirror used to switch between transmission and reflection modes. "Mirror-F" is used to focus the IR signal to the detector. (Reproduced with the permission of the American Chemical Society)

2.2.2 *In situ* high-pressure Raman system

A customized Raman system was used for the Raman measurements. The schematic diagram of the Raman system is depicted in Fig. 2.6.[3] The system is constructed on an optical table. Single longitudinal mode, diode pumped solid state (DPSS) green (wavelength 532.10 nm) or red (780 nm) laser was used as the excitation source. The microscope system (blue area in Fig. 2.6) is used to focus the laser beam onto the specimen containing a 15× eyepiece and 20× objective (Olympus Microscope), while two beam splitters (BS) built inside and a CCD camera allow in-situ imaging. The 3-D manually adjustable sample stage is designed to align the DAC right below the microscope. To record the Raman spectrum, a liquid nitrogen cooled CCD (charge-coupled device) (Spec-10 system, Princeton Instrument) is used to maintain the minus 120 °C operation condition. A 0.5 m monochromator (SpectroPro-2500i, Acton Research Corporation) is used to analyze Raman signals. A triple grating system with different resolutions (300 lines/mm, 1200 lines/mm, and 1800 lines/mm) is housed inside of the spectrometer. The system control and data collection are realized by the WinSpec software. The system is calibrated by using standard neon lines before use. With its calibration, the Raman system can achieve a resolution of $\pm$ 1 cm^{-1}.
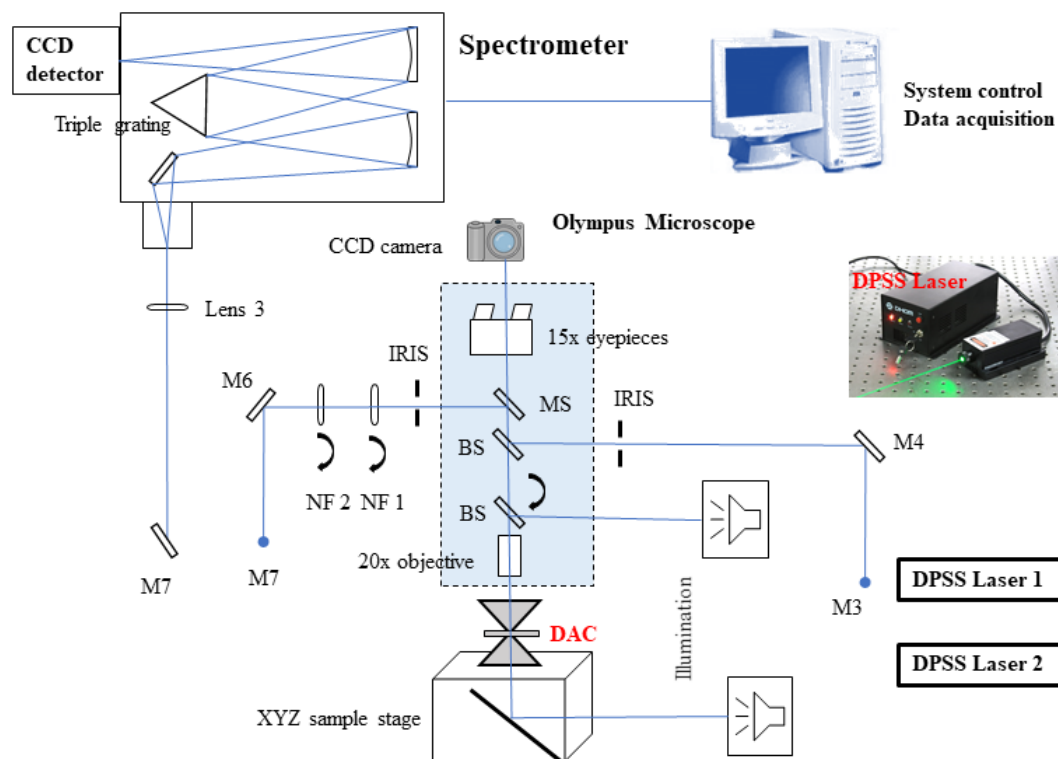
Figure 2.6: Schematic of the Raman system. BPF: band path filter; IRIS: IRIS aperture; M: broadband dielectric reflecting mirrors; BS: beam splitter; NF: notch filter; DAC: diamond anvil cell; Triple gratings: 300 lines/mm, 1200 lines/mm, and 1800 lines/mm. The blue area is the microscope system with a CCD camera, which is perpendicular to the other parts. The two illuminations are top and back light sources used for determing the position of the sample chamber in DAC.

2.3 *Ab initio* calculation

Under the extreme pressure and radiation conditions, chemical reactions of molecular species can sometimes be exotic, which would give rise to foreign molecular products. In such cases, there are no available IR or Raman spectrum for these products in any database or references. Therefore, to assign the obtained IR or Raman spectrum and identify produced products, reliable structural prediction and calculation are necessary. In Chapter 5 of the thesis, *ab initio* calculations were performed using the GAUSSIAN 09 package.[12]

Density functional theory (DFT) with the B3LYP functional with the 6-311++G (2d, p) basis set was utilized to calculate the most stable structure of predicted products, and further calculate the IR and Raman vibrations of the most stable structure. The stationary points were identified with frequency calculations at the same level to verify that minima structures have zero imaginary frequencies.

2.4   References

(1)   Hemley, R. J. *High Pressure Research* **2010**, *30*, 581.
(2)   Lee, R.; Howard, J. A. K.; Probert, M. R.; Steed, J. W. *Chemical Society Reviews* **2014**, *43*, 4300.
(3)   Dong, Z., "High-pressure Study of Molecular Solids and 1D Nanostructures by Vibrational Spectroscopy and Synchrotron X-ray Diffraction", **2012,** 585.
(4)   Forman, R. A.; Piermarini, G. J.; Barnett, J. D.; Block, S. *Science* **1972**, *176*, 284.
(5)   Ceppatelli, M.; Santoro, M.; Bini, R.; Schettino, V. *Journal of Chemical Physics* **2000**, *113*, 5991.
(6)   Aoki, K.; Usuba, S.; Yoshida, M.; Kakudate, Y.; Tanaka, K.; Fujiwara, S. *Journal of Chemical Physics* **1988**, *89*, 529.
(7)   Bernasconi, M.; Chiarotti, G. L.; Focher, P.; Parrinello, M.; Tosatti, E. *Physical Review Letters* **1997**, *78*, 2008.
(8)   Lipp, M.; Evans, W. J.; Garcia-Baonza, V.; Lorenzana, H. E. *Journal of Low Temperature Physics* **1998**, *111*, 247.
(9)   Agnew, S. F.; Swanson, B. I.; Jones, L. H.; Mills, R. L. *Journal of Physical Chemistry* **1985**, *89*, 1678.
(10)   Eckert, B.; Schumacher, R.; Jodl, H. J.; Foggi, P. *High Pressure Research* **2000**, *17*, 113.
(11)   Song, Y. In *Applications of Molecular Spectroscopy to Current Research in the Chemical and Biological Sciences*; InTech, 2016.
(12)   Frisch, M.; Trucks, G.; Schlegel, H.; Scuseria, G.; Robb, M.; Cheeseman, J.; Scalmani, G.; Barone, V.; Mennucci, B.; Petersson, G. *Inc.: Wallingford, CT, USA* **2009**.

Chapter 3

3 Pressure Selected Reactivity and Kinetics Deduced from Photoinduced Dissociation of Ethylene Glycol*

3.1 Introduction

As one of three principal thermodynamic variables, pressure plays an important role to alter the interatomic distances and thus the nature of intermolecular interactions, chemical bonding, molecular configurations, crystal structures and stability of materials. Application of pressure to molecular systems with diversified structures, in particular, offers new and unique ways to produce exotic species that are otherwise not accessible under ambient conditions or using conventional synthetic approach.[1,2] For instance, diamond-like singly bonded poly-nitrogen, which is considered a novel high energy density material, was only accessible at high-pressure and high-temperature conditions (e.g., over 100 GPa and 2000 K) converted directly from molecular nitrogen.[3] Even at a lower pressure range of a few gigapascals, a wide range of molecules were found to undergo transformations including isomerization, polymerization, amorphization and other significant change in molecular structures.[4-9] Furthermore, it was found that the excitation by laser photons can significantly lower the transformation pressure for a number of molecular systems with selective reaction pathways,[10-15] thus providing new avenues to synthesize novel materials.[16,17] For instance, under visible laser irradiations, butadiene can selectively

---

polymerize or dimerize at much lower pressure than by pure compression, suggesting great combined pressure-photon tunability of chemical reactions.[11]

Among the extensive high-pressure photochemical studies, increasing attention has been focused on those initiated by UV radiation. UV photons with energies comparable to the dissociation energy of many chemical bonds, typically in the multiple electronvolt range, provide enhanced opportunities to a wide range of photochemical reactions. It is believed that such high-pressure photon reactivity is predominantly induced via the two-photon (TP) absorption processes[18] in the UV spectral range given the radiation wavelength used (e.g., 350 nm) that is compatible with the high-pressure diamond windows. Although the cross section for TP excitation is relatively small, by carefully tuning the radiation power and reaction pressure, the photochemical reactions can be triggered by UV photons with controlled kinetics and reaction pathways. For instance, Bini and co-workers have extensively used 350 nm multiline UV radiation to initiate chemical reactions at high pressures, such as in ethanol and methanol.[19,20] The dissociative character of the lowest excited singlet electronic state of these molecules allows the production of hydroxyl radicals and hydrogen atoms via the TP absorption of the near UV photons. Following a similar mechanism, excitation energy by two UV photons was utilized to enable new classes of high-pressure photochemical reactions involving mixtures in which water molecules as one of the reagents was used as the radical initiator to produce new molecular species or complexes.[21-24] The novelty of these high-pressure photochemical studies is 2-fold. On one hand, many of high-pressure photochemical reactions result in the formation of desirable products (e.g., H_2) in a mild pressure region (e.g., a few MPa), making the reaction an attractive and unique energy source. On the other hand, reaction conditions involving lower threshold pressure and without the need of solvents or catalysts makes these syntheses highly practical in industry with an appealing, environmentally friendly aspect.

Despite these interesting findings, high-pressure photochemistry in the UV range is discrete, such that many detailed reaction mechanisms are still poorly understood. Therefore, investigation of the photon reactivity of previously investigated molecular systems with specific characteristics under high pressures is of fundamental importance. In particular, factors such as conformational equilibrium and intra- and inter-molecular complexations associated with hydrogen bonding may significantly influence the high-pressure photochemical reactivity. For instance, ethylene glycol (EG, $HOCH_2CH_2OH$) is a model system known as a triple rotor about the C−H, C−C, and C−O bonds for studying photodissociation along these coordinates. Moreover, the two hydroxyl groups that enable intra- and inter-molecular hydrogen bondings in addition to the intrinsic molecular conformations (e.g., trans versus gauche) provide another structural parameter in understanding the high-pressure photon reactivity. Under compression, previous spectroscopic studies showed that liquid EG had a mixture of trans and gauche conformations below 3.1 GPa, which stabilizes to gauche conformation at ~4 GPa upon solidification.[5] Therefore, the relative population of trans and gauche conformations together with hydrogen bondings may substantially influence photochemical reaction channels that are pressure-dependent. Given that EG is widely used in industry with large annual production, any new photoreaction products, if desirable, may offer additional economical applications for EG.

In the present work, we investigate the photochemical reactions of liquid EG triggered by UV radiation at room temperature and different loading pressures from near ambient to ~ 4 GPa. Multiple pressure-selective photon-induced reactions were observed in a different time domain. Using *in situ* FTIR spectroscopy, the primary and secondary processes and products can be monitored and identified. Quantitative analysis allows the understanding of detailed reaction mechanisms and kinetics involving photochemical reactivities of EG under high pressures for the first time. Finally, one of the photodissociation products

involves different structures of CO_2 providing interesting implications for CO_2 sequestration.

3.2 Experimental Details

A symmetric diamond anvil cell (DAC) equipped with a pair of type II diamonds with a culet size of 600 μm was used in the experiment. The liquid anhydrous EG (purity ≥99.8% from Sigma-Aldrich) along with a ruby ball were loaded into a hole with a diameter of 200 μm drilled on a stainless steel gasket that was pre-indented to a thickness of 30-50 μm. The pressure was determined using the well-established ruby fluorescence method. Due to the liquid state of the EG sample and relatively low-pressure range (i.e., < 4 GPa), good system hydrostaticicy is expected and thus no other pressure transmitting medium was used in the present experiments. Moreover, the hydrostaticity is not influenced by the photochemical reactions because the reaction products are predominantly in gas or liquid phase under the experimental pressure (see Results and Discussion) and the ruby fluorescence measurements on different areas across the sample indicate no pressure gradient. The loaded EG samples were compressed to different initial pressures of 0.1, 0.5, 1.0, 1.5, 2.0, and 3.4 GPa for different runs all at room temperature. Sufficient amount of time was allowed for the loaded samples to reach a mechanical and thermal equilibrium before the subsequent photochemical reaction is initiated.

For each loaded sample, the high pressure reactions were triggered by focusing the multiline UV emission with a peak wavelength at ~ 350 nm of an argon ion laser onto the sample with a beam size of ~ 40 μm in diameter and a power ranging from 50 to 750 mW. The reaction progress was monitored by infrared (IR) spectroscopy with the IR absorption spectra collected at half-hour intervals. The reactions were determined complete when no further spectral changes were observed. The time to complete the photochemical reactions was found to be pressure-dependent. Accordingly, the radiation time used for samples loaded at 0.1, 0.5, 1.0, 1.5, 2.0 and 3.4 GPa are 24, 18, 16, 9.5, 14 and 14.5 h, respectively.

In addition, the pressure of the EG sample was found to increase upon UV radiation as a result of photochemical reactions, which was carefully recorded together with each IR measurement.

For infrared absorption measurements, a customized IR micro-spectroscopy system that consists of a Fourier transform infrared (FTIR) spectrometer from Bruker Optics (model Vertex 80v) equipped with a Globar IR light source was used. The detailed instrumentations have been described elsewhere.[25] The system was operated under a vacuum of < 5 mbar, such that the absorption by H_2O and CO_2 was efficiently removed. The variable aperture equipped on the IR microscope allows area-selected IR absorption measurement on different parts of the sample or as a whole. The reference spectrum (i.e., the absorption of diamond anvils) was divided as the background from each measurement. The spectral resolution used was 4 cm^{-1}.

3.3   Results and Discussion

The liquid EG with an initial loading pressure of 0.1 GPa was irradiated by multi-line UV at $\lambda \sim 350$ nm with a power of ~ 700mW and was monitored by visual observations under an optical microscope and by FTIR spectroscopy as a function of time. As shown in Figure 3.1a, no visual changes were observed before the 11th hour. After 13.5 h of irradiation, substantial changes in the physical appearance was observed, including the formation of bubbles and textured materials, indicating the initiation of a photo-induced chemical reaction. With continuing irradiation, the reaction appeared to propagate, and the entire sample had reacted after 24 hours. The photon-induced reactions of EG are further evidenced in the corresponding IR absorption spectra as shown in Figure 3.1b. However, the IR spectra indicate that the photochemical reaction was initiated earlier than 13.5 h. For instance, the IR bands at around 880 cm^{-1} and 1030 cm^{-1} were gradually weakened, while new peaks at 1123, 1724, and 2340 cm^{-1} evolved as early as the third hour and were intensified with time. After 14.5 h, the spectrum showed a strikingly different IR absorption

profile in the spectral region of 1200-1500 cm^{-1} from those before 13.5 h. Thus, two sets of IR spectral evolution with respective radiation time from 0 to 13.5 h, and from 14.5 to 22.5 h, can be identified, indicating a possible sequential photochemical reactions at a switchover time of 13.5 h.

The vibrational bands of EG under 0.1 GPa before radiation agree with the previous IR absorption measurements under ambient conditions (see Table S1 of the supporting information). The disappearance of peaks around 880, and 1030 cm^{-1} indicates the dissociation of the C-C and C-O bonds. Given that the maximum UV absorption wavelength of EG was reported at 198 nm (6.25 eV),[26] two UV photons (λ ~350 nm) are thus expected to have sufficient energy (i.e., ~7 eV) to dissociate the EG. On the basis of the two sets of IR spectra observed, we designate primary and secondary photochemical reactions and products associated with each set in the following analysis. Furthermore, EG was also loaded at other pressures such as 0.5, 1.0, 1.5, 2.0, and 3.4 GPa followed by multi-line UV irradiations with the same power over a different period of time in additional experiments. Similar IR spectral evolutions were observed, as shown in Figures S1-S5 of the supporting information, except that the reaction times were found to be different, indicating the pressure-dependent kinetics which will be discussed in detail later. We will primarily focus on the analysis of photochemical reactions observed at 0.1 GPa as a representative.
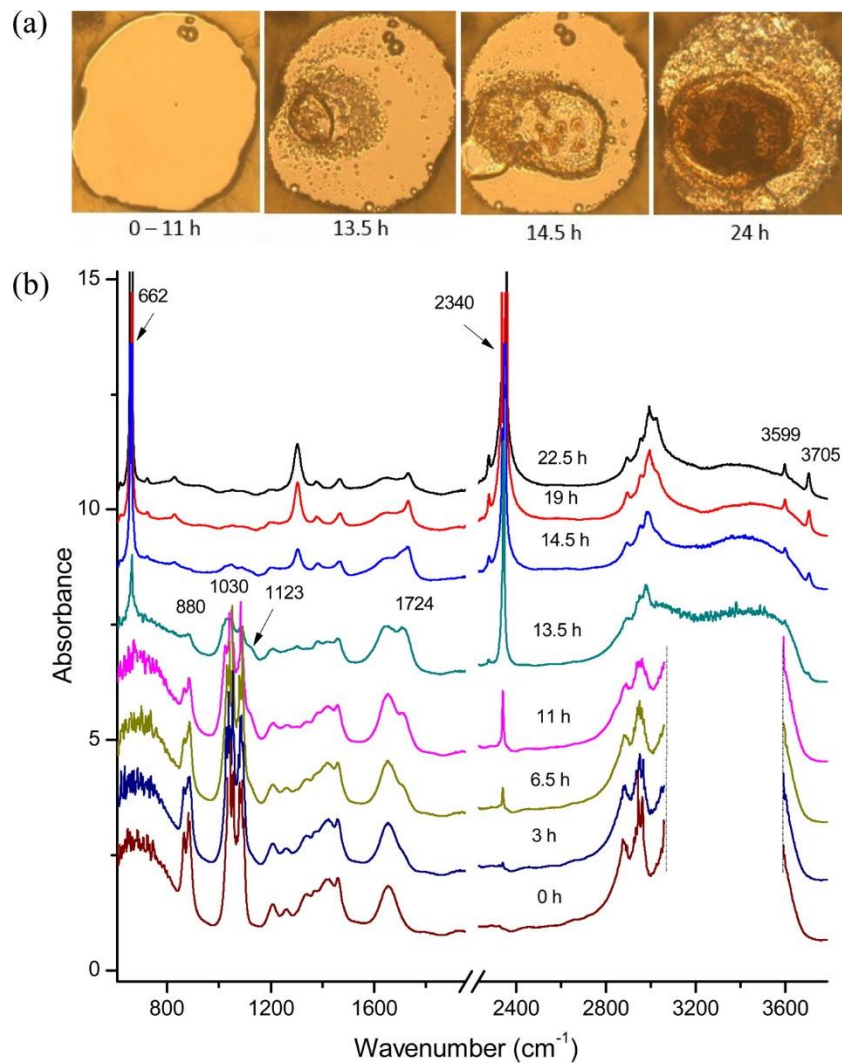
Figure 3.1: Microphotographs of EG samples with an initial loading pressure of 0.1 GPa upon UV irradiation (with λ of ∼350 nm and power of ∼700 mW) collected at (a) different radiation time and (b) selected FTIR spectra of EG collected under the same condition as a function of time. Selected characteristic IR bands emerged at 13.5 h and observed at 22.5 h, indicating sequential photochemical reactions are labeled (see the text). The spectral region in 3000–3500 cm⁻¹ before 13.5 h is truncated due to the saturated IR absorption intensity in this region.

3.3.1 Primary photodissociation products

In Figure 3.2, characteristic IR bands observed at 13.5 h indicating the production of the primary products are examined in the region of 1000-1800 and 2500-3000 cm^{-1}. The intense and well resolved IR peaks at 1213, 1383, 1724, and 2892 cm^{-1} are found to be consistent with those of glycolaldehyde (GA, $HOCH_2CHO$) with reported IR frequencies at 1231, 1372, 1747, and 2867 cm^{-1}, respectively.[27] The strong IR bands at 1092 and 1724 cm^{-1} together with those shown in the inset at 1339, 1396 and 1436 cm^{-1} agree with the characteristic IR bands of acetaldehyde (CH_3CHO) reasonably well, compared to the reported values at 1352, 1395, and 1441 cm^{-1}, respectively.[28] Finally, the two strong IR modes at 1030 and 2947 cm^{-1} are in excellent agreement with the dominant vibrational bands reported for methanol (CH_3OH).[29] Detailed assignments of all peaks in comparison with reported IR modes of GA, acetaldehyde and methanol are listed in Table 3.1.
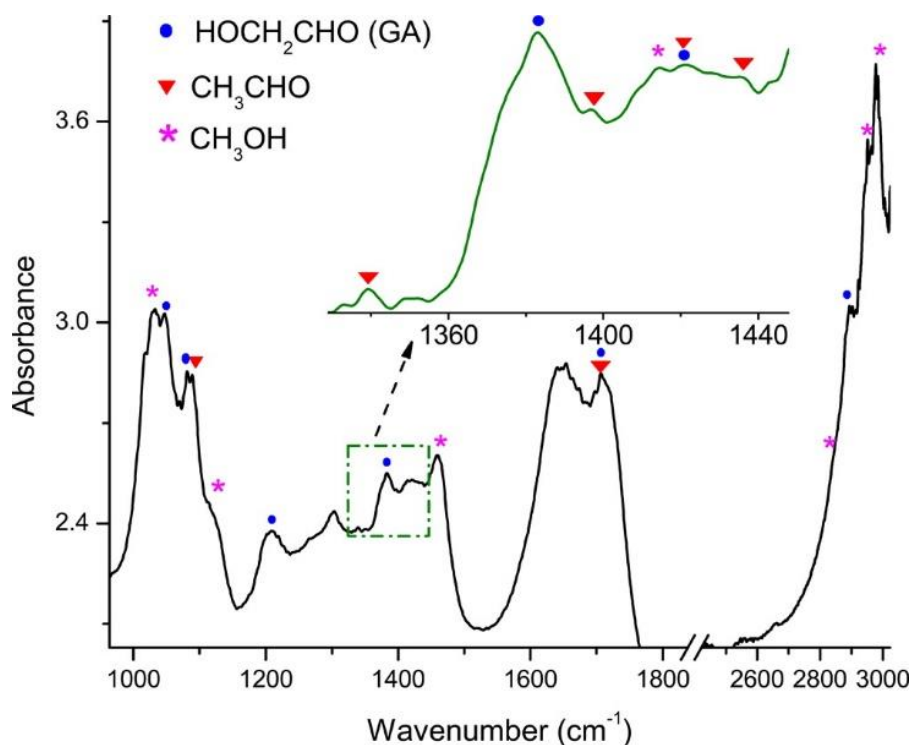
Figure 3.2: FTIR spectrum of EG with an initial loading pressure of 0.1 GPa upon UV radiation for 13.5 h in the selected spectral region where the primary photodissociation products of EG can be identified as labeled by different legends. The inset shows the amplified IR absorption profile in the spectral range of 1320-1450 cm^{-1} that allows the identification of more characteristic IR modes. The peak at 1303 and 1651 cm^{-1} not labeled are associated with a secondary product and original EG respectively (see the text).

Previous studies on UV photolysis ($\lambda = 185$ nm) of 2 M aqueous solutions of EG at ambient condition suggest that hydrogen, formaldehyde, GA, methanol, glycerol and acetaldehyde were the main products.[30] At room temperature, the quantum yields for these products were 0.20 (hydrogen), 0.19 (formaldehyde), 0.08 (GA), 0.07 (methanol), 0.06 (glycerol), 0.02 (acetaldehyde). Our identification of the possible photodissociation products of EG at high pressures is thus consistent with the previous studies. A possible

pathway for the production of GA could follow a straightforward channel by direct cleavage of C-H and O-H bonds as shown below.

$$CH_2OHCH_2OH \rightarrow HOCH_2CHO + 2\dot{H} \qquad (3.1)$$
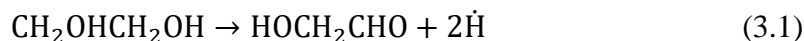
The low intensity of the IR absorbance of the second product acetaldehyde (Figure 3.2) suggests the low abundance of acetaldehyde among other primary products, consistent with the low quantum yield for acetaldehyde (i.e., 0.02) in UV photolysis of EG aqueous solution reported previously.[30] A possible production route for acetaldehyde could be initiated by the dissociation of a C-O bond and an O⋯H intra-molecular hydrogen bonding in the gauche conformation of EG.[5] Subsequently, the C_α-H dissociation and hydrogen transfer from C_α to C_β result in formation of CH_3CHO and water, as shown below.

$$CH_2OHCH_2OH \rightarrow CH_3CHO + H_2O \qquad (3.2)$$
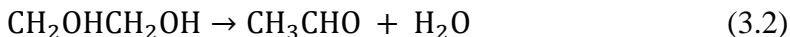
Theoretical calculations on the unimolecular decomposition of EG showed that H_2O-elimination in EG dissociations had the lowest barriers among all the dissociation channels investigated.[31] Our observation is thus consistent with the calculations. Moreover, water as another product that was found to participate in the secondary photochemical reactions further supported our analysis. Detailed processes involving water will be discussed later.

The formation of the third primary product methanol can be inferred from the dissociation of EG that produces CH_2OH radicals (reaction 3.3). Subsequent radical-radical reaction with H radical produced by dissociation of C-H or O-H bonds (e.g., reaction 3.1) may lead to the formation of methanol (reaction 3.4). Indeed, decreasing intensity of the IR bands at around 880 cm^{-1} (see Figure 3.1) may suggest the dissociation of C-C bonds of EG to facilitate the production of CH_2OH radical. More importantly, this channel was predicted to be the lowest-energy dissociation channel among the barrierless reactions of unimolecular decomposition of EG.[31]

$$CH_2OHCH_2OH \rightarrow 2\dot{C}H_2OH \qquad\qquad (3.3)$$

$$\dot{C}H_2OH + \dot{H} \rightarrow CH_3OH \qquad\qquad (3.4)$$
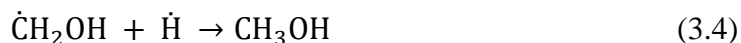
3.3.2 Secondary photochemical reactions

The IR spectrum collected at 22.5 h in Figure 3.1 is the most representative for the analysis of secondary photochemical processes and thus is examined in detail with selected spectral regions shown in Figure 3.3. The IR bands display different intensities ranging from strong (e.g., at 1303 and 3010 cm^{-1}) to medium (e.g., 1375, 1467, 1731, 2340 and 2896 cm^{-1}) and to weak and/or convoluted (e.g., 914, 1060, 1093, 1116, 1200, 1254 cm^{-1}). Our approach to identify the secondary photochemical products is to examine the possible UV photodissociation channels of the primary products, i.e., GA, CH$_3$CHO and CH$_3$OH. The IR frequencies associated with the secondary products identified are listed in Table 3.2. The reaction pathways that lead to the production of both primary and secondary products are summarized in Scheme 3.1.

Table 3.1 The observed IR bands of liquid EG with an initial loading pressure of 0.1 GPa and those of photochemical reaction products after UV irradiation (λ = 350 nm, 750 mW) for 13.5 h.

IR frequencies (cm^{-1})[a]	reference[b]			assignment
	glycolaldehyde (GA)[c]	acetaldehyde (CH$_3$CHO)[d]	methanol (CH$_3$OH)[e]	
662			655S	Torsion
740	752 M			CC=O bend, CH bend
880	861 M	867 M		CC stretch, CH$_3$ rock
908		919 M		CH$_3$ rock
1030			1030 VS	CO stretch
1050	1073 M			O=CCO bend
1082	1108 M			C-O stretch
1092		1104 S		CC stretch
1115			1115W	CH$_3$ rock
1213	1231 M			CH$_2$ twist
1339		1352 S		CH$_3$ s-deform
1383	1372 M			O=CH bend
1396		1395 S		CH bend
1415			1420 M	COH bend
1420	1421 M	1420 S		CH$_2$ wag, CH$_3$ d-deform
1436		1441 S		CH$_3$ d-deform
1463			1455,1480 M	CH$_3$ s, d-deform
1724	1747 S	1732 VS		C=O stretch
2841			2822 S	CH$_3$ s-str, C-H (aldehyde) stretch
2892	2867 S			CH$_3$ d-str, CH$_2$ asymmetric stretch
2947			2934 S	CH$_3$ d-str
2980		2967 M	2980 M	CH$_3$ d-str
3434	3338 vb		3337vb	OH stretch

[a.]This work. [b.]broad, vs= very strong, s=strong, w=weak, m=medium. [c.] Ref. 27.[d.] Ref. 28.[e.] Ref. 29.

Table 3.2 The observed IR bands of liquid EG with an initial loading pressure of 0.1 GPa and those of photochemical reaction products after UV irradiation (λ = 350 nm, 750 mW) for 22.5 h.

IR frequencies (cm^{-1})	reference				
	methoxy methanol[a]	methyl formate[a]	formaldehyde[b]	methane[c]	carbondioxide[d]
662					671
914	925	910			
1060	1067				
1093	1123				
1116		1158			
1200	1200	1208			
1254			1247		
1303	1303			1303	
1375		1371			
1467			1500		
1731		1728	1746		
2340					2325
2896			2843		
3010				3010	
3599					3604
3705					3708

[a]Ref. 20.   [b.]Ref. 36.   [c.] Refs 39, 40.   [d.] Refs 41, 42
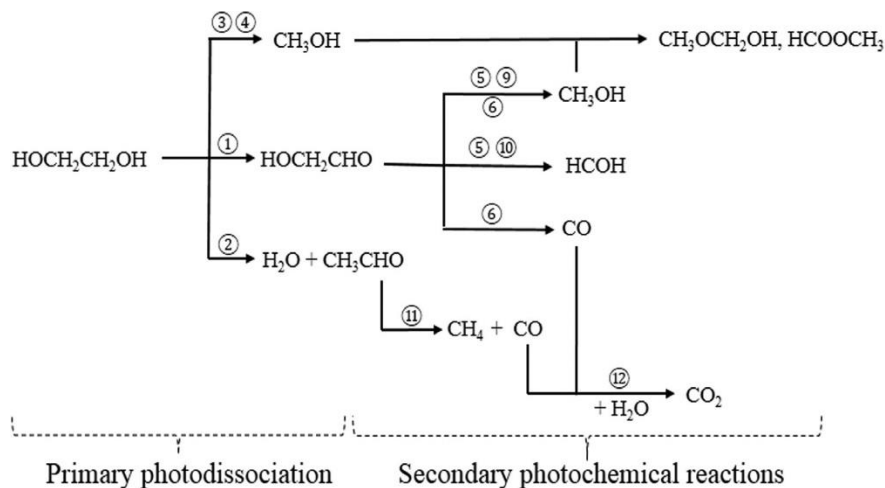
Scheme 3.1: Proposed Photochemical Reactions and Reaction Products upon UV Irradiation on EG. The numbers label the reaction channels discussed in the text.

Photodissociation of GA. The photolysis of GA has been documented both in theoretical calculations and photodissociation experiments using different radiation wavelength. Under the radiation wavelength of 240–400 nm, four possible channels were reported:[32-34]

$$\text{HOCH}_2\text{CHO} + 2h\nu \rightarrow \text{HO}\dot{\text{C}}\text{H}_2 + \text{H}\dot{\text{C}}\text{O} \qquad (3.5)$$

$$\rightarrow \text{CH}_3\text{OH} + \text{CO} \qquad (3.6)$$

$$\rightarrow \text{HO}\dot{\text{C}}\text{HCHO} + \dot{\text{H}} \qquad (3.7)$$

$$\rightarrow \dot{\text{C}}\text{H}_2\text{CHO} + \dot{\text{O}}\text{H} \qquad (3.8)$$
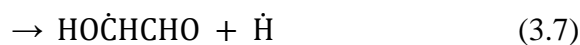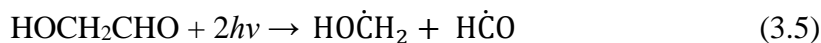
The first channel (reaction 3.5) resulting from the dissociation of the C-C bond was found to be the dominant path with a quantum yield of 65~80%.[32,34] The quantum yield of the second channel (reaction 3.6) was reported to be 15~20%.[33] For the remaining two channels (reactions 3.7 and 3.8), the radical abundance was found to be low.[32] Thus, products from these two channels could be below the detection limit of our IR absorption measurements. Electronic structure calculations of the stationary points and dissociation potential energy surface of GA in the lowest electronic states indicate that with a low

excitation energy of 280–340 nm, the C_α-C bond dissociation facilitated by intersystem crossing from the first excited singlet state (S_1) to first excited triplet state (T_1), was the predominant channel (reaction 3.5). In contrast, the C_α-H bond dissociation leading to reaction 3.7 involving both the S_1 and T_1 states were nearly prohibited due to the relatively high barriers.[35] In addition, the C-C and C-O bond cleavage reactions can occur as a consequence of intersystem crossing via the T_1/S_0 intersection points.

The resulting radical products from the dominant channel 3.5 could subsequently react with $\dot{H}$ from sources discussed above to produce stable species such as methanol and formaldehyde:

$$HO\dot{C}H_2 + \dot{H} \rightarrow CH_3OH \qquad\qquad (3.9)$$

$$H\dot{C}O + \dot{H} \rightarrow H_2CO \qquad\qquad (3.10)$$

Therefore, methanol can be produced from both primary and secondary photochemical processes. Moreover, methanol produced from reaction 3.4, 3.6, and 3.9 could undergo further photochemical reactions under UV irradiation. Investigations on pure methanol have been reported by Fanetti et al. at room temperature between 0.1 and 1.8 GPa,[20] where methoxymethanol and methylformate were identified to be the main products. Our observations of IR bands at 1060, 1200, 914 and 1375 cm^{-1} as shown in Figure 3.3 are indeed consistent with the reported IR frequencies at 1067, 1200 cm^{-1} for methoxymethanol and 910, 1371 cm^{-1} for methylformate, respectively. Noticeably, the lack of IR features associated with methanol observed at 22.5 h suggests that methanol has been completely consumed in the secondary photochemical reactions.
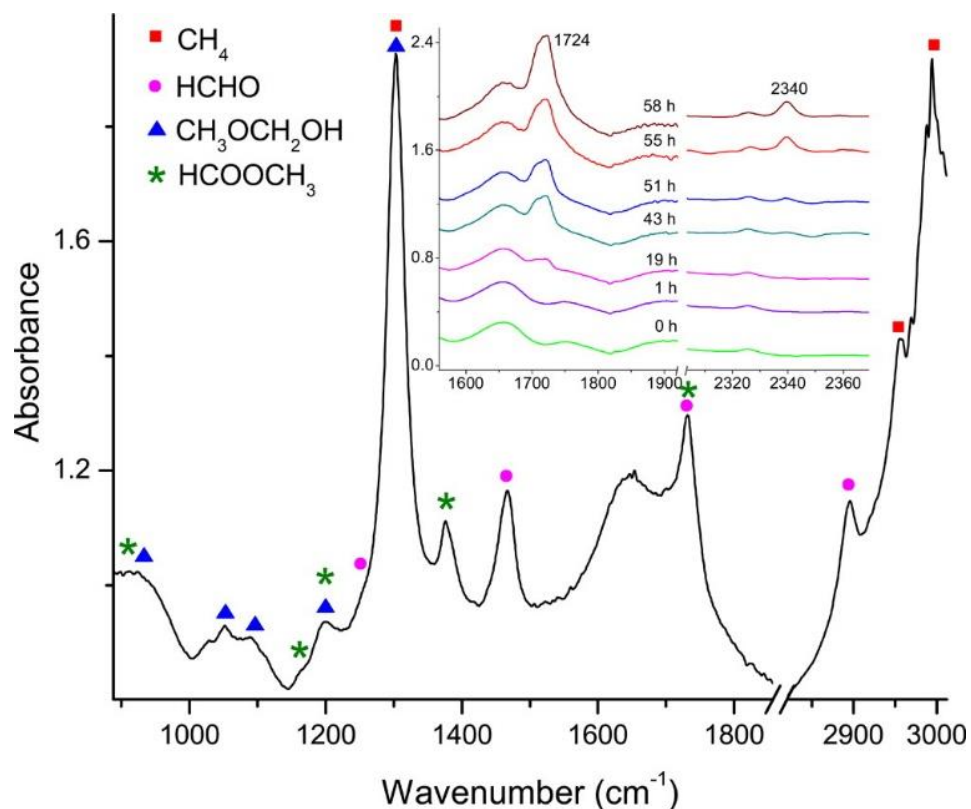
Figure 3.3: FTIR spectrum of EG with an initial loading pressure of 0.1 GPa upon UV irradiation for 22.5 h in the selected spectral region where the secondary photodissociation products of EG can be identified as labeled by different legends. The inset shows selected IR spectra of EG with the same initial loading pressure but irradiated with reduced UV power of ~350 mW collected at different radiation time.

Another possible secondary product, formaldehyde, from reaction 10 can be evidenced by the IR modes observed at 1467, 1731, and 2896 cm^{-1} with medium intensity (see Figure 3.3), consistent with characteristic peaks of formaldehyde reported at 1500, 1746 and 2843 cm^{-1}, respectively.[36] The evidence of production of CO (from reaction 3.6) will be discussed next.

Photodissociation of Acetaldehyde. Previous studies showed that acetaldehyde CH$_3$CHO can be photodissociated by UV radiation at 308 nm.[37,38] A so-called "roaming" mechanism was proposed suggesting that a low-energy pathway involving the methyl and formyl

groups orbiting each other (i.e., CH_3 + HCO), followed by a transfer of a H atom from HCO to CH_3 would result in the formation of CH_4 and CO. This process can be summarized as

$$CH_3CHO \rightarrow CH_4 + CO \tag{3.11}$$

In our experiment, the intense IR absorption bands observed at 1303 and 3010 cm^{-1} as shown in Fig. 3.3 can be assigned as the fundamental IR active modes of CH_4, i.e., the degenerate deformation mode (ν_4) and stretching mode (ν_3), respectively.[39,40] Furthermore, we found the production of CH_4 becomes more prominent with higher initially loading pressure, as evidenced both visually and spectroscopically. For instance, a prominent gas bubble was observed after radiating the sample at 1 GPa for 15 hours as shown in the picture of Figure 3.4. Spatially resolved IR spectra showed distinctively contrasting relative IR intensities between the bubble area and irradiated area. It can be seen that the IR spectrum of the bubble region predominantly consists of two saturated IR absorption peaks at 1303 and 3010 cm^{-1}, unambiguously indicating the production of CH_4 as a major secondary product. Again, the other product CO will be discussed next.
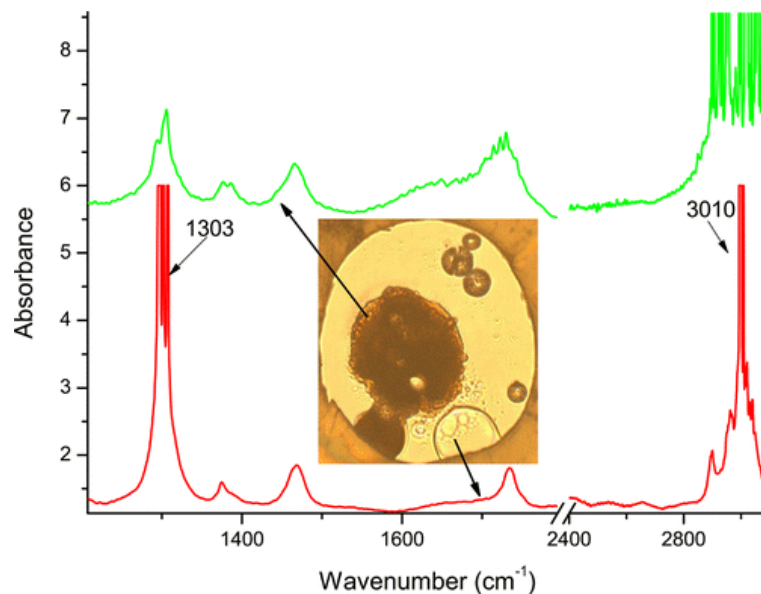
Figure 3.4: Area selected IR spectra of an EG sample with an initial loading pressure of 1.0 GPa after 15 h UV irradiation. The microphotograph was collected under the same conditions. The top and bottom spectra were collected on the dark and bubble areas as labeled, respectively.

Production of Carbon Dioxide. As shown in Figure 3.1, the most distinctive IR bands observed at 22.5h at 662, 2340, 3599, 3705 cm^{-1} strongly suggest the production of CO_2. In particular, the two strong absorption bands at 662 and 2340 cm^{-1} can be attributed to the bending mode (v_2) and asymmetric stretching mode (v_3) of CO_2, respectively. The two high-frequency bands at 3599 and 3705 cm^{-1} can be assigned as the combination modes of $v_3 + 2v_2$ and $v_3 + v_1$, respectively, due to the strong Fermi resonance effect.[41,42] Despite the production channels of 3.6 and 3.11, the expected IR frequency (i.e., ~2140 cm^{-1}) was not observed for CO. Therefore, it is highly likely that CO was consumed instantaneously as a precursor and source for CO_2 via the following reaction.

$$CO + H_2O \rightarrow CO_2 + 2\dot{H} \qquad (3.12)$$

Previous study of photodissociation of water using 350 nm radiation showed that highly reactive OH and H radicals can be produced. Subsequently, hydroxyl radical can undergo dominant reactions such as $H\dot{O} + CO \rightarrow HO\dot{C}O \rightarrow \dot{H} + CO_2$ producing the final products in reaction 3.12.[22]

Given the possible formation mechanism of CO_2 discussed above, CO_2 can be designated as a secondary product instead of primary (i.e., directly produced from EG by photodissociation), thus "contradictory" with the observation of CO_2 production at as early as 3 h together with other primary products (Figure 3.1b). To resolve this conflict, we performed an additional experiment using a reduced UV radiation power (i.e., ~ 350 mW) to slow down the reactions with the results shown in the inset of Figure 3.3. It can be seen that the evolution of the IR band at 1724 cm^{-1} associated with the carbonyl functional group compounds characteristic of primary products (e.g., GA and CH_3CHO) correlates with that at 2340 cm^{-1}, which signifies the production of CO_2, in the sense that appearance of both are substantially delayed by over 40 h due to the reduced radiation power. Furthermore, the production of CO_2 was observed only 24 h later than that of carbonyl containing compounds with dominant abundance over CO_2 at any time. These observations thus strongly suggest that GA and CH_3CHO rather than EG are the major sources of CO that subsequently produce CO_2. Under high radiation power (e.g., ~ 700 mW), GA and CH_3CHO can undergo instantaneous secondary photochemical processes resulting in the observation of CO_2 at as early as 3 h. Under lower radiation power (e.g., ~ 350 mW), however, secondary channels such as 3.6 and 3.11 could be less competitive than the primary channels 3.1 and 3.2 due to smaller TP absorption cross section of GA and CH_3CHO in the UV region [e.g., in the order of EG (198 nm)[26] > GA (277 nm)[34] > CH_3CHO (290 nm)[43]]. As a result, the observation of CO_2 is delayed due to delayed production of GA and CH_3CHO as well as their lower reaction cross-sections.

3.3.3 Pressure-induced CO_2 sequestration

We systematically investigated the photon-induced production of CO_2 from EG at different loading pressures. The IR spectra in the region of the antisymmetric v_3 mode as a function of radiation time are depicted in Figures 3.5 (panels a-d) corresponding to an initial loading pressure of 0.1, 0.5, 1.0, and 1.5 GPa, respectively. The evolution of the asymmetric stretching mode v_3 of CO_2 under pressure shows highly complex IR absorption characteristics with increasing radiation time where both the amplitude of the absorbance and IR frequencies exhibit prominent changes. For instance, the v_3 mode appears singlet at around 2340 cm^{-1} after 11 h irradiation at 0.1 GPa indicating the formation of CO_2 mainly as fluid, but is substantially intensified and split into doublets at 2337 and 2345 cm^{-1} (with saturated intensity) at 13.5 h. Further radiation results in the formation of three peaks at 2337, 2343 and 2351 cm^{-1} at 14.5 h, which become more intensified at 2337, 2348 and 2357 cm^{-1} after 19 h. These spectral evolutions of the antisymmetric mode of CO_2 strongly suggest the formation of distinctive structures of CO_2 under high pressures. The observed IR frequencies of all components of the antisymmetric mode of CO_2 are provided in Table S2 of the supporting information.

The fact that CO_2 can form complexes with water in the form of clathrate hydrates has been very well-established.[23,44] The most commonly observed clathrate hydrate structures include type-I (space group Pm$\bar{3}$n) and type II (space group Fd$\bar{3}$m), each containing 2 small cages (5^{12}), and 6 large cages ($5^{12}6^2$), and 16 small cages (5^{12}) and 8 large cages ($5^{12}6^4$), respectively.[23] Previous high-pressure studies on the mixture of CO_2 with water suggest that hydrate with the type-I structure can be produced,[45,46] where the CO_2 molecules were found to fully occupy the large cages, whereas the occupancy in the small cages increases with pressure up to 100% above 20 MPa.[46] In our work, the frequencies of the first two prominent IR bands (i.e., 2337 and 2349 cm^{-1}) observed at 19 h (Figure 3.5a) can be attributed to the CO_2 occupying the large and small cages, respectively, consistent

with those reported in the type-I structure of CO_2 clathrate hydrate.[47,48] In addition, their intensity ratio of 3:1, which agrees with that predicted for this structure, further confirms the formation of type-I CO_2 clathrate hydrate.[49] The formation of type II CO_2 clathrate hydrate has also been documented previously.[47,48] For instance, CO_2 was found to be capable of stabilizing the type II clathrate hydrate structure through interactions within the small cages with only one characteristic IR band observed at 2349 cm^{-1}.[47] Furthermore, Kumar et al. reported that CO_2 only occupies the small cages in the type II hydrate structure.[48] Considering the pressure-induced blue shift (see Table S2 of the supporting information), in our case, the expected IR band at 2349 cm^{-1} associated with the small cages of type II structure can be extrapolated to lower pressures for 14.5 and 13.5 h corresponding to 2343 and 2337 cm^{-1}, respectively. Therefore, the IR profile at 13.5 h with a shoulder peak at 2337 cm^{-1} can be interpreted by the formation of type II as the only clathrate hydrate structure. This peak at 14.5 h was observed at 2343 cm^{-1}, with an intensity ratio of ~ 1:2 with respect to the proceeding peak at 2337 cm^{-1}, indicating the clathrate hydrate produced here is a mixture of type I and II clathrate structures rather than pure type I (with a corresponding expected intensity ratio of 1:3). The coexistence of the two structure types has been previously reported for CO_2 clathrates contained in natural quartz samples.[50] Starting from 13.5 h, the intense and saturated IR band with the highest frequency labeled with solid circles in Figure 3.5a can be assigned as CO_2 clusters, consistent with the assignment by Barnes and co-workers.[51,52] The rapid blue shift of this mode likely indicates the growth of the cluster size[53] while the increasing and dominant intensity suggest that CO_2 clusters are the most abundant among all observed CO_2 structures under this condition.
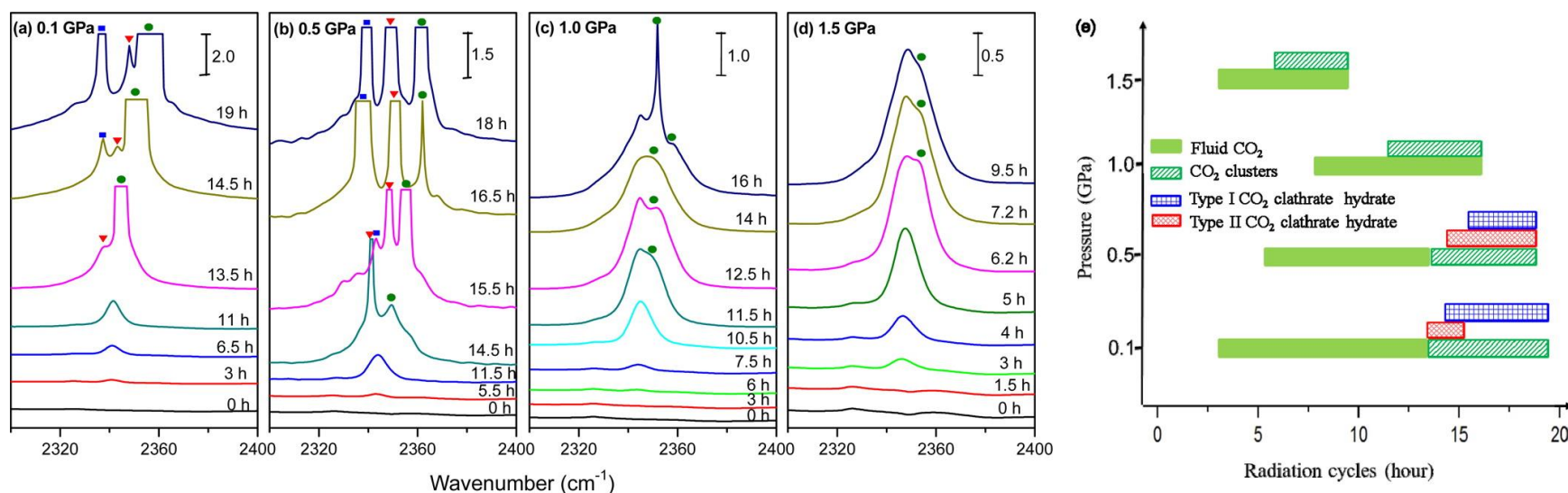
Figure 3.5: IR absorption spectra in the spectral region of the antisymmetry mode of CO₂ as a function of radiation time for EG samples loaded at (a) 0.1 GPa, (b) 0.5 GPa, (c) 1.0 GPa, and (d) 1.5 GPa and (e) CO₂ structural evolution diagram upon UV irradiation of EG samples loaded at these four pressures. The IR modes associated with different CO₂ structures other than fluid form are labeled: CO₂ clusters (green ●), CO₂ in small cages of types I or II clathrate hydrate (red ▼) and CO₂ in large cage of type I clathrate hydrate (blue ■) (see the text).

At 0.5 GPa, the asymmetric stretching mode of fluid CO_2 was observed at 2344 cm^{-1} upon UV irradiation for 11.5 h (Figure 3.5b). This mode splits into a doublet (i.e., at 2341 and 2349 cm^{-1}) at 14.5 h, indicating the formation of type II clathrate hydrate and CO_2 clusters based on the analysis above. Similarly, the IR bands at 2343, 2349, 2355 cm^{-1} observed at 15.5 h can be assigned to the characteristic peaks associated with CO_2 in large cages (type I only), small cages (both type I and II) and CO_2 cluster, respectively. Furthermore, the change in both band intensity and bandwidth from 15.5 to 16.5 h suggests substantially larger amounts of clathrate structures of both type I and II have been produced in this time interval. Further irradiation with UV photons then results in the preferential production of CO_2 clusters, such that all CO_2 structures coexist over a large time window (e.g., at 18 h).

Finally, at initial loading pressures of 1.0 and 1.5 GPa, a less complex spectral profile was observed (Figures 3.5c and 3.5d). The shoulder peak at 2349 cm^{-1} at 11.5h (Figure 3.5c) and 2352 cm^{-1} at 12.5 h (Figure 3.5d) can be attributed to CO_2 clusters. Again, the intensity of this mode increases with radiation time, indicating the sustained production of CO_2 clusters. However, the less prominent blue shift of this mode over time as compared to that observed at 0.1 GPa suggests limited growth of the cluster size and that the CO_2 clusters produced under this pressure are smaller than those produced of 0.1 and 0.5 GPa in general. Interestingly, the IR profile at 16 h for EG loaded at 1.0 GPa exhibits a distinctive intensity distribution with an intense central peak (2352 cm^{-1}) followed by a high-frequency shoulder (2358 cm^{-1}) indicating the preferential formation of CO_2 structures in two particular sizes with the smaller clusters being dominant. Overall, the CO_2 structures from photodissociation of EG at initial loading pressures at 1.0 and 1.5 GPa are mainly fluid and clusters without the observation of clathrates of any kind as observed at lower pressures. The observed CO_2 structures formed at different loading pressures with time are summarized in Figure 3.5e schematically. Evidently, pressure can substantially

influence the reactivity, stabilities of certain structures as well as the reaction kinetics, which will be discussed in detail next.

3.3.4 Reactivity and kinetics of the competitive channels

The above observations clearly suggest that pressure played a regulating role for the formation of specific products. Here we attempt to investigate the pressure dependence in more depth. The approximate relative reaction yields of CH_4 and CO_2 at different loading pressures are evaluated as a function of radiation time by integrating the IR intensity of the characteristic vibrational modes of CH_4 (i.e., v_4) and CO_2 (i.e., v_3), respectively, as plotted in Figure 3.6. The final pressures 0.95, 1.65, 1.86, and 2.70 GPa were measured at the end of irradiation labeled in the figure corresponding to the initial loading pressure 0.1, 0.5, 1.0, and 2.0 GPa, respectively. For CH_4, it is evident that higher loading pressure favors faster kinetics as indicated by the earlier production onset of CH_4. However, no substantially different reaction yield (i.e., all ~ 40-50 with arbitrary unit) for CH_4 produced under different system pressures was observed. In contrast, no preferential pressure effect was observed for the production kinetics for CO_2, where the onset for massive production at ~10 h for EG with all initial loading pressures is evident. However, the reaction yield of CO_2 appears to be monotonically influenced by the system pressure with higher pressure giving lower yield. For instance, the amount of CO_2 produced at initial loading pressure of 2.0 GPa (and final pressure of 2.7 GPa) is estimated to be 85% less than produced at a loading pressure of 0.1 GPa, a substantially reduced reaction yield.
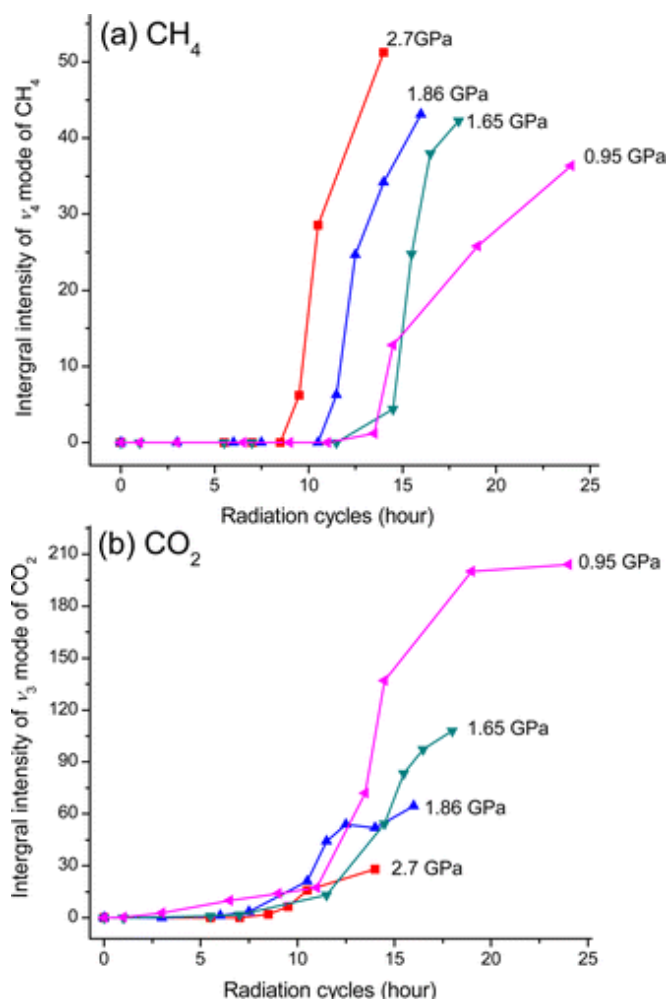
Figure 3.6: Relative photochemical reaction yields of (a) CH₄ and (b) CO₂ estimated by integrating the IR absorbance of the respective characteristic IR modes (v₄ of CH4 and v₃ of CO₂) as a function of radiation time for EG samples with an initial loading pressure of 0.1 (pink ◄), 0.5 (green ▼), 1.0 (blue ▲), and 2.0 (red ▪) GPa. The pressures labeled for each sample denote the final pressure of the system.

To understand such interesting and contrasting pressure effects on different products, the reaction details, especially those involving competitive reaction channels, need to be examined in more depth. Such information may be inferred by monitoring the system pressure as a function of radiation time as shown in Figure 3.7. The system pressure during the photon-induced reactions of EG at different radiation cycles clearly shows two

significant increasing steps at loading pressures 0.1, 0.5, 1.0 and 2 GPa, whereas only one step was observed for the loading pressure of 3.4 GPa. The first step is evident immediately upon the irradiation of EG while the second onset of pressure elevation was observed at 13.2, 12.6, 10.4 and 7.7 h for initial loading pressure of 0.1, 0.5, 1.0, and 2.0 GPa respectively. The general trend of increasing system pressure along the progression of photon-induced reactions suggests the increase in molar density of the materials given the constant reaction volume defined by the gasket sample chamber, consistent with the dissociative nature of the photochemistry of EG.

Among all the primary and secondary photochemical products of EG, we believe the low-density species such as CH_4, CO_2 or CO are likely the major contributors to the elevation of system pressure, especially during the two prominent steps in Figure 3.7. In particular, the fact that the onset time of the 2nd step in Figure 3.7 coincides with the appearance time of CH_4 at each of the four different loading pressures (Figure 3.6a) strongly suggests that CH_4 produced via reaction 3.11 makes a major contribution to the second step of the pressure elevation. This interpretation is also consistent with the timeframe in which CH_4 was produced as secondary products.
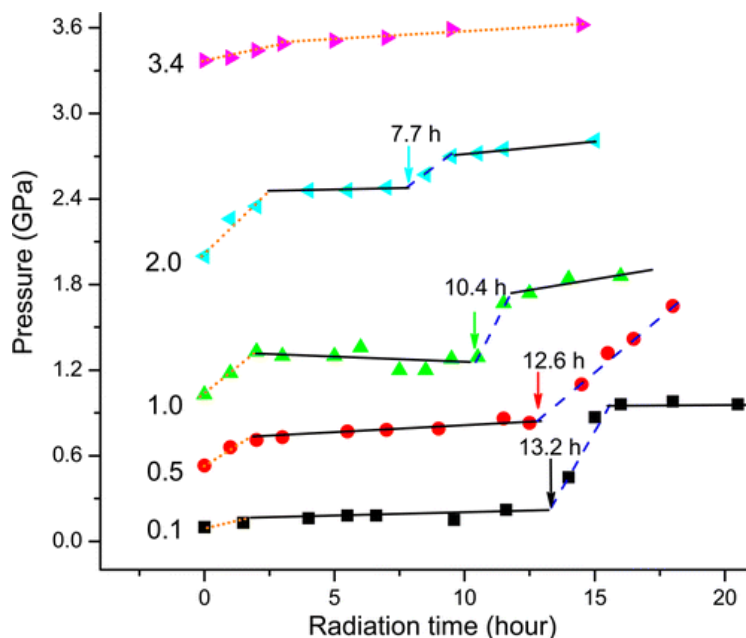
Figure 3.7: Pressure variations caused by the photoinduced reactions of EG as a function of radiation time for samples initially loaded at 0.1, 0.5, 1.0, 2.0, and 3.4 GPa as labeled. All samples except those loaded at 3.4 GPa show two regions of prominent increase in pressure. The first region (dotted line) and second region (dashed line) of pressure increase are mainly associated with the production of CO and CH_4, respectively (see the text). The onset times for the second region are labeled.

Correspondingly, CO_2 or CO or both may contribute to the first step. However, we notice that the time for the first steps in Figure 3.7 is generally earlier than the appearance time of CO_2 indicated in Figure 3.6b, which suggests that the first step is most likely associated with CO. Close examination of reaction channels (e.g., 3.6, 3.11, and 3.12) involving the CO_2 and CO may help to understand this observation. These reactions maybe understood in a way that channel 3.6, and 3.11 are competitive channels for CO production whereas channel 3.12 is promotional for CO by consumption. Given the fact that the formation of CO from reaction 11 is also accompanied by the production of CH_4, a channel that is believed to be open only later contributing to the second step as discussed above, we can infer that the CO produced from reaction 6 predominantly contributes to the first

step, which is consistent with the larger TP absorption cross section of GA. Subsequent CO consumption by reaction 3.12 in the presence of water produced from reaction 3.2 thus leads to the formation of CO_2. Due to the similar density of CO_2 to CO under the reaction conditions, reaction 3.12 is thus not expected to influence system pressure substantially, consistent with the plateau region observed between the two steps. At the second step, the dissociation channel 3.11 opens up thus producing additional CO together with CH_4. This additional CO source can thus convincingly help to interpret the massive production of CO_2 via reaction 3.12 observed after 10 h (Figure 3.6b).

Finally, the absence of the second step in the pressure profile for EG initially loaded at 3.4 GPa shown in Figure 3.7 implies that channel 3.11 has been closed at high pressures. As a result, CH_4 ceased to be produced as evidenced by the lack of v_4 and v_3 modes expected at 1303 and 3010 cm^{-1} (Figure S5). Similarly, all other primary and secondary channels are substantially suppressed. For instance, the disappearance significantly depleted CO_2 characteristic peak at 2340 cm^{-1} (Figure S5) further indicates the essential channels for CO_2 production such as channel 2 have been closed at this pressure.

3.3.5 Implications of combined photon-pressure tunability of reactions

Although both are secondary photodissociation products, CH_4 and CO_2 clearly demonstrated strongly contrasting pressure dependence in terms of productivity and kinetics under UV radiation. In particular, our analysis above shows that the high pressure can effectively accelerate the reactions 3.2, and 3.11 that are essential to produce CH_4 at initial loading pressures up to 2.0 GPa, but can inhibit these reactions when the pressure is above ~ 2 GPa and substantially shut down these channels at 3.4 GPa. The acceleration of dissociation reactions of EG under specific conditions was also predicted in the theoretical calculations of EG unimolecular decomposition.[31] In particular, the temperature-dependent rate constant calculations in the temperature range of 500-2000 K have shown that the H_2O elimination reaction by surmounting potential energy barriers was predominant at lower

temperatures. Given that high pressure and low temperature often exert similar effects on materials with common phase diagram, we speculate that the H_2O elimination reaction 3.2 would be a kinetically favorable path with increasing pressure in the range up to 1.5 GPa. Very high system pressures (e.g., 3.4 GPa), although still kinetically driving the reactions forward, will necessarily suppress most reaction channels thermodynamically that are dissociative in nature. Therefore, reactions requiring a high mobility of the reacting units can be completely prohibited.[1]

Finally, the pressure-dependent photochemical reactivity of EG provides important implications in the production of useful species with great tunability and controllability. For instance, the production of CH_4 as a fuel molecule produced photochemically from EG could be developed as a new application of EG that has already been widely used in industry. By carefully selecting the favorable pressure, temperature as well as the radiation energy, the reaction channels producing CH_4 may be tuned and optimized to selectively generate the desired product. Furthermore, the observation of CO_2 in the form of clathrate hydrates under specific pressure range may provide a solution to sequestrate and store CO_2 as an undesirable intermediate or product.

3.4 Conclusions

In summary, high-pressure photochemistry of liquid ethylene glycol was investigated at room temperature using multi-line UV radiation at ~350 nm and monitored by FTIR spectroscopy. Representative IR spectra of EG show two sets of profiles after specific reaction times suggesting multiple photon-induced chemical reactions designated as primary and secondary processes. Spectral analysis results in the identification of glycolaldehyde, acetaldehyde and methanol as the primary products. Subsequent photoreactions of these primary products gave rise to secondary products including methane, formaldehyde, methoxymethanol, methylformate, and carbon dioxide. The possible reaction mechanisms and production pathways of these products were proposed.

We further found that initial loading pressure of EG not only can substantially influence the reaction kinetics, but controls the accessibilities for some reaction channels such as for CH_4. Quantitative analysis of the antisymmetric stretching mode of CO_2 formed at different loading pressures suggests the formation of CO_2 clathrate hydrates as well as CO_2 clusters. The stabilities as well as relative abundance of these CO_2 species are found to be dependent on both pressure and radiation time. These observations revealed interesting pressure-induced CO_2 sequestration behaviors as a result of photochemical reactions of ethylene glycol.

3.5   References

(1)   Hemley, R. J. *Annual Review of Physical Chemistry* **2000**, *51*, 763.
(2)   Schettino, V.; Bini, R. *Chemical Society Reviews* **2007**, *36*, 869.
(3)   Eremets, M. I.; Gavriliuk, A. G.; Trojan, I. A.; Dzivenko, D. A.; Boehler, R. *Nature Materials* **2004**, *3*, 558.
(4)   Schettino, V.; Bini, R. *Physical Chemistry Chemical Physics* **2003**, *5*, 1951.
(5)   Murli, C.; Lu, N.; Dong, Z.; Song, Y. *Journal of Physical Chemistry B* **2012**, *116*, 12574.
(6)   Dong, Z.; Seemann, N. M.; Lu, N.; Song, Y. *Journal of Physical Chemistry B* **2011**, *115*, 14912.
(7)   Murli, C.; Song, Y. *Journal of Physical Chemistry B* **2010**, *114*, 9744.
(8)   Dong, Z.; Beilby, N. G.; Huang, Y.; Song, Y. *Journal of Chemical Physics* **2008**, *128*.
(9)   Sabharwal, R. J.; Huang, Y.; Song, Y. *Journal of Physical Chemistry B* **2007**, *111*, 7267.
(10)   Ceppatelli, M.; Santoro, M.; Bini, R.; Schettino, V. *Journal of Chemical Physics* **2000**, *113*, 5991.
(11)   Citroni, M.; Ceppatelli, M.; Bini, R.; Schettino, V. *Science* **2002**, *295*, 2058.
(12)   Ciabini, L.; Santoro, M.; Bini, R.; Schettino, V. *Physical Review Letters* **2002**, *88*.
(13)   Santoro, M.; Ceppatelli, M.; Bini, R.; Schettino, V. *Journal of Chemical Physics* **2003**, *118*, 8321.
(14)   Bini, R. *Accounts of Chemical Research* **2004**, *37*, 95.
(15)   Citroni, M.; Fanetti, S.; Bini, R. *Journal of Physical Chemistry C* **2014**, *118*, 10284.
(16)   Ceppatelli, M.; Bini, R. *Macromolecular Rapid Communications* **2014**, *35*, 787.
(17)   Rademacher, N.; Bayarjargal, L.; Morgenroth, W.; Winkler, B.; Ciezak-Jenkins, J.; Batyrev, I. G.; Milman, V. *Chemistry-a European Journal* **2014**, *20*, 11531.

(18)   Nikogosyan, D. N.; Oraevsky, A. A.; Rupasov, V. I. *Chemical Physics* **1983**, *77*, 131.

(19)   Ceppatelli, M.; Fanetti, S.; Citroni, M.; Bini, R. *Journal of Physical Chemistry B* **2010**, *114*, 15437.

(20)   Fanetti, S.; Ceppatelli, M.; Citroni, M.; Bini, R. *Journal of Physical Chemistry C* **2012**, *116*, 2108.

(21)   Ceppatelli, M.; Bini, R.; Schettino, V. *Proceedings of the National Academy of Sciences of the United States of America* **2009**, *106*, 11454.

(22)   Ceppatelli, M.; Bini, R.; Schettino, V. *Journal of Physical Chemistry B* **2009**, *113*, 14640.

(23)   Ceppatelli, M.; Bini, R.; Schettino, V. *Physical Chemistry Chemical Physics* **2011**, *13*, 1264.

(24)   Ceppatelli, M.; Bini, R.; Caporali, M.; Peruzzini, M. *Angewandte Chemie-International Edition* **2013**, *52*, 2313.

(25)   Dong, Z.; Song, Y. *Journal of Physical Chemistry C* **2010**, *114*, 1782.

(26)   Xu, H.; Zhu, T.; Yu, R.-p. *Spectroscopy and Spectral Analysis* **2007**, *27*, 1381.

(27)   Hudson, R. L.; Moore, M. H.; Cook, A. M. In *Space Life Sciences: Astrobiology: Steps toward Origin of Life and Titan before Cassini*; Bernstein, M., NavarroGonzalez, R., Raulin, R., Eds., 2005; Vol. 36; pp 184.

(28)   Evans, J. C.; Bernstein, H. J. *Canadian Journal of Chemistry-Revue Canadienne De Chimie* **1956**, *34*, 1083.

(29)   Falk, M.; Whalley, E. *Journal of Chemical Physics* **1961**, *34*, 1554.

(30)   Vanderli.Hj; Sonntag, C. V. *Photochemistry and Photobiology* **1971**, *13*, 147.

(31)   Ye, L.; Zhao, L.; Zhang, L.; Qi, F. *Journal of Physical Chemistry A* **2012**, *116*, 55.

(32)   Zhu, C.; Zhu, L. *The Journal of Physical Chemistry A* **2010**, *114*, 8384.

(33)   Magneron, I.; Mellouki, A.; Le Bras, G.; Moortgat, G.; Horowitz, A.; Wirtz, K. *The Journal of Physical Chemistry A* **2005**, *109*, 4552.

(34)   Bacher, C.; Tyndall, G. S.; Orlando, J. J. *Journal of Atmospheric Chemistry* **2001**, *39*, 171.

(35)   Cui, G.; Fang, W. *Chemphyschem* **2011**, *12*, 1351.

(36)   Blau, H. H.; Nielsen, H. H. *Journal of Molecular Spectroscopy* **1957**, *1*, 124.

(37)   Houston, P. L.; Kable, S. H. *Proceedings of the National Academy of Sciences of the United States of America* **2006**, *103*, 16079.

(38)   Heazlewood, B. R.; Jordan, M. J. T.; Kable, S. H.; Selby, T. M.; Osborn, D. L.; Shepler, B. C.; Braams, B. J.; Bowman, J. M. *Proceedings of the National Academy of Sciences of the United States of America* **2008**, *105*, 12719.

(39)   Momose, T.; Miki, M.; Wakabayashi, T.; Shida, T.; Chan, M. C.; Lee, S. S.; Oka, T. *Journal of Chemical Physics* **1997**, *107*, 7707.

(40)   Nelander, B. *Journal of Chemical Physics* **1985**, *82*, 5340.

(41)   Hanson, R. C.; Jones, L. H. *Journal of Chemical Physics* **1981**, *75*, 1102.

(42)   Giordano, V. M.; Gorelli, F. A.; Bini, R. *Low Temperature Physics* **2006**, *32*, 1067.

(43)   Hallquist, M.; Wangberg, I.; Ljungstrom, E. *Environmental Science & Technology* **1997**, *31*, 3166.

(44)   Sloan, E. D. *Nature* **2003**, *426*, 353.

(45)   Udachin, K. A.; Ratcliffe, C. I.; Ripmeester, J. A. *Journal of Physical Chemistry B* **2001**, *105*, 4200.

(46)   Circone, S.; Stern, L. A.; Kirby, S. H.; Durham, W. B.; Chakoumakos, B. C.; Rawn, C. J.; Rondinone, A. J.; Ishii, Y. *Journal of Physical Chemistry B* **2003**, *107*, 5529.

(47)   Fleyfel, F.; Devlin, J. P. *Journal of Physical Chemistry* **1991**, *95*, 3811.

(48)   Kumar, R.; Lang, S.; Englezos, P.; Ripmeester, J. *Journal of Physical Chemistry A* **2009**, *113*, 6308.

(49)   Manakov, A. Y.; Dyadin, Y. A.; Ogienko, A. G.; Kurnosov, A. V.; Aladko, E. Y.; Larionov, E. G.; Zhurko, F. V.; Voronin, V. I.; Berger, I. F.; Goryainov, S. V.; Lihacheva, A. Y.; Ancharov, A. I. *Journal of Physical Chemistry B* **2009**, *113*, 7257.

(50)   Prasad, P. S. R.; Prasad, K. S.; Thakur, N. K. *Current Science* **2006**, *90*, 1544.

(51)   Barnes, J. A.; Gough, T. E. *Journal of Chemical Physics* **1987**, *86*, 6012.

(52)   Cardini, G.; Schettino, V.; Klein, M. L. *Journal of Chemical Physics* **1989**, *90*, 4441.

(53)   Oliaee, J. N.; Dehghany, M.; McKellar, A. R. W.; Moazzen-Ahmadi, N. *Journal of Chemical Physics* **2011**, *135*.

Chapter 4

4 Pressure Selected Reactivity between 2-Butyne and Water Induced by Two-Photon Excitation*

4.1 Introduction

Application of external pressure on molecular systems can effectively shorten the intermolecular and intramolecular distances, subsequently causing reversible or irreversible transformations in the molecular structures and associated electronic, optical, or mechanical properties.[1,2] Therefore, pressure becomes one of the most effective tools to produce new materials even starting from simple molecular solids, especially those with unsaturated bonds or conjugate ring structures.[2,3] For example, pressure-induced transformations have been reported for acetylene,[4] cyanogen,[5] butadiene,[6] benzene,[7] and others.[2] These transformations, however, require pressures ranging from several to dozens of gigapascals (GPa). As a result, the application of these reactions to produce useful materials is strongly limited by the high pressures required and thus is difficult for large-scale production. Recently, the electronic excitation by laser photons has been demonstrated to be a very efficient way in reducing the threshold pressure for polymerization and other reactions.[8] Moreover, an enhanced selectivity and (or) the access to new reaction paths might be also achieved.[9,10] Thus, the combination of high pressure and electronic excitation provides attractive alternative routes to synthesize novel materials.

Selective electronic excitation of a reactant molecule can initiate a reaction not just by bringing the molecule to the necessary activation energy level, but also by changing the molecular symmetries and electronic configurations, opening otherwise inaccessible reaction paths. The excited molecule can have a reduced bond order that determines bond strengths and molecular reactivity, lowered rotational or torsional barriers, an increase in polarity, and even spontaneous dissociation and ionization characters.[11] The electronically excited molecules can be particularly aggressive from a chemical point of view and, depending on their lifetime and free mean path, can trigger and propagate a reaction to a different extent under different physical conditions. Therefore, high pressure may efficiently promote photoreactions because the increasing density of the materials results in reduced intermolecular distances that favor the interaction between electronic excited state and ground state molecules. The efficiency of these processes has been studied in pure condensed unsaturated hydrocarbon systems using near-UV excitations from continuous or pulsed wave laser sources.[9,10,12-15]

Among unsaturated hydrocarbons with triple bonds, for example, polymerization of acetylene as the simplest model system has been studied by applying high pressure and (or) laser-assisted high-pressure methods.[4,16,17] High-pressure reactivity of 2-butyne as a substituted acetylene, in contrast, is much less understood. Upon compression, Baonza *et al*. reported two phase transitions at 0.2 and 0.9 GPa deduced from the pressure evolution of Raman spectra of 2-butyne.[18] Above 2.6 GPa, the rotation hindrance of the methyl groups along the molecular axis was indicated, and no polymerization of 2-butyne was observed up to 4 GPa, indicating that much higher pressure is required for polymeric transformations. Polyacetylene and poly(2-butyne) as conductive polymers have a very attractive electrical conductivity induced by the conjugated bonds. For instance, combination of doping and photoexcitation of polyacetylene led to substantially enhanced electrical conductivity comparable with that of amorphous carbon.[19] Therefore,

understanding the high-pressure reactivity of 2-butyne is of great interest in producing useful materials.

Photochemical reactivities of alkynes have been investigated in mono- or di-substituted acetylenes in which the substituents are alkyl, aryl, or alkoxycarbonyl.[20] Many simple alkynes are reported to undergo efficient hemolytic bond cleavage on (vacuum) ultraviolet irradiation in the vapor phase. For instance, the cleavage of 2-butyne at shorter wavelengths gave rise to a diyne (eq. 4.1).[20]

$$CH_3C \equiv CCH_3 \xrightarrow{h\nu} CH_3C \equiv CH_2CH_2C \equiv CCH_3 + CH_3CH = CHCH_3 \quad (4.1)$$
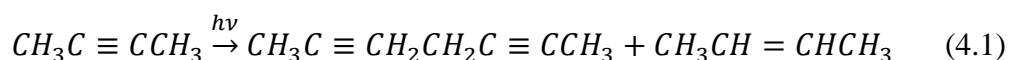
Unlike the wealth of photochemistry reported for alkenes, alkynes have a greater tendency to undergo photopolymerization than any other reactions upon irradiation, particularly in solution phase. Thus, applying pressure to liquid 2-butyne could even further favor the photopolymerization of the sample. Given the very high projected pressure required for the polymerization of 2-butyne, in particular, laser activation might lower the pressure threshold for polymerization and other reactions. In this work, we apply near-UV radiation on condensed 2-butyne at high pressures and monitor the photoreactions by FTIR spectroscopy. We found that 2-butyne is highly reactive when mixed with even a small amount of H_2O to produce distinctive products selectively at different pressures, although the polymerization is still not favored under the combined pressure-photon conditions. The observed reactions and products demonstrate the feasibility and efficiency of a pure physical route to synthesis the relevant materials with great selectivity and controllability.

4.2   Experimental section

2-Butyne (purity ≥98%) was purchased from Alfa Aesar and used as obtained. A symmetric diamond anvil cell (DAC) equipped with a pair of type II diamonds with a culet size of 600 μm was used to generate the high static pressure. Briefly, a ruby ball was firstly

loaded into a hole with a diameter of 250 μm drilled on a stainless steel gasket that was pre-indented to a thickness of 30-50 μm. Then 2-butyne was cryogenically loaded into the DAC which was pre-cooled with dry ice due to the high volatility of 2-butyne at room temperature (i.e., boiling point: 27 ˚C). During this loading process, a small amount of water condensed from the surrounding air was loaded as well. The pressure was determined using the well-established ruby fluorescence method. Excellent system hydrostaticity was observed due to the liquid state of the sample and relatively low-pressure range (i.e., < 1 GPa). The loaded samples were compressed to different initial pressures of 0.04, 0.14, 0.27, 0.52, and 0.9 GPa for different runs all at room temperature. The relative ratios of 2-butyne and H_2O in the DAC for each loading were estimated from the IR spectra (see Fig. 4.1a). Specifically, the relative amount of 2-butyne and H_2O are estimated by integrating the IR band $2v_3$ of 2-butyne and OH stretching mode of H_2O, respectively. The relative intensities of the $2v_3$ band of 2-butyne for each loading pressure are normalized to 100%, and the maximum water content loaded at 0.52 GPa is arbitrarily set with 1:1 ratio with 2-butyne as the reference level to allow the estimate of relative amount of water loaded at other pressures. No reactivity for 2-butyne and H_2O mixture under high pressure at ambient temperature was found, which was evidenced by the invariant IR spectra collected from a fresh loading sample to up to 240 h aged under 0.5 GPa.

For each loaded sample under high pressure, reactions were triggered by focusing the multiline UV emission with a peak wavelength of ∼350 nm from an argon ion laser onto the sample with a beam size of ∼60 μm in diameter and a power of 250 mW. The reaction progress was monitored by IR spectroscopy, with the IR absorption spectra collected at a 5-10 min interval. The reactions were determined complete when no further spectral changes were observed (see Results and Discussion). For IR absorption measurements, a customized IR micro-spectroscopy system that consists of a Fourier transform IR (FTIR) spectrometer from Bruker Optics (model Vertex 80v) equipped with a Globar mid-IR light source was used. The detailed instrumentations have been described elsewhere.[21] The

system was operated under a vacuum of <5 mbar, such that the absorption by H_2O and CO_2 was efficiently removed. The reference spectrum (i.e., the absorption of diamond anvils that was collected before samples were loaded) was divided as the background from each measurement. The spectral resolution used was 4 cm^{-1}.
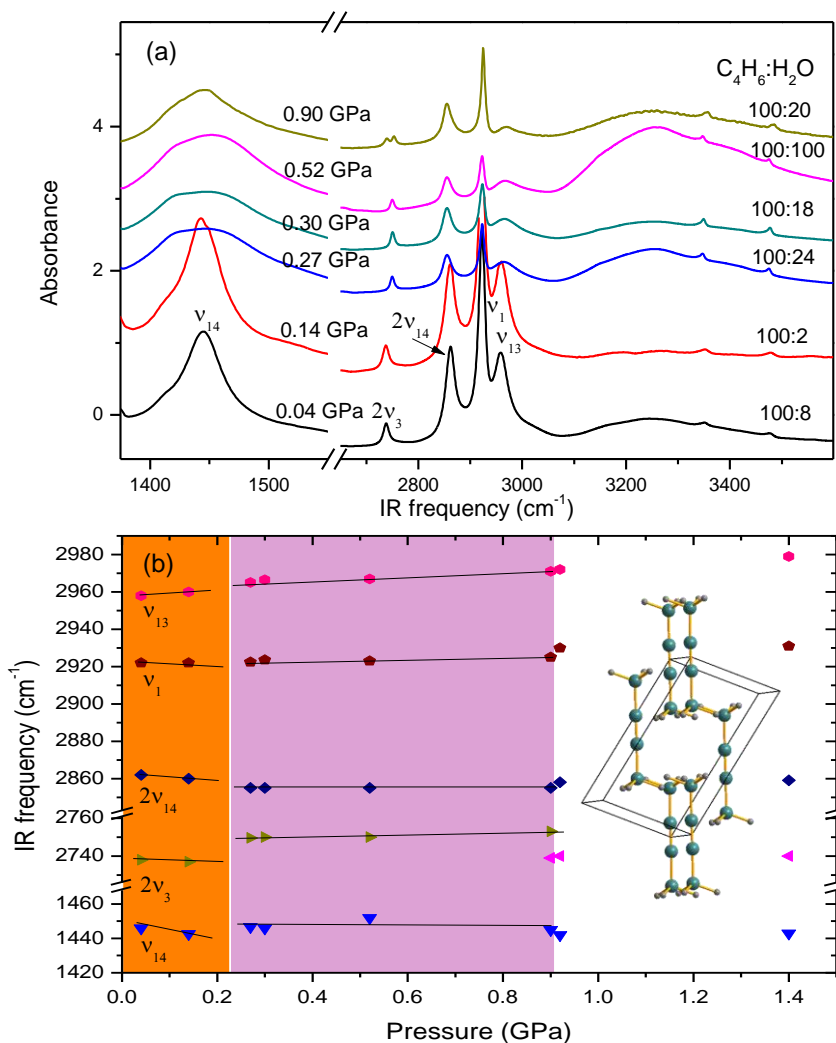
Figure 4.1: (a) Selected IR spectra of 2-butyne mixed with small amount of water collected at room temperature on compression. (b) Pressure dependence of IR band shifts of 2-butyne mixed with small amount of water (the inset shows the crystal structure of 2-butyne in phase II).

4.3 Results and Discussion

4.3.1 Pressure-induced phase transitions of 2-butyne below 1.4 GPa

As a starting point, we performed multiple loadings of 2-butyne samples with different initial pressures and collected the IR absorption spectra as reference (shown in Fig. 4.1a) prior to the irradiation with UV laser. IR absorption bands of 2-butyne and their assignments at the lowest initial pressure of 0.04 GPa are listed in Table 4.1, and are consistent with the previous report using Raman spectroscopy.[18] Analysis indicates that for all samples, a trace amount of water from the moisture of atmosphere was condensed and inevitably trapped in the sample chamber during the cryogenic loading, as indicated by the broad OH IR absorption band around 3300 cm^{-1}. Quantitative analysis of the IR intensity allows an estimate of water content, as indicated in Fig 4.1a. Pressure-induced phase transitions of 2-butyne leading to the changes in intermolecular distances and orientations of molecules in different phases has been reported previously.[18] Therefore, frequency shifts of characteristic IR modes of 2-butyne upon compression are plotted in Fig. 4.1b to examine the possible pressure-induced phase transitions. Pressure dependence of IR modes at 1440 (v_{14}), 2740 ($2v_3$), 2860 ($2v_{14}$), 2920 (v_1) and 2960 (v_{13}) cm^{-1} clearly show two phase transition boundaries. The first boundary at around 0.25 GPa suggests a phase transition from liquid to solid phase I, which is consistent with the transition observed at 0.2 GPa in a previous Raman study of pure 2-butyne upon compression.[18] Moreover, the full width at half maximum (FWHM) of IR band v_{14} becomes much larger at 0.27, 0.30, and 0.52 GPa (i.e., ~107 cm^{-1}) than those in liquid phase (i.e., ~50 cm^{-1}). Concurrently, the intensities of IR modes $2v_{14}$, v_1 and v_{13} are significantly reduced. These observations indicate the molecular disorder in phase I. Indeed, a low-temperature neutron powder diffraction study on 2-butyne suggested that this phase likely adopts a rhombohedral structure with three molecules per unit cell with highly disordered nature.[22] The IR frequency shifts vs. pressure and appearance of a new mode at 2740 cm^{-1} indicate another phase transition from phase I

to phase II at 0.9 GPa, which is also consistent with the previous Raman study.[18] The low-temperature neutron powder diffraction study indicated that phase II has a monoclinic structure (space group *C2/m*) with two molecules per unit cell (as shown in Fig. 4.1b).[22]

Table 4.1 Assignment and Frequencies of Observed Infrared Modes in Comparison with References.

Mode	IR (in cm^{-1})	Raman	Description
v_{13}	2961	2963	CH_3 stretching
v_1	2916	2921	C-H stretching
$2v_{14}$	2862	2863	CH_3 deformation
$2v_3$	2744	2738	CH_3 deformation
$2v_8$	2330	2315	C-C stretching
v_2	----	2238	C≡C stretching
v_{14}	1448	1448	CH_3 deformation
v_3	----	1379	CH_3 deformation
v_{11}	1035	----	CH_3 rocking

Note: IR values are from this paper and Raman values, as well as descriptions, are from Ref. 18.

4.3.2 Photochemical reactions of 2-butyne with H_2O

Starting from these phases at pressures of 0.04 (liquid), 0.27 (liquid-phase I mixture), 0.52 (phase I), and 0.90 GPa (phase II), we carried out photochemical studies by irradiating with multiline UV at λ ~350 nm with a power of 250 mW. The reaction progress is monitored by visual observations under an optical microscope and by FTIR spectroscopy as a function of radiation time. We observed that the photon-induced reactions at 0.04 GPa are the same as the those at 0.27 GPa as evidence by almost identical IR evolution profiles. Here, we show the photochemical evolution at 0.27 GPa as an example (Fig 4.2a). Clearly, after 30 min irradiation, new IR bands at 675 and 966 cm^{-1} appear and are intensified with further radiation. At 45 min, more IR bands, e.g., at 816, 884, 910, 1065, and 1303 cm^{-1} (Fig. 4.2a) as well as 1660, 1729, and 3020 cm^{-1} are observed (Fig. 4.3a).

Table 4.2: The Observed IR Bands of 2-butyne and water with an initial loading pressure of 0.27, 0.52, 0.90 GPa and those of photochemical reaction products after UV irradiation (λ = 350 nm, 250 mW).

This work						2-butene (solid)[a]		2-butanone[b]
0.27GPa				0.52 GPa	0.90 GPa	cis	trans	(solid)
0min	30	45	100	100	135			
	676	676	676	676		682vs		
		752	752	752	746			745m
		770	770	770	768			768s
		883	886	887		868vw		
		910		910				937s
	966	969	969	968		972s	974vs	
	976			978	973		983vs	995s
1040	1041	1038	1037	1036	1039	1038m	1043s	
		1065	1065	1067			1061s	
		1093		1090	1090			1087s
1145	1145	1145	1150	1150	1146			
		1303	1302	1302			1303w	
	1660	1660	1661	1661	1661	1661m		1668m
		1724	1722	1717	1719	1722w		1716vs
2855	2856	2859	2862	2870	2865	2860m	2860m	
2923	2923s	2923s	2923	2925	2925	2922s	2918m	2920m
2965	2964	2964s	2963	2962	2965	2965s	2966s	
	3020	3023s	3023	3025w		3014s	3014s	

[a] McKean et al.[23]   [b]Durig et al.[31]
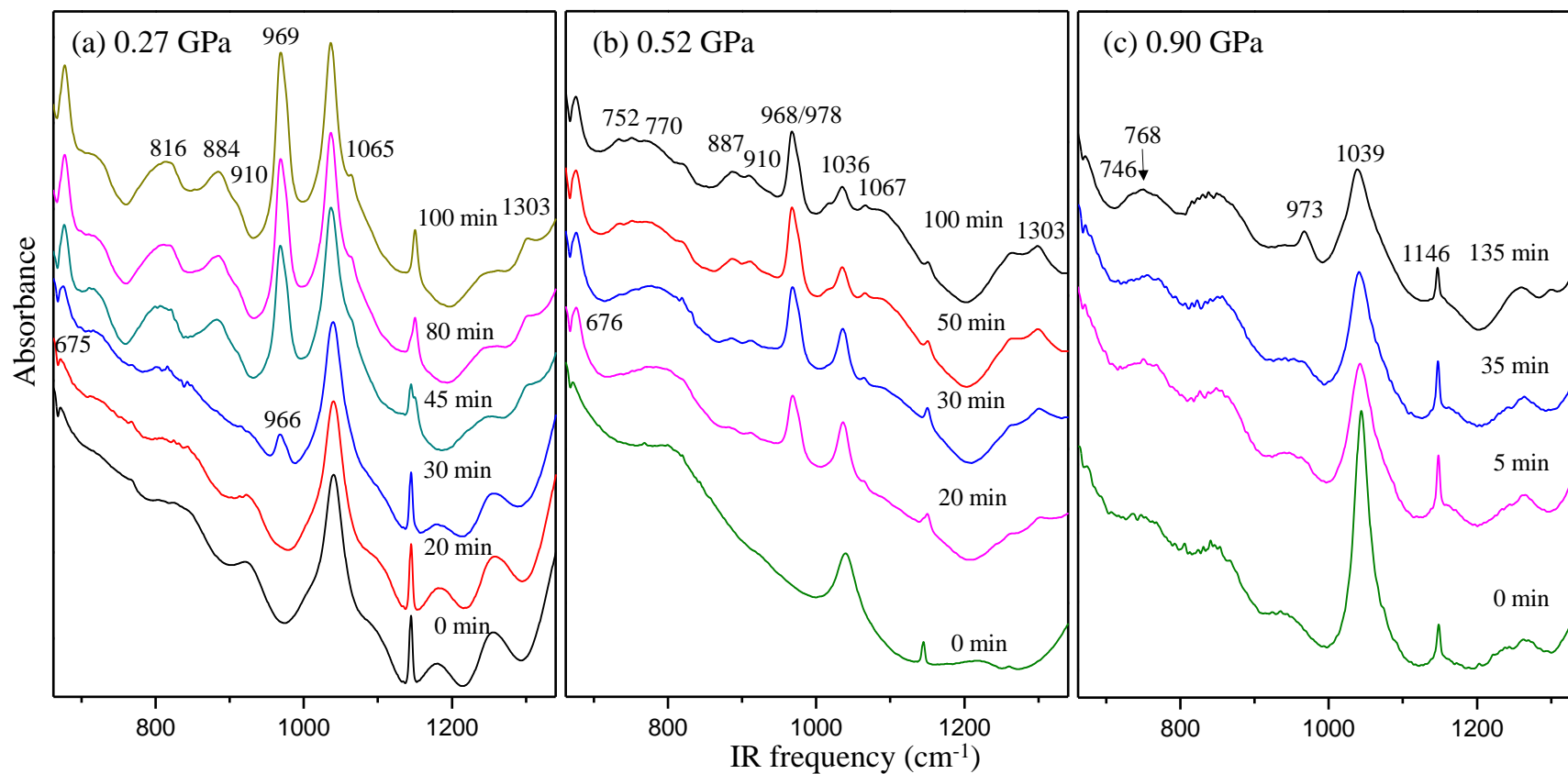
Figure 4.2: IR spectra of 2-butyne and H_2O at pressure 0.27, 0.52 and 0.90 GPa upon UV irradiation (with λ of ~350 nm and power of ~250 mW) as a function of time in the spectral region of 670−1310 cm^{-1}.
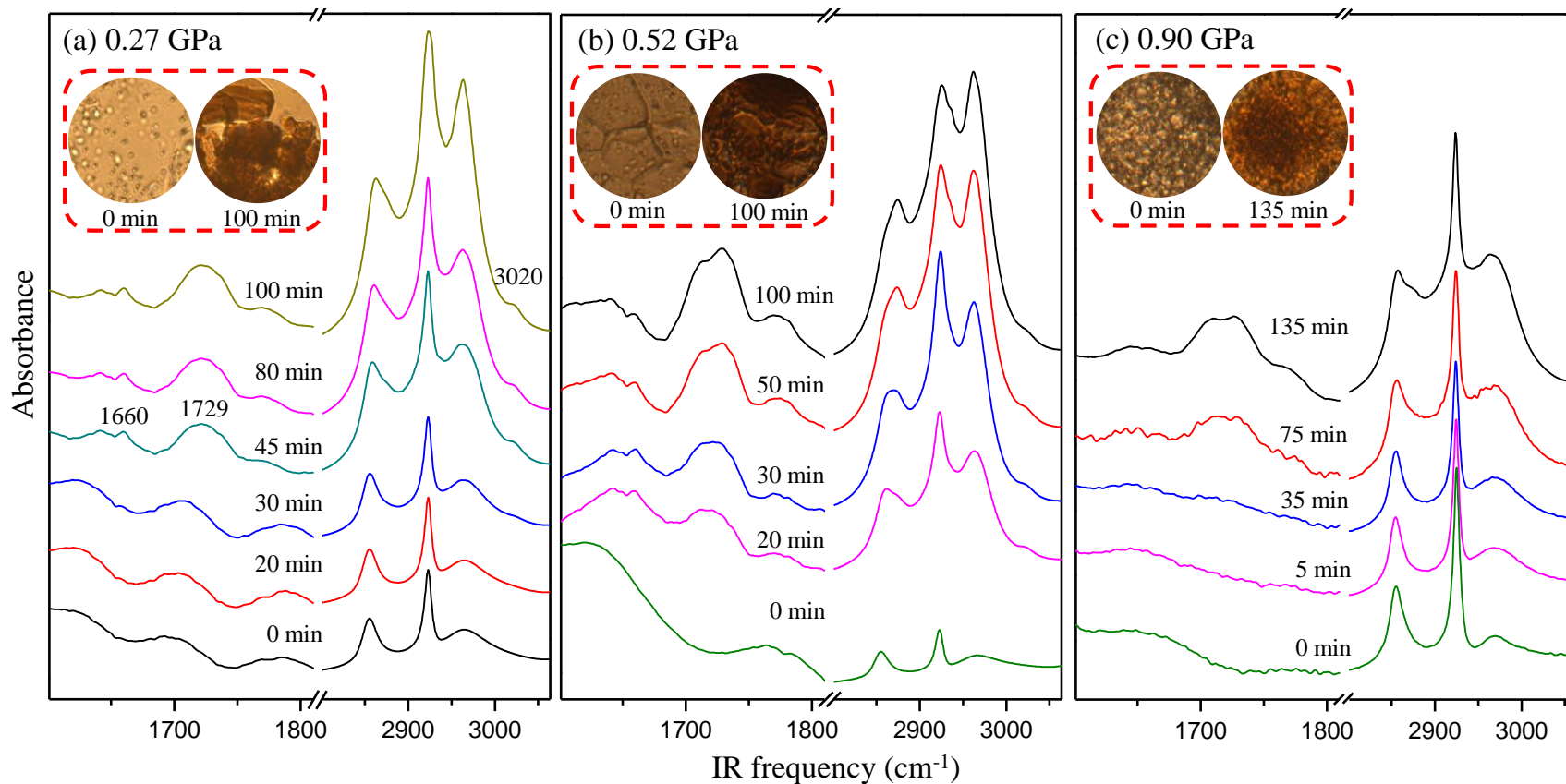
Figure 4.3: IR spectra of 2-butyne and H$_2$O at pressure 0.27, 0.52 and 0.90 GPa upon UV irradiation (with λ of ∼350 nm and power of ∼250 mW) as a function of time in the spectral region of 1600−1800 cm^{-1}. The insets show corresponding microphotographs (60 micro in diameter) of the 2-butyne/H$_2$O mixture collected before and after radiation.

After 100 min, these IR peaks become extremely intense but no more time-dependent changes of the IR profile were observed, indicating the completion of the photochemical reactions under the given conditions. As a result, a brownish solid as the product can be observed under the microscope as shown in the inset of Fig. 4.3a.

Partial hydrogenation of 2-butyne

In order to identify the possible photochemical products, we examined the database of the characteristic IR absorption frequencies of several possible 2-butyne derivatives. The observed IR peaks at 969 cm^{-1} (=C-H bend) and 3020 cm^{-1} (=C-H stretch) both suggest a possible formation of alkenes. By comparing the IR spectra at 30, 45, and 100 min with corresponding characteristic IR peaks of 2-butene in Table 4.1, the new peaks at 676, 969, 1661, 2862, and 3023 cm^{-1} exhibit an excellent agreement with the IR bands of solid cis 2-butene ($H_3CCH=CHCH_3$), which absorbs at 682, 972, 1661, 2860, and 3014 cm^{-1}, respectively.[23] From 30 min to 45 min, the IR bands in the range of 2800-3000 cm^{-1} were significantly intensified (Fig. 4.3a), which also supports the progressive formation of cis 2-butene as the primary photochemical product (Table 4.2). In addition, we observed a slight shift of the peak at 966 to 969 cm^{-1} at 45 min with a strong and relatively broad IR profile (Fig. 4.2a) as well as the appearance of new peaks at 1065 and 1303 cm^{-1}. These features strongly suggest a photo-induced partial isomerisation of cis 2-butene to trans 2-butene, as summarized in Table 4.2.

The formation of 2-butene requires a cleavage of the triple carbon-carbon bond of 2-butyne and subsequent reaction with H atoms. The source of H atoms therefore is of fundamental importance for the formation of 2-butene. As discussed below, the energetics strongly disfavor the dissociation of hydrogen from methyl groups of 2-butyne, leaving the other reactant, H_2O as the more probable source of hydrogen. The early studies showed

that irradiating liquid water with VUV light favorably promotes the dissociation process:[24-26]

$$H_2O_{(l)} + h\nu \rightarrow H_{(aq)} + OH_{(aq)} \qquad (4.2)$$
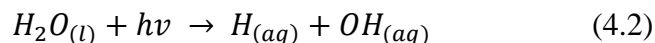
Furthermore, the photon energies that can be effectively absorbed by liquid water were reported to be in the range of 6-6.5 eV.[27,28] Therefore, the energy required for reaction in eq. 4.2 can be achieved by two-photon absorption of 350 nm near-UV radiation (i.e., 7 eV) under the current experiment condition. By using the transient absorption spectroscopy, Elles *et al.* found that the average initial separation of H and OH fragments from the dissociation channel at the lower excitation energy (e.g., 8.3 eV) is about 7 Å. The relatively large separation of the dissociation products suggests that H atoms are formed with enough kinetic energy to escape the solvent cage or several layers of solvent shells.[26] Moreover, previous molecular dynamics calculations on the mobility of the H atoms and OH radicals also showed that H atoms could move long distances up to 60 Å even through solid H_2O and remain reactive.[29] Under these conditions, it is therefore highly likely for liquid water to produce reactive radicals with the feasible photon energies. As shown in Fig. 4.4, the photodissociation of water via the two-photon process allows the production of a pair of radicals within the cage of water molecules. The H and OH radical pair can either escape the water cage and persist separately in solution or diffusively recombine to form the starting molecule. Alternatively, the radical pair could also remain the original water cage and recombine on a much faster timescale than for diffusive recombination.[30] Therefore, water cages play a prominent role to sequestrate reactive OH radicals but release H atoms for subsequent reactions. Ultimately, the light H atom with enough kinetic energy survives the recombination process and thus favorably reacts with the C-C triple bond of 2-butyne to produce 2-butene (Fig. 4.4).
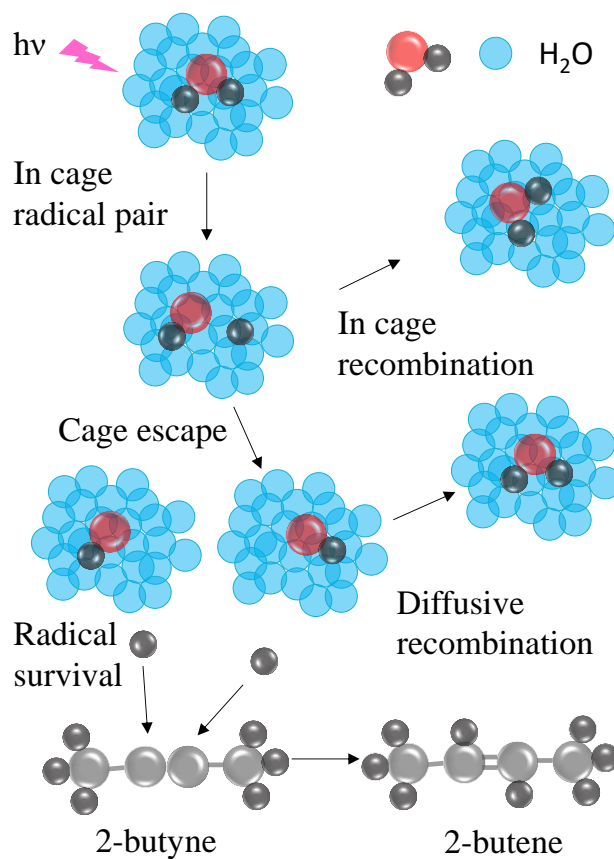
Figure 4.4: Carton showing three possible results following a photodissociation event that produces a pair of H and OH radicals within a water cage. The H and OH radical pair can escape the solvent cage and persist separately in solution or diffusively recombine to form original H₂O molecule. The H and OH radical pair could also remain within the original H₂O cage and recombine on a much faster timescale than that for diffusive recombination (see Harris et al.[30]). The escaped H atoms are proposed to react with 2-butyne and give rise to 2-butene.

Hydration of 2-butyne and tautomerism

In addition to 2-butene, the IR profiles suggest the formation of other possible photochemical products. In Fig. 4.3a, for instance, the broad peak centered at 1729 cm^{-1} indicates the vibration of the carbonyl group. Together with IR bands at 752, 770, and 910

cm^{-1} observed in Fig. 4.2b, these characteristic peaks provide strong evidence for the formation of solid 2-butanone, which exhibits characteristic IR absorptions at 745, 768, 937, and 1716 cm^{-1} for instance (Table 4.2).[31] The IR signatures for solid 2-butanone become more prominent at 0.52 GPa.

The formation of 2-butanone can be easily understood from the highly reactive nature of the H and OH radicals produced via the two-photon dissociation of water molecules by near-UV radiation at 350 nm at moderate pressures. It has been reported that these radicals are the essential initiators to induce chemical reactions in the mixtures such as red phosphorus-H$_2$O system and in clathrate hydrates.[11,32-34] Similarly, the highly reactive H and OH radicals can attack the triple bond of 2-butyne and undergo a photochemical anti-Markownikoff addition to produce the enol form (H$_3$CHC=COHCH$_3$) as the hydration product. In the IR spectrum, however, no enol form can be identified. Moreover, the hydration of alkyne has been alternatively achieved catalytically followed by tautomerization:[35]

$$CH_3C \equiv CCH_3 + H_2O \rightarrow H_3CHC = COHCH_3 \xleftrightarrow{tautomerization} C_2H_5COCH_3 \quad (4.3)$$

Under ambient and catalytic conditions, the reaction in eq. 4.3 suggests a tautomerism equilibrium between the enol and ketone forms. The fact that no enol form was observed in experiments suggests that the ketone is the energetically favorable form over the enol under the specific conditions where combined pressure-photon acts as an effective driving force for one-way tautomerization.

At higher pressure (e.g., 0.9 GPa), interestingly, the IR spectra suggests that instead of 2-butene, only 2-butanone is produced (Figs. 4.2c, 4.3c, and Table 4.2). The closure of the production channel for 2-butene at this pressure could be primarily due to the fact that H$_2$O and (or) 2-butyne transformed to crystalline phases (Ice VI and phase II, respectively). At room temperature, specifically, the phase transition pressures for both liquid H$_2$O $\rightarrow$ Ice

VI and phase I → phase II of 2-butyne were reported in pressure region of 0.9-1GPa.[18,36] The crystallization of water would significantly impact the formation of water cages, which are essential to preserve the reactive H atoms, and thus the formation of 2-butene.

4.3.3 Possibility of other photochemical reactions and polymerizations of 2-butyne

We systematically investigated the influence of pressure and water content on the photochemical reactions between 2-butyne and H_2O in an extended pressure region and by varying the water content. However, no other reaction channels and especially the originally expected polymerization of 2-butyne, were observed. To minimize the reactive contribution from H_2O, we loaded almost pure 2-butyne (e.g., at 0.14 GPa where the extremely weak IR band of OH stretch suggests negligible water content, as shown in Fig. 4.1a) for subsequent photochemical studies. However, the appearance of the most characteristic IR band at 969 cm^{-1} at 130 min radiation (the most intense IR peak of 2-butene and 2-butanone in Fig. 4.2 suggests that the reactions still proceed via the dissociation of H_2O slowly instead of polymerization reactions of 2-butyne. Photochemical reactions of pure 2-butyne have been studied both experimentally and theoretically.[37-39] Upon excitation by a 193 nm UV (6.42 eV) laser,[38] for instance, two dominant dissociation paths were identified as follows.[37,40,41]

$$H_3CC\equiv CCH_3 \rightarrow H_3CC\equiv CCH_2 + H \qquad 3.78 \quad eV \qquad (4.4)$$

$$\rightarrow H_3CC\equiv C + CH_3 \qquad 3.84 \quad eV \qquad (4.5)$$
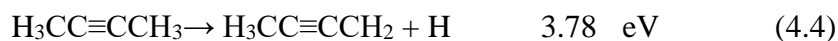
However, the possible products from reactions of these fragments (e.g., $H_3CC\equiv CCH_2CH_3$, $H_3CC\equiv CH$) can be ruled out by examining documented IR spectra of the products. Moreover, excitation energy at near-UV 350 nm (3.5 eV) in our experiment is insufficient to reach the reaction threshold.

4.3.4 Selectivity and kinetics of the competitive reactions under pressure

Finally, we examined the effects of loading pressures on the reaction kinetics quantitatively for more in-depth understanding of the reaction mechanisms. The yield of two primary products can be estimated by the integrated intensity of the characteristic IR bands, e.g., 675 cm^{-1} for 2-butene and 1729 cm^{-1} for 2-butanone. The integrated intensity of the characteristic peaks as a function of radiation time is plotted in Fig. 4.5. For 2-butene, the relative reaction yield suggests that low pressure (i.e., < 0.27 GPa) is favorable for its production whereas relatively high pressure (e.g., 0.52 GPa) significantly reduces the production. Moreover, the production channel for 2-butene is completely closed at 0.9 GPa (see above discussion). For 2-butanone, in contrast, the relative reaction yield is less affected by different loading pressures. In particular, this production channel remains open even under a high pressure of 0.9 GPa (Fig. 4.5b).

In terms of reaction rate, evidently, higher loading pressures favor faster kinetics for the production of both 2-butene and 2-butanone. Specifically, the reaction initiation time at 0.04 GPa is significantly shortened from 100 min to less than 20 min or almost instantaneous when the initial loading pressure is increased to 0.52 GPa. However, above 0.52 GPa (e.g., 0.9 GPa), it reduces the reaction rate for 2-butanone with initiation time close to 40 min (Fig. 4.5b). These observations show the similar pressure effect on photochemical reaction kinetics for ethylene glycol and styrene we reported previously,[15,42] where pressure generally accelerates a photochemical reaction up to an optimal pressure beyond which the reaction is significantly slowed down and/or completely prohibited. In these studies, we established that the activation volume typically decreases with increasing pressure until reaching an optimal pressure giving a zero activation volume and thus a barrierless reaction. The reduced kinetics for the production of 2-butanone above 0.52 GPa thus implies the activation volume reached the minimum at this pressure and increases

significantly at 0.9 GPa. More importantly, higher pressure may substantially suppress the reaction channels that are dissociative in nature, such as the production of H and OH radicals from water. The reduced supply of H and OH radicals as essential reactants for the production of 2-butanone may further contribute to the reduced reaction rate.
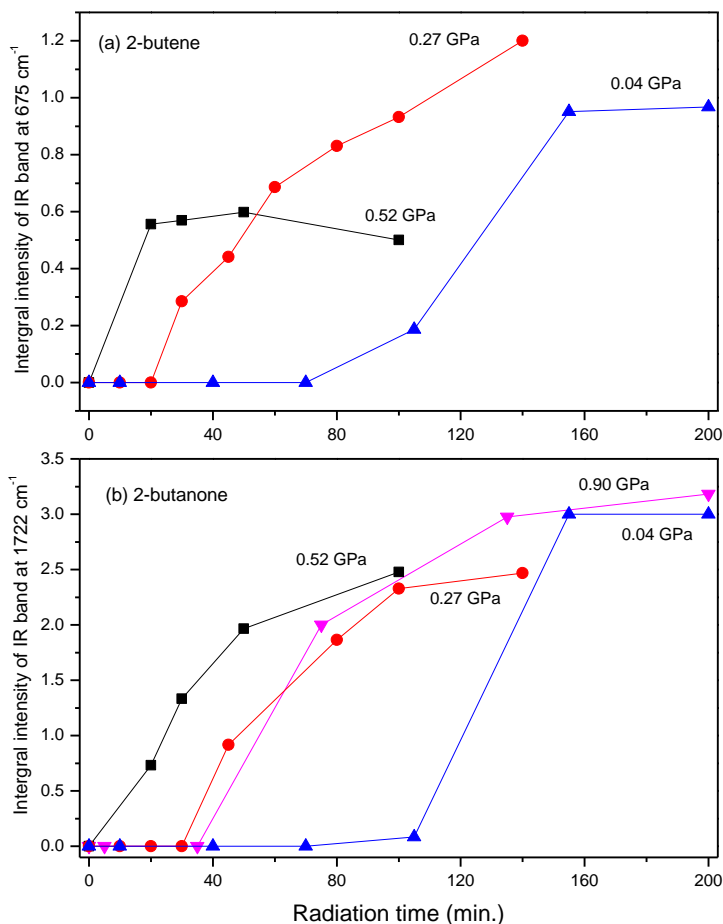
Figure 4.5: Relative photochemical reaction yields of (a) 2-butene and (b) 2-butanone estimated by integrating the IR absorbance of the respective characteristic IR modes as a function of radiation time for 2-butyne-water mixture with an initial loading pressure of 0.04, 0.27, 0.52 and 0.90 GPa.

Overall, the pressure-dependent photochemical reactivity of 2-butyne/H_2O system provides important implications in the production of useful species with great tunability and controllability. In particular, the production of 2-butene can be a cost effective and

efficient method to produce the precursor for the production of gasoline and butadiene. In addition, the unique synthesis of 2-butanone as an industrially versatile material that is currently produced on a large scale (i.e., 700 million kilograms annually[43]) may shed light on its production using an alternative approach. By carefully selecting the favorable pressure, temperature, and the radiation energy, the reaction channels may be tuned and optimized to selectively generate the desired product. Furthermore, the methods we use to synthesis these products are in the absence of solvents, catalysts, and radical initiators and thus greatly promote green chemistry.

4.4 Conclusions

In summary, the photon-induced reactivity of 2-butyne with trace amount of water was investigated in a DAC at pressures up to ~1 GPa and ambient temperature. Near-UV radiation at $\lambda = 350$ nm was employed to initiate the photochemical reactions via two-photon absorption processes. In situ FTIR spectroscopy allows reaction progress to be probed in real time. Spectral analysis suggests the production of cis, trans-2-butene and 2-butanone from the photoreactions of the 2-butyne/water fluid at relatively lower loading pressures. At higher loading pressures of 0.9 GPa, only 2-butanone is selectively produced. The possible reaction mechanisms and pathways of these products are proposed, where the photodissociation of H_2O is believed to be the essential step of the reactions. We further explored the pressure-dependence of the reaction kinetics for the production of 2-butene and 2-butanone. Both the reaction yield and rate are found to be highly pressure dependent, which can be understood in terms of activation volume as well as the production efficiency of radicals. The study demonstrates an attractive route to produce useful materials with great selectivity via an environmental friendly synthetic approach.

4.5 References

(1)   Schettino, V.; Bini, R. *Physical Chemistry Chemical Physics* **2003**, *5*, 1951.

(2)   Schettino, V.; Bini, R.; Ceppatelli, M.; Ciabini, L.; Citroni, M. In *Advances in Chemical Physics, Vol 131*; Rice, S. A., Ed., 2005; Vol. 131; pp 105.

(3)   Hemley, R. J. *Annual Review of Physical Chemistry* **2000**, *51*, 763.

(4)   Aoki, K.; Usuba, S.; Yoshida, M.; Kakudate, Y.; Tanaka, K.; Fujiwara, S. *Journal of Chemical Physics* **1988**, *89*, 529.

(5)   Yoo, C. S.; Nicol, M. *Journal of Physical Chemistry* **1986**, *90*, 6726.

(6)   Citroni, M.; Ceppatelli, M.; Bini, R.; Schettino, V. *Journal of Chemical Physics* **2003**, *118*, 1815.

(7)   Citroni, M.; Bini, R.; Foggi, P.; Schettino, V. *Proceedings of the National Academy of Sciences of the United States of America* **2008**, *105*, 7658.

(8)   Bini, R. *Accounts of Chemical Research* **2004**, *37*, 95.

(9)   Citroni, M.; Ceppatelli, M.; Bini, R.; Schettino, V. *Science* **2002**, *295*, 2058.

(10)   Ciabini, L.; Santoro, M.; Bini, R.; Schettino, V. *Physical Review Letters* **2002**, *88*.

(11)   Ceppatelli, M.; Bini, R.; Schettino, V. *Proceedings of the National Academy of Sciences of the United States of America* **2009**, *106*, 11454.

(12)   Ceppatelli, M.; Bini, R. *Macromolecular Rapid Communications* **2014**, *35*, 787.

(13)   Evlyukhin, E.; Museur, L.; Traore, M.; Nikitin, S. M.; Zerr, A.; Kanaev, A. *Journal of Physical Chemistry B* **2015**, *119*, 3577.

(14)   Citroni, M.; Ceppatelli, M.; Bini, R.; Schettino, V. *Journal of Physical Chemistry B* **2007**, *111*, 3910.

(15)   Guan, J. W.; Song, Y. *Journal of Chemical Physics* **2016**, *144, 214904*.

(16)   Bernasconi, M.; Chiarotti, G. L.; Focher, P.; Parrinello, M.; Tosatti, E. *Physical Review Letters* **1997**, *78*, 2008.

(17)   Sakashita, M.; Yamawaki, H.; Aoki, K. *Journal of Physical Chemistry* **1996**, *100*, 9943.

(18)   Baonza, V. G.; Montoro, O. R.; Taravillo, M.; Caceres, M.; Nunez, J. *Journal of Chemical Physics* **2004**, *121*, 11156.

(19)   Chiang, C. K.; Fincher Jr, C.; Park, Y. W.; Heeger, A. J.; Shirakawa, H.; Louis, E. J.; Gau, S. C.; MacDiarmid, A. G. *Physical Review Letters* **1977**, *39*, 1098.

(20)   Chelazzi, D.; Ceppatelli, M.; Santoro, M.; Bini, R.; Schettino, V. *The Journal of Physical Chemistry B* **2005**, *109*, 21658.

(21)   Dong, Z. H.; Song, Y. *Journal of Physical Chemistry C* **2010**, *114*, 1782.

(22)   Ibberson, R. M.; Prager, M. *Acta Crystallographica Section B-Structural Science* **1995**, *51*, 71.

(23)   McKean, D. C.; Mackenzie, M. W.; Morrisson, A. R.; Lavalley, J. C.; Janin, A.; Fawcett, V.; Edwards, H. G. M. *Spectrochimica Acta Part a-Molecular and Biomolecular Spectroscopy* **1985**, *41*, 435.

(24)   Thomsen, C. L.; Madsen, D.; Keiding, S. R.; Thogersen, J.; Christiansen, O. *Journal of Chemical Physics* **1999**, *110*, 3453.

(25)   Elles, C. G.; Rivera, C. A.; Zhang, Y.; Pieniazek, P. A.; Bradforth, S. E. *Journal of Chemical Physics* **2009**, *130*.

(26)   Elles, C. G.; Shkrob, I. A.; Crowell, R. A.; Bradforth, S. E. *Journal of Chemical Physics* **2007**, *126*.

(27)   Nikogosyan, D. N.; Angelov, D. A. *Chemical Physics Letters* **1981**, *77*, 208.

(28)   Nikogosyan, D. N.; Oraevsky, A. A.; Rupasov, V. I. *Chemical Physics* **1983**, *77*, 131.

(29)   Andersson, S.; Al-Halabi, A.; Kroes, G. J.; van Dishoeck, E. F. *Journal of Chemical Physics* **2006**, *124*.

(30)   Harris, S. J.; Murdock, D.; Zhang, Y. Y.; Oliver, T. A. A.; Grubb, M. P.; Orr-Ewing, A. J.; Greetham, G. M.; Clark, I. P.; Towrie, M.; Bradforth, S. E.; Ashfold, M. N. R. *Physical Chemistry Chemical Physics* **2013**, *15*, 6567.

(31)   Durig, J. R.; Feng, F. S.; Wang, A. Y.; Phan, H. V. *Canadian Journal of Chemistry-Revue Canadienne De Chimie* **1991**, *69*, 1827.

(32)   Ceppatelli, M.; Bini, R.; Schettino, V. *Journal of Physical Chemistry B* **2009**, *113*, 14640.

(33)   Ceppatelli, M.; Bini, R.; Caporali, M.; Peruzzini, M. *Angewandte Chemie-International Edition* **2013**, *52*, 2313.

(34)   Ceppatelli, M.; Bini, R.; Schettino, V. *Physical Chemistry Chemical Physics* **2011**, *13*, 1264.

(35)   Reusch, W. Text Book of Organic Chemistry, **1999**.

(36)   Wagner, W.; Saul, A.; Pruss, A. *Journal of Physical and Chemical Reference Data* **1994**, *23*, 515.

(37)   Collins, S. *Journal of Physical Chemistry* **1990**, *94*, 5240.

(38)   Lee, H. Y.; Kislov, V. V.; Lin, S. H.; Mebel, A. M.; Neumark, D. M. *Chemistry-a European Journal* **2003**, *9*, 726.

(39)   Palmer, M. H.; Walker, I. C. *Chemical Physics* **2007**, *340*, 158.

(40)   Deschênes, J.; Deslauriers, H.; Collin, G. J. *Canadian Journal of Chemistry* **1980**, *58*, 2108.

(41)   Fahr, A.; Laufer, A. H. *Journal of Physical Chemistry A* **2005**, *109*, 2534.

(42)   Guan, J. W.; Song, Y. *Journal of Physical Chemistry B* **2015**, *119*, 3535.

(43)   Hoell, D.; Mensing, T.; Roggenbuck, R.; Sakuth, M.; Sperlich, E.; Urban, T.; Neier, W.; Strehlke, G. *Ullmann's Encyclopedia of Industrial Chemistry* **2009**.

Chapter 5

5 Photochemical Liquid-to-Crystal, Crystal-to-Crystal versus Liquid-to-Liquid Phase Transitions of Stilbene at High Pressure: From Product Selectivity to Electronic State Compressibility

5.1 Introduction

Photoinduced phase transitions (PIPT) have been established in various materials, and are now developing into a method for exploring new structures and properties of materials and realizing new phases that are not formed in thermal equilibrium.[1-4] PIPT examples extend from the liquid-to-solid,[5,6] liquid-to-liquid,[4] solid-to-liquid,[7] to solid-to-solid transitions.[3] Those phenomena become particularly attractive and are technologically important when the phase transformation occurs rapidly or permanently depending on the material, because a phase transition is often accompanied by drastic changes in electric, dielectric, optical and magnetic properties; For example, photoinduced insulator–metal, semiconductor-metal phase transition,[8,9] and photochemical transition from the equilibrium nematic to the non-equilibrium isotropic phase in liquid crystals (LCs).[4,10] The last one involves structural changes of a chromophoric moiety such as stilbene or azobenzene molecule doped in LCs. At ambient conditions, the doped molecules are well known photoactivated systems and show reversible trans/cis isomerization upon UV and visible irradiation (see scheme 5.1). Upon radiation, the reversible trans-cis photoisomerization can exert large effects on the properties of LCs. The rod-like shape of the trans isomer is compatible with LC phases, while the bent shape of the cis isomer is incompatible with them, which, in the case of nematic LCs, can give rise to an isothermal

photochemical nematic-isotropic phase transition.[4] At the ambient pressure, this PIPT plays a striking role in imaging and display devices as well as high-speed information processing due to the fast transformation induced by light.

Influences of external thermodynamic factors such as temperature and pressure need to be considered as they could have several impacts on the phase transitions and chemical stability of the phases. Prasad et al. have observed that increasing pressures significantly shift the photoinduced nematic-isotropic transition temperature.[11] Iwai et al. found that high pressure enhances the nonlinearity of the photoinduced insulator-to-metal transition in a layered organic salt.[12] In fact, pressure-temperature tuning has been exploited as a powerful tool to induce structural phase transitions in materials over the last few decades.[13] In recent years, it is more interesting to study high-pressure effects on photo-induced phase transitions, particularly, photochemical phase transformations.[14-19] The studies have demonstrated that high pressure can have a profound impact on photochemical phase transitions and occasionally create new technological important materials. For instance, crystalline benzene has been forced to photolyze and produce an amorphous hydrogenated carbon phase (a-C:H) at high pressure.[14] By tuning the pressure and laser wavelength, Chelazzi et al. obtained a highly crystalline polymeric phase from liquid ethylene.[15] However, up to the present, we have little knowledge about high-pressure effects on photochemical phase transitions due to other types of photoreactions such as the trans-cis photoisomerization reaction. This knowledge is necessary for further evaluating high-pressure effects on photochemical nematic-isotropic phase transition in LCs as well as exploring new photoinduced states.
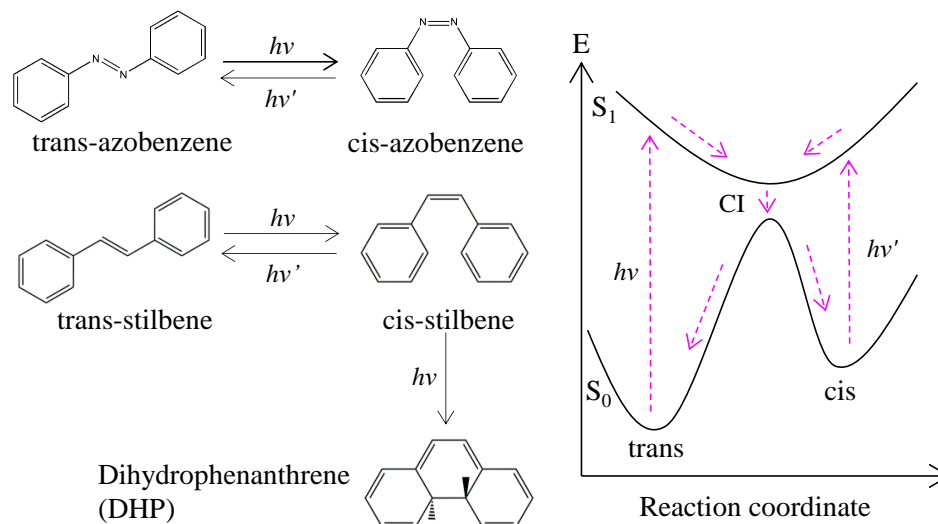
Scheme 5.1: Photochemical reactions and products of azobenzene and stilbene at normal conditions. No dimerization can be induced from cis-stilbene at normal conditions.

Another fundamental issue concerns the role of electronic states on photochemical phase transitions, especially when the system suffers from high pressures. The issue remains far from being fully understood. It is known that the photochemical phase transition undergoes electronic excitation and electron configuration change of a target molecule as the most important step.[20] More basically, each electronic state of a molecule is represented by a potential energy surface (PES) that describes the change in energy of the system on changing nuclear coordinates.[21] The PESs allow us to visualize not only the radiative and radiationless deactivations of excited states but also their evolution towards reaction products. In previous studies, dissociation or polymerization type reactions are intrinsically caused by an adiabatic energy dissipation,[22-24] where the molecule in the excited electronic state follows a single, adiabatic surface to the reaction product. The effect of increasing pressure is to reduce the energy gap between the ground and excited electronic states (vertical contribution) of the molecule.[25] In contrast, the trans/cis photoisomerization type reaction processes a non-adiabatic energy dissipation at ambient

pressure.[26] The non-adiabatic processes mean non-radiative de-excitation transitions from the excited state to a new ground state (see scheme 5.1). The process is achieved by a conical intersection (CI) point, a single point where the wave function is degenerate, allowing a rapid transition between the excited electronic state (S_1) and ground state electronic state (S_0).[27-30] Because of the existence of the CI at ambient conditions, the cis conformer and trans conformer can interconvert upon suitable wavelengths. More importantly, the non-adiabatic process of such systems creates opportunities and allows us to explore pressure effects on the displacement behavior of electronic states (especially the horizontal contribution). Given these backgrounds, we use cis-stilbene as a representative of the non-adiabatic systems. The cis-stilbene upon UV irradiation was found to geometrically isomerize to trans-stilbene or undergo an electronic rearrangement process to generate 4a,4b-dihydrophenanthrene (DHP) in solution.[31] Herein, we have examined effects of high pressure on the photochemical phase transition of cis-stilbene in the condensed phase. The results clearly demonstrate the tuning capacity of high pressure on the photochemical phase transitions and the corresponding electronic state behaviors, and further show potential synthetic usages of high pressure on selected PIPT from functional molecular systems containing stilbene or azobenzene derivatives.

5.2   Experiments and calculations

Symmetric diamond anvil cells (DAC) equipped with a pair of type I (culet size 600 µm) or II (800 µm) diamonds were used in the experiment. The liquid cis-stilbene (97%, Alfa Aesar) along with a ruby ball was loaded into a hole with a diameter of 170 µm drilled on a stainless-steel gasket that was pre-indented to a thickness of 20–40 µm. The pressure was determined using the well-established ruby fluorescence method. The reaction of the sample was carried out at 6 loading pressures (e.g., 0, 0.11, 0.25, 0.36, 0.52 and 0.80 GPa).

Upon each loading, the reactions were subsequently triggered by focusing multi-line UV radiation with a peak wavelength at ~350 nm of an argon ion laser onto the sample

with a beam size of ~170 µm in diameter and a power 5 mW. The reaction progress was monitored by Fourier transform infrared (FTIR) spectroscopy and micro-Raman spectroscopy with the vibrational spectra collected at an appropriate time interval. Single crystals (α phase) of trans-stilbene (96%, Aldrich) were obtained by recrystallization from toluene. The IR and Raman spectrum of the α phase were collected and used as references in comparison with the vibrational spectra of the photochemical products.

For IR absorption measurements, a customized IR micro-spectroscopy system that consists of a FTIR spectrometer from Bruker Optics (model Vertex 80v) equipped with a Globar IR light source was used. The detailed instrumentations have been described elsewhere.[32] The system was operated under a vacuum of <5 mbar, such that the absorption by H_2O and CO_2 was efficiently removed. The reference spectrum, i.e., the absorption of diamond anvils that was collected before the samples were loaded, was divided as the background from each measurement. The spectral resolution used was 4 cm^{-1}.

A customized Raman micro-spectroscopy system was used to collect the Raman spectra. A single longitudinal mode, diode pumped solid state (DPSS) green laser with wavelength 532.10 nm was used as the excitation source. The laser was focused to < 5 µm on the sample by a 20× Mitutoyo objective. The Raman signal was detected with backscattering geometry by the same objective lens. The Rayleigh scattering was removed by a pair of notch filters. The scattered light was then dispersed using an imaging spectrograph equipped with a 1200 lines/mm grating achieving a 0.1 cm^{-1} resolution. The Raman signal was recorded using an ultrasensitive, liquid nitrogen cooled, back-illuminated, charge-coupled device (CCD) detector from Acton. The system was calibrated by neon lines with an uncertainty of ±1 cm^{-1}.

Ab initio calculations were performed using the GAUSSIAN 09 package.[33] Density functional theory (DFT) with the B3LYP functional with the 6-311++G (2d, p) basis set was utilized to obtain infrared spectra of the possible products. The stationary points were

identified with frequency calculations at the same level to verify that minima structures have zero imaginary frequencies.

5.3   Results and Discussion

5.3.1 Liquid-to-crystal phase transition via photoisomerization

In the beginning, we explore photochemical reactivity of liquid cis-stilbene at ambient pressure. The sample is loaded and sealed into the DAC. Next, the liquid sample is irradiated using the UV multi-line (UVML) emission of an Ar ion laser centered at 350 nm with a power density ~1.6 mW/cm^2. As shown in Fig. 5.1(a), micro-photographs suggests a liquid-to-crystal phase transition upon the UV radiation at ambient pressure. *in situ* IR measurements show that liquid cis-stilbene is completely converted to trans-stilbene crystal after 60s of radiation, which is signified by the disappearance of characteristic IR peaks of the cis isomer (1407 cm^{-1} labeled with an asterisk). The characteristic IR peaks of products show good consistency with the ones collected from the trans-stilbene crystal (α phase).
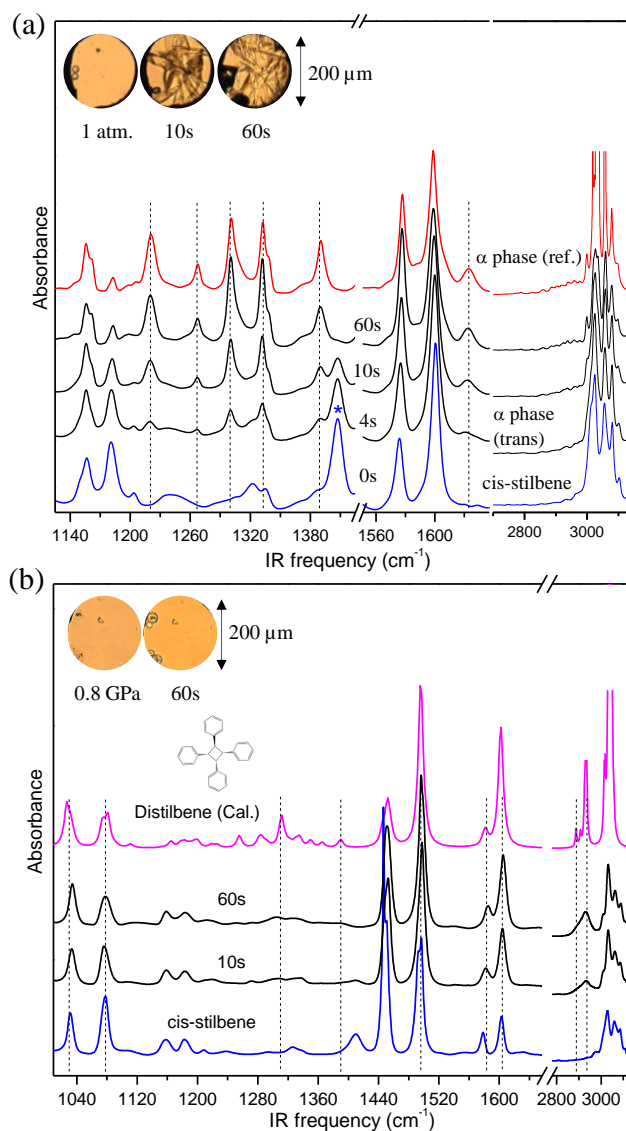
Figure 5.1: IR spectral evolution in the selected region of liquid cis-stilbene upon ~350 nm UV radiation (a) at normal pressure, (b) at 0.8 GPa. The insets show the corresponding microphotographs: (a) liquid-to-crystal, (b) liquid-to-liquid phase transitions. The top shows (a) IR spectrum of the trans-stilbene crystal (α phase) and (b) the calculated IR spectrum of a stilbene dimer. In (a), the cis/trans isomerization and subsequent crystallization to α phase are ON but the cyclization as shown in scheme 1 leading to DHP is OFF. At high pressure (b), a new reaction, dimerization from cis-stilbene is ON.

5.3.2 Liquid-to-liquid phase transition via 2+2 photodimerization

When repeated at a higher pressure 0.8 GPa, the photoreaction course is strikingly different. As shown in Fig. 5.1(b), the liquid cis-stilbene is completely converted to a new product after 60 s and a characteristic IR profile around 2929 cm^{-1} can be observed in contrast with the IR spectrum in Fig. 5.1(a). The IR spectrum of the photoproduct at 0.8 GPa is mostly consistent with the calculated IR spectrum of a stilbene dimer (distilbene or 1,2,3,4-tetraphenylcyclobutane) and no IR signatures of trans-stilbene can be found. More evidently, the evolution of micro-photographs shows a liquid-to-liquid phase transition unlike the liquid-to-solid phase transition in Fig. 5.1(a). This product is formed via [2+2] photodimerization of cis-stilbene but it is prohibited under normal conditions (scheme 5.1). This distilbene product processes an unique stereo-structure. Our calculations show that distilbene can have four stereoisomers depending on the positions of four phenyl groups (see Fig. 1S of the supporting information). Only the IR spectrum of type-III, where three phenyl groups are above and one phenyl group are below the cyclobutane ring is consistent with the experimental IR spectrum. Therefore, the result suggests that high pressure creates a photo-induced phase from the originally prohibited 2+2 dimerization and the new phase is type-III distilbene.

5.3.3 Two new crystal solids and their photo-induced phase transition

The opening of 2+2 dimerization and the closure of the isomerization at 0.8 GPa is unexpected since no factors have been reported to close the cis/trans photoisomerization. We further examine photochemical reactions at a smaller pressure increment (0.1-0.2 GPa). From these experiments, it turns out that the dimerization is strongly competitive with the photoisomerization. As shown in Fig. 5.2(a), when the photoreaction is induced at 0.25 GPa, after 2s irradiation, the liquid sample becomes an opaque solid in contrast with the transparent solid in Fig. 5.1(a). The IR spectrum shows new peaks at 908, 964, 971, 1221

cm^{-1}. At 8 s, the IR peak at 971 cm^{-1} disappears while an IR peak at 1164 cm^{-1} appears and the IR band at 1221 cm^{-1} is red-shifted to 1217 cm^{-1}. The IR bands at 1164, 1217 cm^{-1} become extremely intense at 31s. With the aid of the optical microphotographs, these spectral changes suggest two phase transitions: liquid cis-stilbene to solid trans-stilbene γ phase (TSγ), the γ phase to trans-stilbene β phase (TSβ). The spectral assignments and structures of TSγ and TSβ will be discussed below. The two-phase transitions are further evidenced by *in situ* Raman measurements at the same pressure. As shown in Fig. 5.2(b), the γ phase appears at 2-7s radiation (green lines). Further irradiation produces the β phase. From the γ phase to β phase, the Raman mode at 229, 349 cm^{-1} red-shifts to 222, 324 cm^{-1} respectively. The Raman mode at 1156 cm^{-1} disappears while two Raman modes appear at 1145, 1163 cm^{-1}.
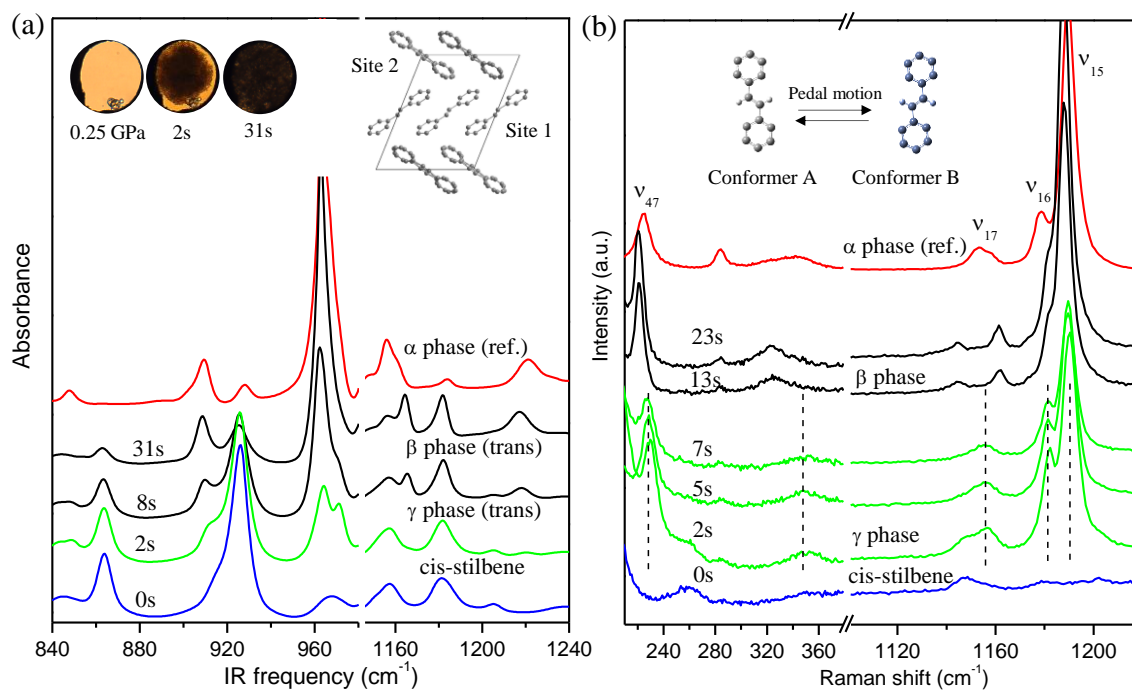
Figure 5.2: (a) Selected IR spectra and (b) Raman spectra of liquid cis-stilbene upon ~350 nm UV radiation at 0.25 GPa. The insets show the corresponding photographs (200 μm in diameter) under optical microscopy: liquid-to-solid and solid-to-solid phase transitions. The solid-to-solid phase transition is revealed from the spectral evolution (green to black). At the site 2 of α phase as shown in (a), the two trans-stilbene conformers (A and B) are in bicycle pedal motions (bold molecular structures). The IR and Raman spectra (red) of α phase are collected and used as references.

As shown in Fig. 5.2, IR and Raman spectra of trans-stilbene crystal (TSα phase) are collected as references. The α phase shows different vibrational characteristics to the β phase and γ phase. To find structural connections between TSα and the two new phases (β and γ), we first examine the crystal structure of the α phase. The crystal structure of the α phase has been reported to be monoclinic (space group: $P2_1/a$) with orientational disorder in the unit cell.[34] In the α phase, there are two crystallographically independent molecules in the asymmetric unit (the crystal structure is shown in Fig. 5.2(a)). Trans-stilbenes at site

1 are static, while those at site 2 are in dynamic motion, where trans-stilbene conformer A (or conformer B) on site 2 reversibly transforms to conformer B (or conformer A) like a bicycle pedal (see Fig. 5.2(b)).[35-37] The A-B interconversion changes the orientation of the -HC=CH- unit. Therefore, once the pedal-motion in the crystal is prohibited by external factors, for instance, high pressure, it is expected that trans-stilbenes on site 2 will have two states: conformer A or conformer B. This leads to two isostructural phases for TSα. This hypothesis is confirmed by results below. Our calculation shows that the Raman v_{47} mode is the vibration from the -HC=CH- unit (Fig. 2S of the supporting information). The measured red-shift of this mode in Fig. 5.2(b) suggests the orientation change of this unit, which is evidence for the expected changes from the γ to β phase transition, and for the production of the two phases. Moreover, by deconvoluting the experimental Raman spectra of the α phase (Fig. 3S of the supporting information), the selected Raman peaks of the α phase can be deconvoluted into two components. These components are consistent with the measured Raman peaks from the β and γ phases. Therefore, we assign the β and γ phases as a second and third polymorph of trans-stilbene crystals and they have the same space group (P2₁/a) as TSα but without molecular disorder in the unit cell.
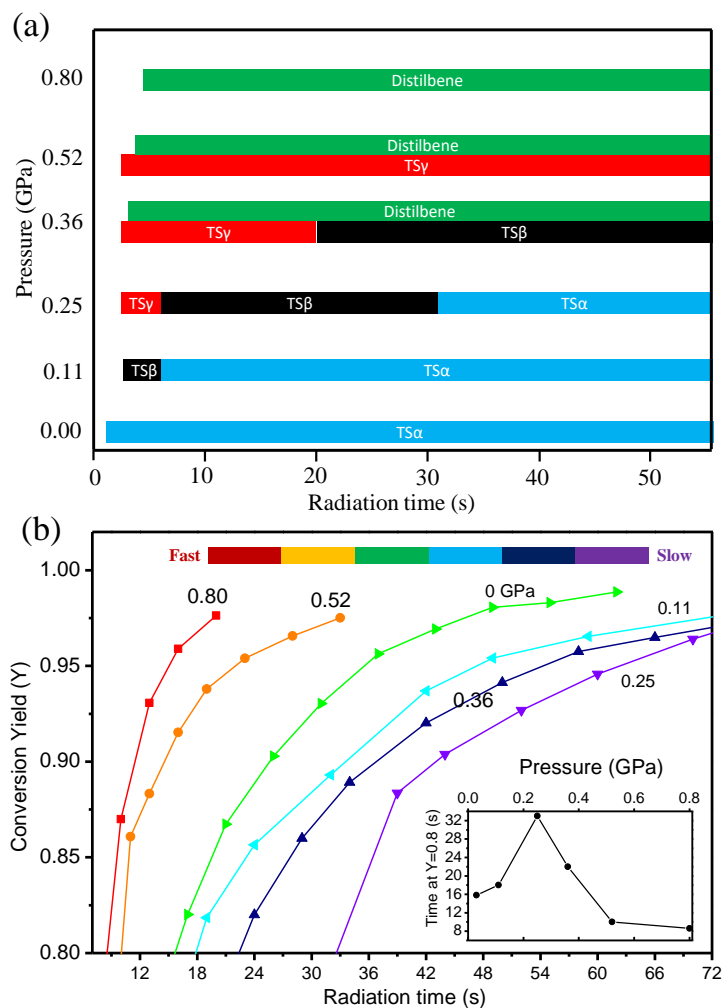
Figure 5.3: (a) The evolution of each photoproduct at different pressures. The appearance time of each photoproduct during UV radiation are determined by their characteristic IR absorption peaks. As pressure increases, reaction pathways lead to the β phase, γ phase and distilbene are successively opened. (b) The photochemical conversion ratio from liquid cis-stilbene to products as a function of radiation time at different pressures. The inset shows the measured radiation time to yield 80% products as pressure increases. From 0 to 0.25 GPa, the transformations are slowing down. Above 0.25 GPa, the transformations are speeding up, which are attributed to the opening of a new and efficient reaction channel, dimerization as revealed by (a).

5.3.4 Pressure tuning on the competitive phase transitions

Now we have identified four products (TSα, TSβ, TSγ, and distilbene). Firstly, the formation of the four products highly depends on the loading pressures. Examining the characteristic IR absorptions of each product, a detailed evolution as a function of radiation time at six pressures are summarized in Fig. 5.3(a). At 1 atm (~0 GPa), liquid cis-stilbene is transformed to TSα. However, at 0.11 GPa, the sample is transformed to TSβ initially before thermally transforming to TSα (Fig. 4S of the supporting information). When the pressure is increased to 0.25, 0.36 GPa, the other new product TSγ appears first. It is evident that the production of γ and β phases become more favorable as pressure increases. However, at 0.36 GPa and above, the [2+2] dimerization starts to be involved and becomes the dominant reaction at 0.8 GPa. The dimerization results in a liquid (cis-stilbene) to liquid (distilbene) photochemical phase transition.

Secondly, the yields of each product highly depend on the radiation time as well. To examine the radiation time-dependency, revealing kinetic information of the reactions, the integral intensity of an IR peak of the reactant is calculated and normalized at increasing radiation time at each pressure. An equation: $Y=1-I_t/I_0$ (I_0 is the integral intensity of the IR peak of the reactant before irradiation) is used to calculate the production yield Y at time t. The production yield Y versus irradiation time t can give kinetic information of the reactions. As shown in Fig. 5.3(b), the kinetics show that the reaction rate is initially deaccelerated as pressure increases to 0.25 GPa, however, it is accelerating at 0.36, 0.52 and 0.80 GPa. For instance (see inset), at Y=0.8, the required radiation time increases from 16s (0 GPa) to 32s (0.25 GPa) and reduces to 8s as pressure increases to 0.8 GPa.

The acceleration of the reaction is due to the opening of the dimerization channel at 0.36 GPa as shown in Fig. 5.3(a). However, the deacceleration of the reaction below 0.36 GPa is anomalous. Below 0.36 GPa, TSα, TSβ, and TSγ are produced and the production relies on pressure. Nevertheless, we know that TSα, TSβ, and TSγ are trans-stilbene

crystals and are produced from the cis/trans photoisomerization reaction. To explain the anomalous pressure-dependence of the reaction rate and selectivity, we need to understand the photoisomerization processes in depth. The processes have been well studied by time-resolved spectroscopy[29,38,39] and advanced theoretical calculations.[30] The whole processes are summarized in scheme 5.2, plotting 3-dimensional isomerization PESs of the ground state S_0 and excited electronic state S_1 states of stilbene along the isomerization coordinates (θ and φ). At first, cis-stilbene has two minima on the PES of S_0. On UV excitation, cis-stilbene at the two minima is excited to S_1 and twists the ethylenic double bond by $\theta=90^0$ to the minimum of the S_1 via a relaxation process. After the C=C twist, there are two possible isomerization pathways. The new coordinate either involves pyramidalization (rehybridization) of one ethylenic C atom or a twist of the adjacent C-C single bond by φ. The former is known as one-bond-flip (OBF) path and the latter is called as Hula-twist (HT) path. At room temperature, the cis/trans isomerization will procced along the OBF path, while at low temperature, cis/trans was found to isomerize along the HT path.[40] The HT path from the cis to the trans is a volume-conserving reaction and is favored when temperature decreases, the viscosity of solvent increases or the hydrogen-bonding interaction is enhanced.[41,42] Increasing pressure is known to increase the viscosity of molecular liquids. Therefore, the trans-stilbenes (conformer A in the scheme) from the OBF path gives rise to TSα, TSβ at low pressures. Instead, higher pressures increase the viscosity of liquid cis-stilbene and could favor the reaction proceeding along HT path. The produced conformer B subsequently crystalizes into TSγ.
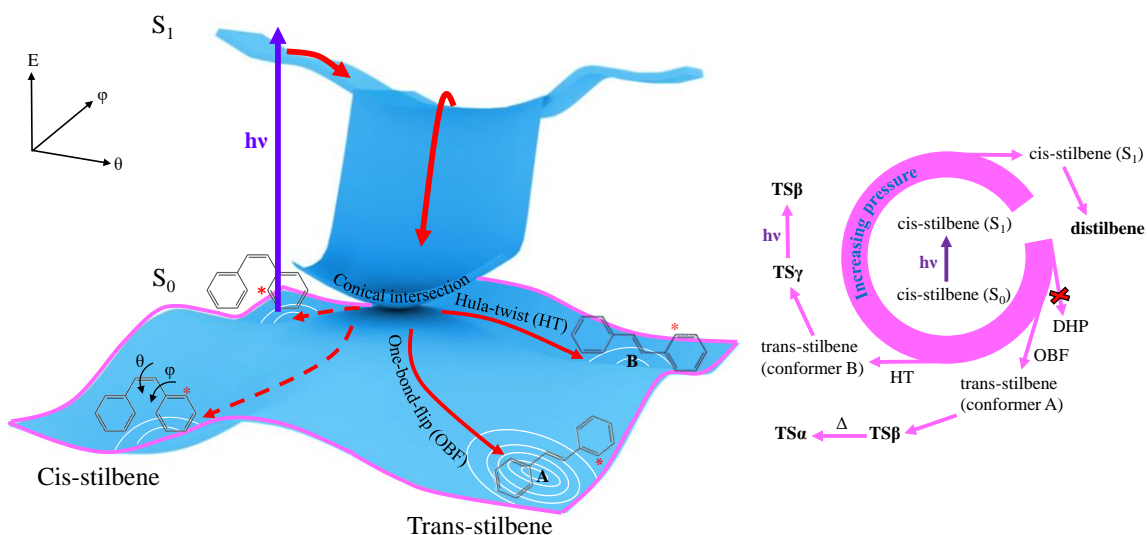
Scheme 5.2: The reaction mechanisms from cis-stilbene to each photoproduct at different pressures. The left is an illustration of the potential energy surfaces and molecular structures of cis/trans photoisomerization at electronic states S_0, S_1. Suggested surfaces and topology of the S_1/S_0 conical intersection show possible energy dissipation paths. The energy is not to scale. The structures corresponding to the minima of the lower surface S_0. On the right is the detailed reaction pathways and phase transitions as pressure increases. The dimerization of cis-stilbene producing distilbene at high pressure suggests pressure induces a significant horizontal displacement between the S_0 and S_1 potential energy surfaces, which eventually results in a cancellation of the conical intersection (CI) points. The cancellation of the CI switches non-adiabatic photoisomerization reactions (producing TSα, TSβ and TSγ) to the adiabatic photodimerization reaction (producing distilbene).

Moreover, the high pressures or high viscosity promoting cis/trans isomerization via the HT path could be fundamentally due to the PES displacement of the S_0 and S_1 states. For example, in scheme 5.2, a slight horizontal displacement of S_1 towards positive ϕ clearly favors the reaction via HT path. Such pressure effect is immediately revealed by the opening of the 2+2 photodimerization at the more drastic pressure. The 2+2

photodimerization reaction is known to be a reaction between the electronic excited molecule and neighboring molecule.[43] Thus, the reaction requires the energy of the excited cis-stilbene on the S_1 PES to be dissipate adiabatically (via fluorescence emission or reacting with neighboring species). However, we know that electronically excited cis-stilbene at ambient pressure dissipates energy non-adiabatically and the energy transfers from S_1 to S_0 via the CI (see scheme 5.2). The dimerization as the single reaction at 0.8 GPa suggests that the isomerization via the non-adiabatically energy dissipation must be closed at this pressure. This can only be achieved by a "disconnection" of the S_0 and S_1 surfaces (disappearance of the CI). Thus, the dominance of dimerization as pressure increases in the region 0.36-0.80 GPa suggests a pressure-induced horizontal displacement of the S_1 and S_0 of cis-stilbene. The higher the pressure, the larger the displacement, resulting in a slower isomerization and faster dimerization. At 0.8 GPa, the severe horizontal displacement "cancels" the CI and closes the isomerization. Consequently, no crystallization products (TSα, TSβ, TSγ) from cis/trans isomerization can be detected at this pressure. In addition, a vertical displacement along positive E (broadening of the energy gap) is not the case since the isomerization is proceeding when the dimerization is opened.

We further confirm the pressure-induced horizontal displacement of the two states experimentally. If the horizontal displacement is induced in the first place, the cis/trans isomerization would not happen when the sample is compressed to extremely high pressure. Without UV irradiation, we compress the sample up to 18.2 GPa. As shown in Fig. 5.4, the ν_8 (C_{ring}-C_{ring} s-stretching), ν_9 (C_{ring}-C_{ring} a-stretching) and C_{ring}-H stretching modes in 3000-3100 cm^{-1} blue-shift and become broad as pressure increases. Upon decompression, a broad IR absorption at 2900 cm^{-1} gradually appears. The recovered sample shows new IR peaks at 1583, 2917 cm^{-1} (blue asterisk) in contrast with the IR spectrum of liquid cis-stilbene. Thus, the reaction is induced when the maximum pressure is 18.2 GPa. In fact, when the maximum pressure is 12.5 GPa, the recovered sample starts

to have the weak IR absorption at 2917 cm^{-1} (Fig. 5.4) suggesting a lower threshold pressure. The two characteristic IR peaks are consistent with the IR signatures of the photoproduct distilbene at 0.8 GPa. Therefore, pure high pressure indeed can not induce isomerization suggesting the electronic states (S_1 and S_0) of cis-stilbene have been horizontally displaced.

Finally, the two polymorphic phases of trans-stilbene are produced for the first time. Since trans-stilbene crystal is a well-known scintillation material used for the detection of high-energy neutrons in the presence of strong gamma radiation,[44] producing trans-stilbene crystals by the photochemical liquid-to-crystal phase transition at high pressure could be an alternative to the traditional Bridgman melting technique. Moreover, the stilbene dimers, type I and II, have been photosynthesized from trans-stilbene in solution.[45-46] The production of type III, to our knowledge, is successfully achieved for the first time. Our results suggest that pressure is a very versatile tool to induce [2+2] photodimerization reaction and the photosynthesis of new stereoisomers that are prohibited by conventional methods at ambient pressure. Especially, [2+2] photodimerization, as a very important synthetic reaction,[47] can be used in the synthesis of natural products.[48,49] More importantly, by identifying those products and analyzing reactions kinetics, the effects of pressure on photochemical phase transitions are clearly presented. The evidence suggests that the horizontal displacement of S_1 and S_0 of cis-stilbene along configuration coordinates occurs under high pressure, in comparison with the reported vertical displacement of unsaturated hydrocarbons under pressure.[14,50,51]
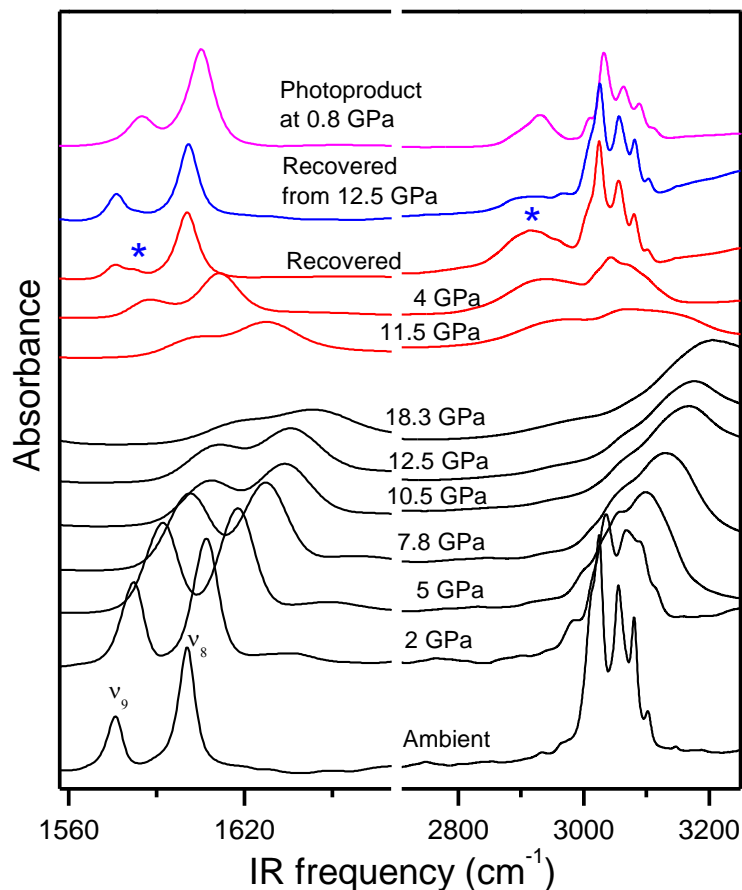
Figure 5.4: Selected FT-IR in the spectral region of 1560-3230 cm^{-1} of cis-stilbene collected upon compression (black lines) and decompression (red lines). IR spectrum of products recovered from 12.5 GPa (blue line) and IR spectrum of the photodimer (pink line) are also presented as comparisons. The results show that pressure induces dimerization of liquid cis-stilbene above 12.5 GPa. No evidence of crystallization and cis/trans isomerization can be found. These results further support the pressure-induced horizontal displacement of the electronic states.

5.4   Conclusion

In summary, we explore the pressure effects on the photochemical phase transitions of liquid cis-stilbene. Two polymorphs (β-form, γ-form) of crystalline trans-stilbene via different isomerization paths of cis-stilbene are produced as pressure increases. The trans-

stilbenes in the two crystals are pedal motionless at high pressure, unlike molecular motions in α-form obtained at ambient pressure. Under much higher pressures, a new reaction, [2+2] photodimerization pathway from cis-stilbene is induced, which leads to a recoverable liquid at ambient conditions. Those products are prohibited at ambient pressure and have not been reported previously. Furthermore, mechanism studies via reaction kinetics suggest that the selectivity of products is due to pressure-induced horizontal displacement of the electronically excited state S_1 and ground state S_0 of cis-stilbene. The higher the pressure, the larger the horizontal displacement. This finding is unprecedented, and the work provides sufficient evidence for this pressure effect. The observed pressure effects could potentially be used to tune the phase transitions of functional materials (e.g., the nematic-isotropic transition in liquid crystal) containing stilbene or azobenzene derivatives and access new phases from the dimerization reaction.

5.5   References

(1)   Tokura, Y. *Journal of the Physical Society of Japan* **2006**, *75*.
(2)   Nasu, K.; Ping, H.; Mizouchi, H. *Journal of Physics-Condensed Matter* **2001**, *13*, R693.
(3)   Bennemann, K. H. *Journal of Physics-Condensed Matter* **2011**, *23*.
(4)   Prasad, S. K.; Nair, G. G.; Rao, D. S. S. *Liquid Crystals* **2009**, *36*, 705.
(5)   Veesler, S.; Furuta, K.; Horiuchi, H.; Hiratsuka, H.; Ferte, N.; Okutsu, T. *Crystal Growth & Design* **2006**, *6*, 1631.
(6)   Okutsu, T. *Journal of Photochemistry and Photobiology C-Photochemistry Reviews* **2007**, *8*, 143.
(7)   Norikane, Y.; Uchida, E.; Tanaka, S.; Fujiwara, K.; Koyama, E.; Azumi, R.; Akiyama, H.; Kihara, H.; Yoshida, M. *Organic Letters* **2014**, *16*, 5012.
(8)   Semenov, A. L. *Physics of the Solid State* **2007**, *49*, 2303.
(9)   Xue, X.; Jiang, M.; Li, G. F.; Lin, X.; Ma, G. H.; Jin, P. *Journal of Applied Physics* **2013**, *114*.
(10)   Tong, X.; Wang, G.; Zhao, Y. *Journal of the American Chemical Society* **2006**, *128*, 8746.
(11)   Prasad, S. K.; Rao, D. S. S.; Jeyagopal, P. *Physical Review E* **2001**, *64*.
(12)   Iwai, S.; Yamamoto, K.; Hiramatsu, F.; Nakaya, H.; Kawakami, Y.; Yakushi, K. *Physical Review B* **2008**, *77*.
(13)   Badding, J. V. *Annual Review of Materials Science* **1998**, *28*, 631.

(14)   Ciabini, L.; Santoro, M.; Bini, R.; Schettino, V. *Physical Review Letters* **2002**, *88*.

(15)   Chelazzi, D.; Ceppatelli, M.; Santoro, M.; Bini, R.; Schettino, V. *Nature Materials* **2004**, *3*, 470.

(16)   Salzillo, T.; Bilotti, I.; Della Valle, R. G.; Venuti, E.; Brillante, A. *Journal of the American Chemical Society* **2012**, *134*, 17671.

(17)   Guan, J. W.; Song, Y. *Journal of Chemical Physics* **2016**, *144*.

(18)   Konieczny, K.; Bakowicz, J.; Turowska-Tyrk, I. *Crystengcomm* **2015**, *17*, 7693.

(19)   Konieczny, K.; Bakowicz, J.; Turowska-Tyrk, I. *Journal of Photochemistry and Photobiology a-Chemistry* **2016**, *325*, 111.

(20)   Klessinger, M.; Michl, J. *Excited states and photochemistry of organic molecules*; Wiley-VCH, 1995.

(21)   Robb, M. A.; Olivucci, M. *Journal of Photochemistry and Photobiology a-Chemistry* **2001**, *144*, 237.

(22)   Citroni, M.; Ceppatelli, M.; Bini, R.; Schettino, V. *Science* **2002**, *295*, 2058.

(23)   Fanetti, S.; Ceppatelli, M.; Citroni, M.; Bini, R. *Journal of Physical Chemistry B* **2011**, *115*, 15236.

(24)   Fanetti, S.; Ceppatelli, M.; Citroni, M.; Bini, R. *Journal of Physical Chemistry C* **2012**, *116*, 2108.

(25)   Citroni, M.; Bini, R.; Foggi, P.; Schettino, V. *Proceedings of the National Academy of Sciences of the United States of America* **2008**, *105*, 7658.

(26)   Nakamura, T.; Takeuchi, S.; Taketsugu, T.; Tahara, T. *Physical Chemistry Chemical Physics* **2012**, *14*, 6225.

(27)   Waldeck, D. H. *Chemical Reviews* **1991**, *91*, 415.

(28)   Tamai, N.; Miyasaka, H. *Chemical Reviews* **2000**, *100*, 1875.

(29)   Bao, J.; Weber, P. M. *Journal of Physical Chemistry Letters* **2010**, *1*, 224.

(30)   Minezawa, N.; Gordon, M. S. *Journal of Physical Chemistry A* **2011**, *115*, 7901.

(31)   Sension, R. J.; Repinec, S. T.; Szarka, A. Z.; Hochstrasser, R. M. *Journal of Chemical Physics* **1993**, *98*, 6291.

(32)   Dong, Z. **2012**.

(33)   Frisch, M.; Trucks, G.; Schlegel, H.; Scuseria, G.; Robb, M.; Cheeseman, J.; Scalmani, G.; Barone, V.; Mennucci, B.; Petersson, G. *Inc.: Wallingford, CT, USA* **2009**.

(34)   Hoekstra, A.; Meertens, P.; Vos, A. *Acta Crystallographica Section B: Structural Crystallography and Crystal Chemistry* **1975**, *31*, 2813.

(35)   Harada, J.; Ogawa, K. *Journal of the American Chemical Society* **2001**, *123*, 10884.

(36)   Harada, J.; Ogawa, K. *Journal of the American Chemical Society* **2004**, *126*, 3539.

(37)   Harada, J.; Ogawa, K. *Chemical Society Reviews* **2009**, *38*, 2244.

(38)   Bao, J.; Weber, P. M. *Journal of the American Chemical Society* **2011**, *133*, 4164.

(39)   Fuss, W.; Kosmidis, C.; Schmid, W. E.; Trushin, S. A. *Angewandte Chemie-International Edition* **2004**, *43*, 4178.

(40)   Yang, L. Y.; Harigai, M.; Imamoto, Y.; Kataoka, M.; Ho, T. I.; Andrioukhina, E.; Federova, O.; Shevyakov, S.; Liu, R. S. H. *Photochemical & Photobiological Sciences* **2006**, *5*, 874.

(41)   Liu, R. S. H. *Accounts of Chemical Research* **2001**, *34*, 555.

(42)   Liu, R. S. H.; Hammond, G. S. *Accounts of Chemical Research* **2005**, *38*, 396.

(43)   Loutfy, R.; Mayo, P. D. *Canadian Journal of Chemistry* **1972**, *50*, 3465.

(44)   Zaitseva, N.; Glenn, A.; Carman, L.; Martinez, H. P.; Hatarik, R.; Kapper, H.; Payne, S. *Nuclear Instruments & Methods in Physics Research Section a-Accelerators Spectrometers Detectors and Associated Equipment* **2015**, *789*, 8.

(45)   Fulton, J. D. *British Journal of Pharmacology and Chemotherapy* **1948**, *3*, 75.

(46)   Dunitz, J. D. *Acta Crystallographica* **1949**, *2*, 1.

(47)   Penn, J. H.; Gan, L. X.; Eaton, T. A.; Chan, E. Y.; Lin, Z. *The Journal of Organic Chemistry* **1988**, *53*, 1519.

(48)   Schreiber, S. L. *Science* **1985**, *227*, 857.

(49)   Alcaide, B.; Almendros, P.; Aragoncillo, C. *Chemical Society Reviews* **2010**, *39*, 783.

(50)   Drickame.Hg; Slichter, C. P.; Frank, C. W. *Proceedings of the National Academy of Sciences of the United States of America* **1972**, *69*, 933.

(51)   Bini, R. *Accounts of Chemical Research* **2004**, *37*, 95.

Chapter 6

6 Pressure-induced Amorphization and Reactivity of Solid Dimethyl Acetylene Probed by in situ FTIR and Raman Spectroscopy*

6.1 Introduction

High-pressure is a particularly attractive tool for performing mechanochemical synthesis of polymers without using catalysts and initiators[1]. At high pressures, polymerization of a molecular solid which contains unsaturated bonds is favored as the produced polymer possesses a reduced volume with saturated networks. In recent years, pressure-induced polymerization has been reported for several molecules such as ethylene,[2] cyanogen,[3] acetylene,[4-6] cyanoacetylene,[7,8] acrylic acid,[9] benzene,[10-12] styrene,[13] etc. In particular, polymerization of molecules with triple bonds (e.g., $C\equiv C$ or $C\equiv N$) is of enormous interest as the molecules can be used as a precursor to produce conjugated polymers. Currently, conjugated polymers are considered to be one of the most promising classes of smart materials for future technologies[14]. For instance, the electrical conductivity, optical absorption, or electrochemical properties of the conjugated polymers could be utilized as the sensing parameters in gas sensors based on their redox reactions with certain gases or vapors.[15] In addition, the ability of conjugated polymers to form the basic components required for solar energy conversion,[16] organic electronics and opto-electronics[17] is appealing to both basic research and practical applications in multiple fields, such as biophysics or sustainable energy.

Due to its simple structure, acetylene (HC≡CH) has been extensively studied as a prototype system in high-pressure solid-state polymerization of alkynes. It has been polymerized at room temperature from the orthorhombic phase (space group Cmca or D_{2h}^{18}, Z=2) at a pressure of 4.2 GPa without a catalyst.[6] Unfortunately, the recovered polyacetylene is not air-stable and reacts favorably with atmospheric moisture.[4] Alternatively, polymerization of substituted acetylenes has been considered because they could yield air-stable conjugated polymers.[18-20] Dimethyl acetylene or DMA (H_3C-C≡C-CH_3) is an example of such substituted acetylenes since steric effects of the substituting CH_3 groups may protect and stabilize the produced polymer. Moreover, once the liquid DMA molecules crystalize at low temperature or high pressure, the polymerization from the crystalline solid is interesting because the crystal lattice may guide the reaction to proceed along a preferential path following topochemical principles.[21] As a result, polymerization in the crystalline state could selectively provide us with a well-ordered polymeric structure. Crystal structures and phase transitions of DMA at low temperature have been widely investigated via various techniques, including X-ray diffraction, NMR spectroscopy, vibrational spectroscopy, and neutron diffraction.[22-29] It was found that liquid DMA freezes at 241 K and becomes a highly disorder solid (phase I). Upon further cooling, the phase I undergoes a phase transition at 154 K to a crystalline solid (phase II). Ibberson et al. reported that phase II has a monoclinic lattice (space group C2/m, Z=2) using neutron powder diffraction (with crystal structure shown in Fig 6.1).[29]
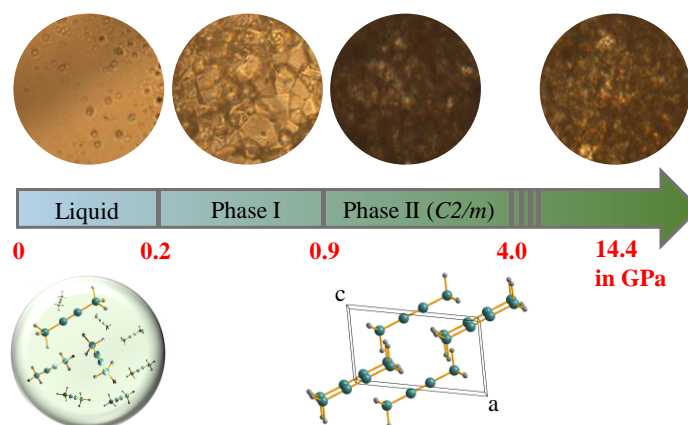
Figure 6.1: Microphotographs (~ 200 µm in diameter) of dimethyl acetylene (DMA) under high pressures: transparent liquid (0-0.2 GPa), transparent solid phase I (0.2-0.9 GPa) and opaque solid phase II (above 0.9 GPa). Graphs below are illustrations of the liquid and the crystal structure of phase II viewed along the b axis. In the phase II, the bright color at 14.4 GPa is due to the compression-reduced sample thickness that enhances the transmitted illumination.

In contrast, studies of DMA under high pressure are very sparse. So far, pressure-induced phase transitions of DMA have been studied by Raman spectroscopy only up to 4 GPa.[30] The Raman spectra showed a liquid-to-phase I transition at 0.2 GPa and phase I-to-II transition at 0.9 GPa. Moreover, no polymerization was observed in that pressure region, indicating that much higher pressure is required for the polymeric transformation. In fact, polymerization of DMA is rarely successful by conventional catalytic methods either. To our knowledge, polymerization of DMA has only been achieved with aid of a nickelocene based catalyst.[31] In this work, we compress DMA to much higher pressures (up to 24.4 GPa) and investigate the stability and reactivity of the sample via *in situ* FTIR and Raman spectroscopy. We here report the first successful polymerization of solid DMA using pure external compression at room temperature. The detailed transformation mechanism from phase II crystalline DMA to amorphous and polymeric phase is examined. Finally, the relations between pressure, concentration of crystal defects and polymerization are investigated via fluorescence analysis.

6.2 Experimental Section

Sample preparation. Dimethyl acetylene (purity ≥98% from Alfa Aesar) was purchased and used as obtained. High static pressure was generated by symmetric diamond anvil cells (DAC) equipped with a pair of type I and II diamonds with a culet size of 250 μm or 600 μm, which were used for Raman and IR measurements, respectively. Briefly, a ruby ball was first loaded into a hole with a diameter of 80 μm or 200 μm drilled on a stainless-steel gasket that was pre-indented to a thickness of 30-50 μm. Then the sample was cryogenically loaded into a DAC that was pre-cooled with dry ice because of the high volatility of the sample at room temperature (i.e., with boiling point of 27 °C). The pressure was measured by the shift of the R1 photoluminescence line of the ruby.

Micro-FTIR spectroscopy. For infrared (IR) absorption measurements, a customized IR micro-spectroscopy system that consists of a Fourier transform infrared (FTIR) spectrometer from Bruker Optics (model Vertex 80v) equipped with a Globar IR light source was used. The detailed instrumentations have been described elsewhere.[32] The system was operated under a vacuum of < 5 mbar, such that the absorption by H_2O and CO_2 was efficiently removed. The reference spectrum, i.e., the absorption of diamond anvils that was collected before the liquid sample was loaded, was divided as the background from each measurement. The spectral resolution used was 4 cm^{-1}.

Micro-Raman spectroscopy. *In situ* high-pressure Raman measurements were carried out with a customized Raman spectroscopy system. The 532 and 780 nm solid-state lasers were used as the excitation sources. The scattered light was then dispersed using an imaging spectrograph (SpectraPro-2500i, Acton Research Corporation) equipped with a 1200 line per mm grating achieving a 0.1 cm^{-1} resolution. The Rayleigh scattering was removed by wavelength specific edge filters. The Raman signal was recorded by an ultrasensitive liquid nitrogen-cooled back-illuminated charge coupled device (CCD) detector from Acton. The system was calibrated using neon lines with an uncertainty of ±1 cm^{-1}.

6.3   Results and Discussion

6.3.1 Effects of pressure on crystalline DMA up to 12 GPa

First, we load the liquid DMA into the DAC and compress it from 0.04 GPa. The microphotographs (Fig. 6.1) show obvious physical differences as pressure reaches the phase transition thresholds (0.2 and 0.9 GPa). Specifically, phase I in 0.2-0.9 GPa is a transparent solid whereas phase II above 0.9 GPa is an opaque solid. These phase transitions below 4 GPa were further verified by *in situ* FTIR and Raman spectroscopic measurements. Our results are in excellent agreement with previous reports[30,33] and thus no detailed discussion is necessary for this pressure region. We therefore collected IR and Raman spectra of DMA at slightly above 4 GPa (i.e., 4.1 and 4.7 GPa respectively) as the starting point and list the observed vibrational frequencies in Table 6.1. These frequencies are assigned and compared with previously reported values for phase II DMA measured at ambient pressure and low temperatures.[26,27] Evidently, the vibrational modes corresponding to C-H stretching (v_9, v_{13}, v_6, v_1) and C≡C vibration (v_2) are significantly blue-shifted (≥ 20 cm^{-1}) due to compression. Moreover, the two lattice modes observed for phase II which can be assigned to R_x, R_y lattice liberations suggest the DMA remains in a highly ordered crystalline structure.[27]

We then compress the DMA stepwise and collect the IR and Raman spectra at each pressure with selected IR spectra in the selected spectral region shown in Fig. 6.2. Evidently, the v_{11} mode exhibits a prominent splitting at 4.1 GPa. Moreover, as pressure increases, the v_{11} and v_{14} modes become broader. At 8.5 GPa, shoulder peaks appear for the IR modes. All these changes could indicate pressure-induced structural modifications, e.g., a phase transition following the selection rule. To verify the possible phase transitions, we examined the pressure dependence of the all major IR and Raman modes as depicted in Fig. 6.3. Other than the pressure-induced blue shift of all modes indicating bond stiffening upon compression, however, no discontinuity in pressure dependence of any characteristic IR or Raman mode up to 12 GPa was observed. More importantly, the two lattice modes exhibit a constant pressure coefficient and maintained their spectral profile indicating that phase II DMA remains in the monoclinic structure up to 12 GPa without pressure-induced phase transitions or chemical transformations.

Table 6.1: Assignment and Frequencies of Observed Raman and Infrared Modes of Solid Dimethyl Acetylene in Phase II.

Vibration number	Description[a]	IR (Ref.)[b]	IR (4.1 GPa)	Raman (Ref.)[b]	Raman (ref)[a]	Raman (4.7 GPa)
9	v (C-H)	2965 s	3003			
		2958 sh	2981			
13	v (C-H)			2964 ms	2960 s	3023
				2954 ms		2989
6	v (C-H)	2924 s	2944			
1	v (C-H)			2926 m	2921 s	2958
	$2v_{14}$	2862 m	2864		2863 m	
	$2v_3$		2760		2737 w	
	v_3+v_8	2536 vw	2390		2521 vw	
	$v_{15}+v_{14}$	2489 w	2364		2473 vw	
	v_3+v_{15}	2413 w	2348		2408 vw	
	$2v_8$			2309 s	2312 ms	2356
2	v(C≡C)			2231 vs	2236 s	2256
14	δ(CH$_3$)	1443 vs	1445		1448 m	
7	δ(CH$_3$)	1367 s	1364			
8	v (C-C)	1143 w	1153		1147 vw	
11	CH$_3$ rock	1045/1042 s	1051/1045	1044	1040 sh	1054
15	CH$_3$ rock			1037 m	1028 m	1036
4	v (C-C)			700 m	697 m	735
16	δ(C-C-C-C)			383 vs	378 vs	396
	R_y			138 s		258
	R_x			102 s		183

[a] From Ref. 27 measured at 10 K and ambient pressure.

[b] From Ref. 26 measured at 77 K and ambient pressure.
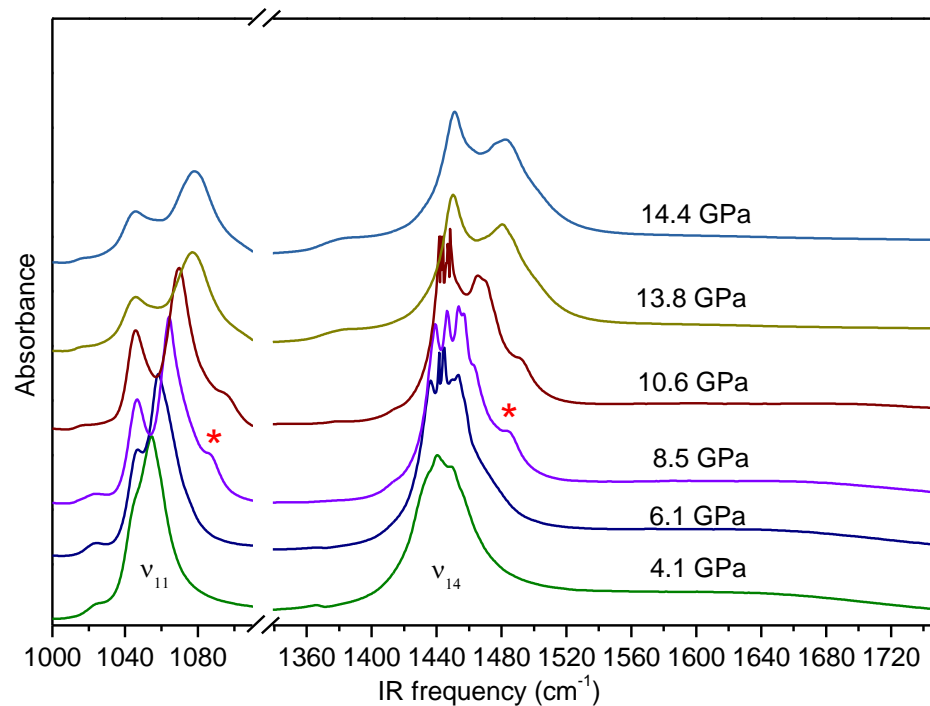
Figure 6.2: Selected spectral evolution of the IR modes ν_{11} and ν_{14} of DMA as function of pressure in the range of 4.1-14.4 GPa. The two IR shoulder peaks labeled with asterisk are observed at 8.5-10.6 GPa. The noisy feature of IR absorption ν_{14} is due to the signal saturation of IR absorption.
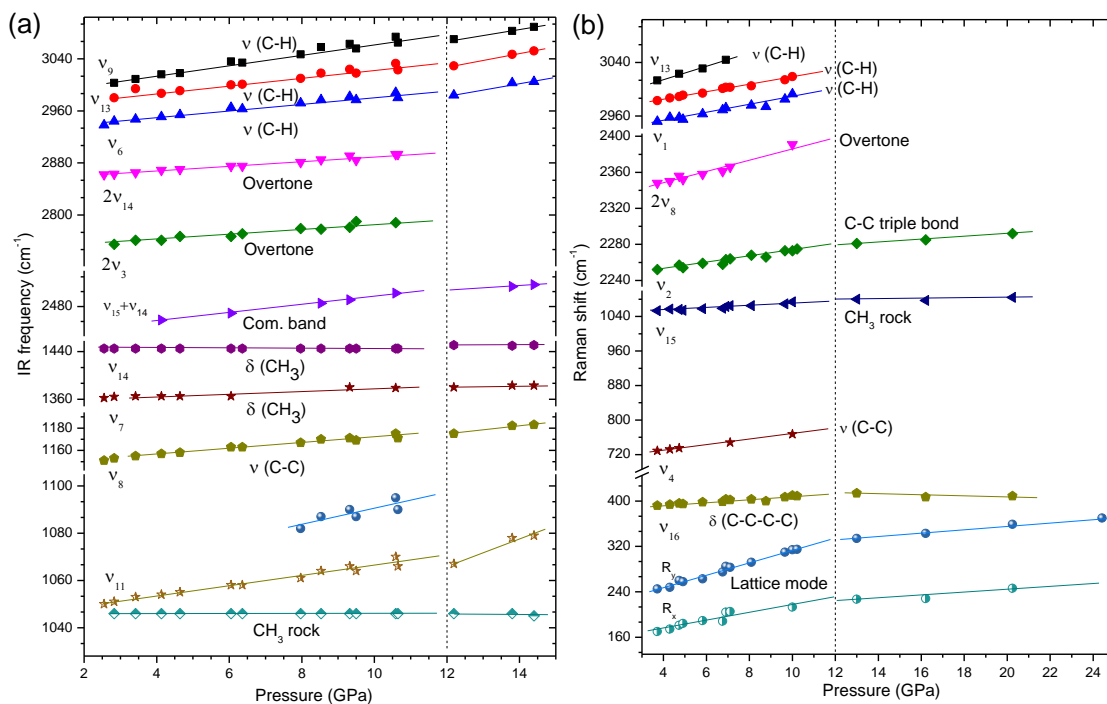
Figure 6.3: Pressure dependence of the observed (a) IR modes in the range 2-15 GPa and (b) Raman modes in the range 3-25 GPa. The assignments of these modes are also labeled in the figure. The vertical lines indicate the transformation threshold pressure (see text).

The v_{11} and v_{14} IR modes have been assigned to methyl rocking and deformation modes, respectively.[26,30] The IR mode v_{11} and the Raman mode v_{15} are fourfold degenerate as suggested by a recent high-resolution experiment.[34] Mohaček et al. reported the breaking of the fourfold degenerate (v_{11}/v_{15}) mode into two modes in phase II of DMA.[27] Further investigations from Baonza et al. concluded that the hindered rotation by the interaction of the methyl groups with the surrounding molecules has significant effect on the splitting of v_{15} starting from 2.6 GPa.[30] To better understand the changes in the methyl deformation and rocking modes appearing in the 1000-1500 cm^{-1} range, we provide a correlation diagram for phase II of DMA as shown in Table 6.2. It has been shown previously that the double group, G_{36}^{+}, is needed to describe the symmetry of non-rigid DMA molecule.[26] Thus, the irreducible representations for DMA are shown as equation 6.1.

$$\Gamma_{vib}^{G_{36}} = 4A_{1S}(Raman) + A_{3s}(Inactive) + 3A_{4s}(IR)$$

$$+4E_{1d}(IR/Raman) + 4E_{2d}(IR/Raman) \qquad (6.1)$$

According to the selection rule as shown in the Table 6.2, in phase II, the IR active E_{2d}, A_{4s} and E_{1d} modes could all split into $(A_u + B_u)$, respectively. Thus, significant correlation splitting from the degenerate modes (e.g., v_{11}) in phase II is expected. Upon compression, the broadening of the v_{11}, v_{14} lines indeed suggest a severe splitting of the degenerate modes. Additionally, the compression of phase II could only affect the site symmetry of the crystal, whereas the space group remained as the C2/m. For instance, the change from the C_i symmetry with 2 molecules to C_s symmetry with 2 molecules is allowed for the C2/m unit cell, according to site symmetries of space groups. Such site symmetry change can result in an equal number of lattice modes. This is supported by our observations that the no extra lattice modes appear up to 12 GPa. Moreover, the site effect is possible to cause further splitting of the degenerated modes and even activate the silent modes, e.g., A_{3s} mode. The latter could lead to the appearance of new IR peaks (e.g., at 8.5 GPa).

Table 6.2: Correlation diagram for solid DMA in phase II.

Point group		Site symmetry	Factor group	
G_{36}^+	D_{3d}	C_i	C_{2h}^3 (C2/m)	
A_{1s}	A_{1g}		A_g	Raman
	A_{2g}	A_g		
E_{2d}	E_g		A_u	IR
	A_{1u}			
A_{4s}	A_{2u}	A_u	B_g	Raman
E_{1d}	E_u		B_u	IR

Our results show that the phase II crystal structure of DMA is surprisingly stable at high pressure up to 12 GPa, in strong contrast to the stability of acetylene and its other derivatives. For instance, both acetylene and phenylacetylene are found to polymerize around 4 GPa.[6,20] As a disubstituted acetylene, the reaction threshold pressure for diphenyl acetylene via the C≡C bond was significantly higher (i.e., above 9 GPa) suggesting the steric hindrance from the aromatic substitutes, although the threshold pressure for chemical reactions via the phenyl rings was also found to be around 4 GPa.[18] Similarly, in case of DMA, a substantially higher threshold pressure (i.e., a minimum of

12 GPa) is expected for polymeric transformation likely due to a certain degree of rotational freedom of the methyl groups in the low-pressure region and the prominent steric hindrance imposed by both non-reactive methyl substituents.

6.3.2. Compression-induced amorphization and decompression-induced polymerization of the crystalline DMA

We then examined the threshold pressure that is required to induce structural or chemical transformations. Indeed, when compressed to higher pressures, e.g., above 14.4 GPa, DMA exhibits prominent changes in the pressure dependence of most of the characteristic Raman and IR modes (Fig. 6.3), even though the spectral profile only undergoes gradual changes with pressure. In particular, the IR modes ($2v_{14}$ and $2v_3$) and the Raman modes (v_{13}, v_1, $2v_8$ and v_4) are found to successively diminish above 12 GPa. These observations suggest structural disorder with contribution from the anisotropic compression as no pressure transmitting medium was used in the experiments. Moreover, as shown in Fig. 6.3(b) and Fig. 6.4, pressure-induced amorphization process initiated from the increasing structural disorder is rather sluggish, spanning from 12 GPa to 24.4 GPa. Above 12 GPa, the possibility of chemical reactivity of solid DMA is evidenced from the following detailed experimental observations. Firstly, when we compress the sample to pressures less than 12 GPa and release the pressure to ambient, liquid DMA is recovered suggesting a reversible pressure modification of the DMA below 12 GPa. Secondly, when the sample is compressed to higher pressures (e.g., 14.4 GPa and 24.4 GPa) and retained at these pressures for few days, we found no spectral changes indicating no reactivity or extremely slow reactions at high pressures. In contrast, when the pressure is released from 14.4 GPa to the ambient pressure, a solid product is recovered that is completely different than the initial sample (i.e., a transparent liquid). Moveover, upon the decompression from 14.4 GPa to 6 GPa, the IR spectrum shows broader IR peaks at 1400 and 1450 cm^{-1} (Fig. 6.5) as well as a new IR absorption at 1650 cm^{-1}, which can be assigned to C=C stretching vibrations indicating the formation of the sp^2 carbons. Finally, the IR spectrum of the recovered solid shows a totally different IR profile than that of initial DMA especially with the evident vibrational mode of C=C bond (labeled with asterisks in Fig. 6.5). A detailed analysis of the product will be

discussed below. Therefore, we can conclude that the amorphization of the crystalline phase II starts from 12 GPa and the decompression of the DMA sample from this threshold pressure is a necessary condition to induce chemical reactions.
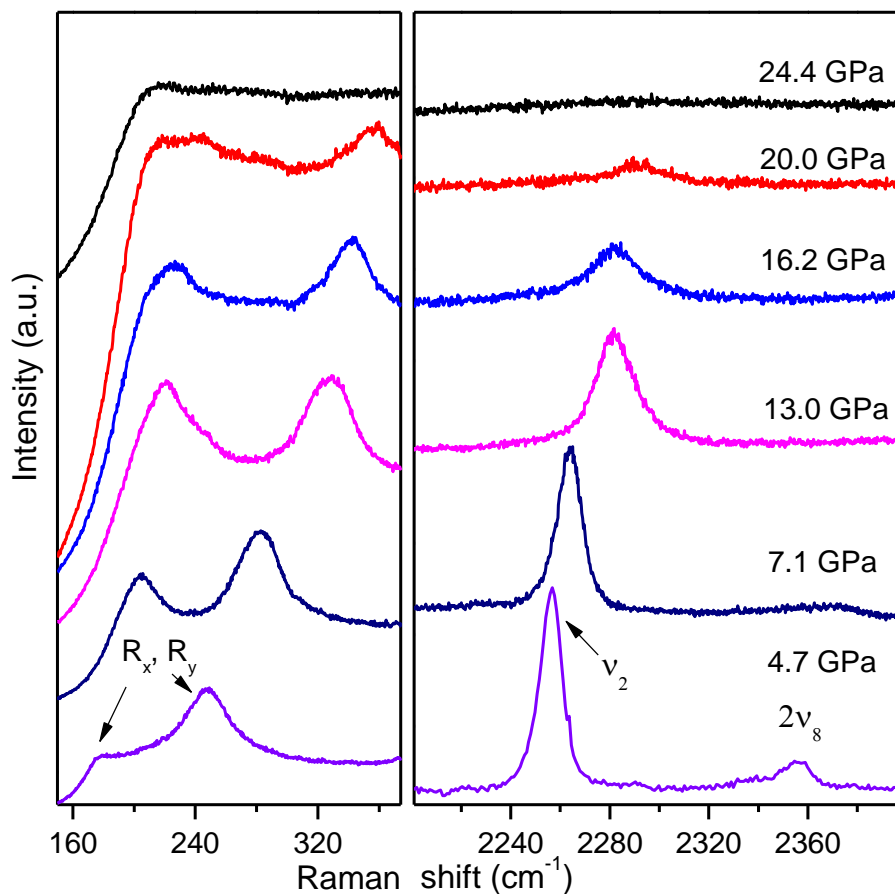
Figure 6.4: Phonon and selected intramolecular Raman spectra of DMA as function of pressure in the range of 4.7-24.4 GPa collected upon compression.
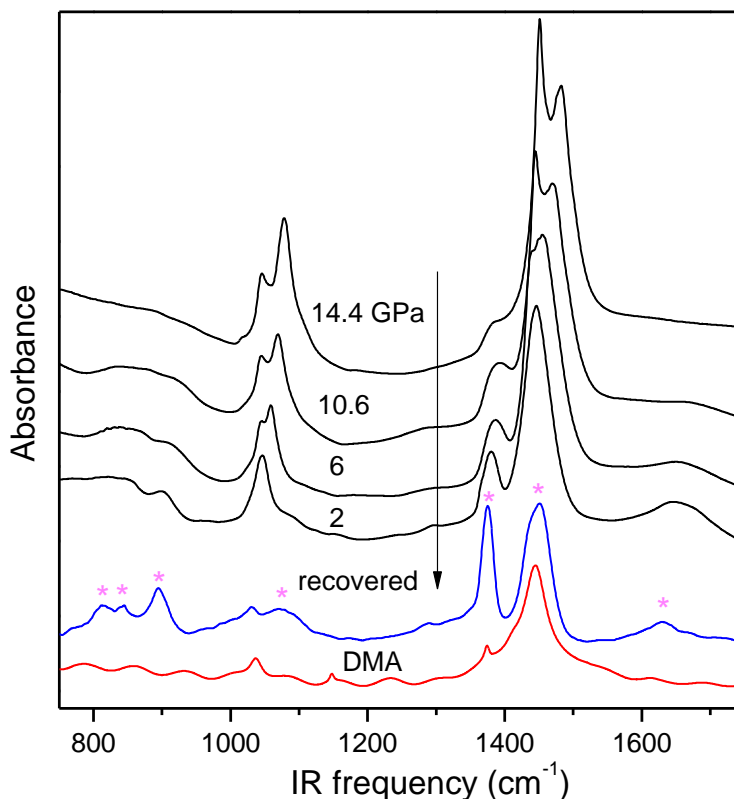
Figure 6.5: IR spectral evolution in the range of 750-1750 cm^{-1} collected upon decompression from 14.4 GPa. The IR spectrum of the recovered product show obvious differences (labeled by asterisks) compared to the IR spectrum of original DMA.

Knowledge of the activation volume and crystal defects are important aspects in understanding the high-pressure reactivity of a crystalline solid. Firstly, in contrast to the polymerization of analog unsaturated hydrocarbons that were induced in the compression cycle,[2,35] the polymeric reaction of solid DMA was induced in the decompression cycle, similar to some simple aromatic molecules such as benzene, furan, thiophene and pyridine reported previously (ref. 36 and refs therein). In these cases, the reaction occurring mainly on decompression indicates a positive activation volume for the formation of the extended reaction product. Secondly, studies of pyridine and benzene indicated that defects in the crystals played a fundamental role in driving the reaction.[37] The defects of crystals can be easily formed under nonhydrostatic pressure conditions,[38] and the concentration of crystal defects can be evaluated by the measurement of

fluorescence as a function of pressure.[37,38] Thus, considering the nonhydrostatic pressure conditions in the present experiments, we further examine the effects of crystal defects on the reactivity of crystalline DMA by analyzing the fluorescence intensity from the Raman spectra in three designed experiments, as described below.

   Specifically, we collected the Raman spectra on three separate loadings on compression to three different maximum pressures, i.e.., 10.22, 15.32 and 24.4 GPa, respectively, followed by decompression. We then analyzed the fluorescence intensity in a selected spectral region as a function of pressure (Fig 6.6). Due to the extremely intense fluorescence of the sample compressed to 24.4 GPa, we used 785 nm as the excitation source whereas 532 nm was used for the samples compressed to 10.22 and 15.32 GPa. All other experimental parameters are kept the same. As shown in Fig. 6.6, the fluorescence intensity is enhanced as pressure increases to 10.22, 15.32, 24.4 GPa, respectively. When the maximum compression pressure (e.g., 10.22 GPa) is less than the reaction threshold pressure (i.e., ~ 12 GPa), a reversible fluorescence level was observed during the pressure annealing cycle despite some hysteresis (Fig 6.6(a)). In contrast, fluorescence intensity is irreversibly modified during the compression-decompression cycles with maximum pressures of 15.32 and 24.4 GPa corresponding to the irreversible transformation to solid products at these pressures that enhance the fluorescence intensity. Compared to the pressure annealing cycle to 15.32 GPa, where unreacted DMA is recovered together with polymeric product, the dramatically enhanced fluorescence intensity observed when the sample is decompressed from 24.4 GPa to 3 GPa suggests that the transformation is completed at this pressure and the fluorescence is entirely attributed to the fluorescence emission of the reaction product (Fig. 6.6(c)). The enhancement of the fluorescence intensities upon compression and irreversible behavior upon decompression suggest that crystal defects caused by the non-hydrostaticity and the pressure-induced structural disorder lead to the formation of excimers. This is consistent with the conclusions from recent fluorescence studies of anthracene and pyridine under high pressures[37,38] that excimer formation occurs at crystal defects and the intensity of fluorescence can be enhanced by pressure due to the increasing concentration of defects. Consequently, the high concentration of defects irreversibly produced at 24.4 GPa may efficiently induce chemical reactions with a relatively high yield.
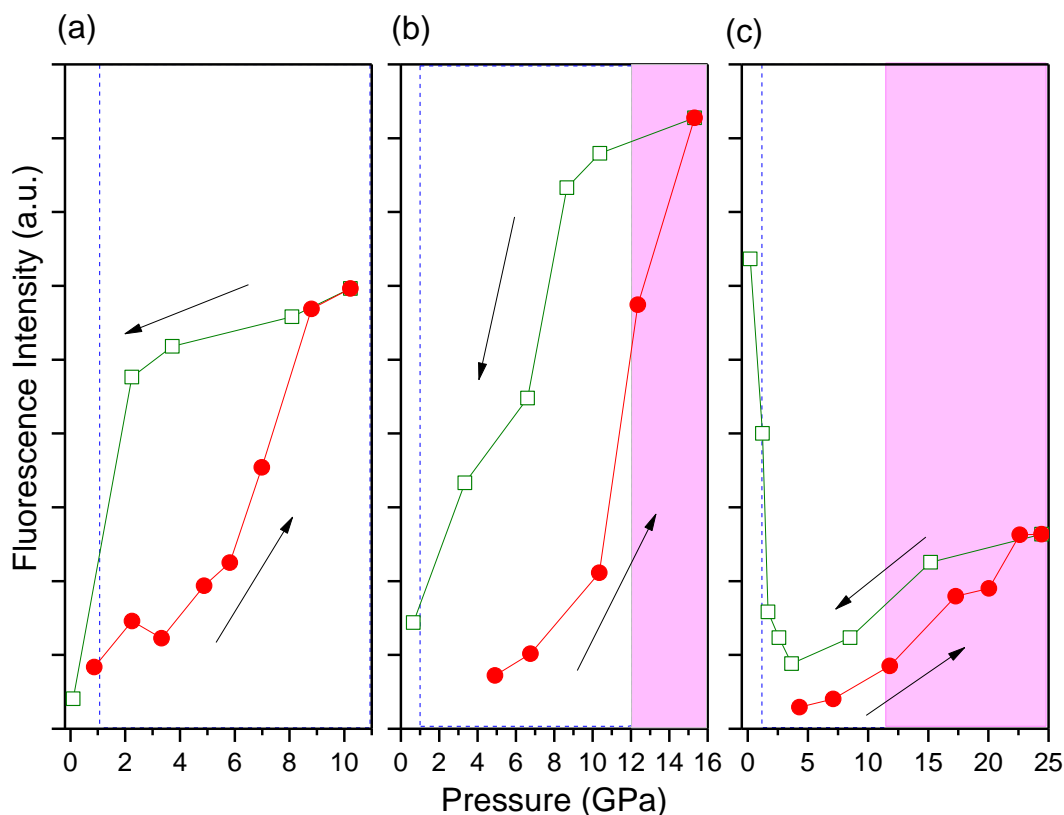
Figure 6.6: Fluorescence intensities of the selected spectral region upon compression (solid circles) and decompression (open squares) to three different pressures (a) 10.22 GPa, (b) 15.32 GPa and (c) 24.42 GPa. The vertical dashed line at 0.9 GPa denotes the pressure that liquid DMA transforms to crystalline phase II. The shaded area indicates the pressure region where the amorphization of the crystalline phase II starts at 12 GPa and completes at higher pressures.

6.3.3. IR and Raman spectra of the recovered polymers

To analyze structures of the decompression-synthesized polymeric products, major IR absorption frequencies of the products are listed in Table 6.3 in comparison with the IR frequencies of a poly(DMA) synthesized by Stanislaw et al. using a nickelocene based catalyst.[31] The reported poly(DMA) has 12-25 monomeric molecular units in the conjugated chains based on the molecular weight. Table 6.3 shows that the IR frequencies of the synthesized polymeric DMA in our study are mostly consistent with the reference values with only minor differences (e.g., at 894 cm^{-1}). Some other

differences include the IR absorption for the C=C stretch mode of the polymer recovered from 14.4 GPa that is observed at a lower frequency of 1630 cm^{-1} than the reference value (i.e., 1664 cm^{-1}), but observed at higher frequency (i.e., 1687 cm^{-1}) when the polymer is produced by compression to and decompression from 24.4 GPa.

Table 6.3: IR frequencies of polymerization products recovered from 14.4 and 24.4 GPa in comparison with those of poly(DMA) synthesized catalytically.

IR Frequency (cm^{-1})		
14.4 GPa	24.4 GPa	Ref. 31
814	814	800 (s)
844	844	846 (s)
894	892	
1030	1034	1020 (s)
1074	1076	1093 (s)
1285		1261 (s)
1375	1375	1380 (m)
1450	1450	1446 (m)
1630	1687	1664 (w)
2875	2876	2882 (w)
2920	2930	2905 (s)
2962	2963	2963 (s)

The IR profile and frequencies provide a fingerprint of the recovered products. First, the consistency between the IR absorption frequencies of our products and the poly(DMA) suggest that the recovered products contain poly(DMA). Secondly, any minor discrepancies could be due to either structural differences of polymers or additional reaction products (e.g., amorphous hydrogenated carbon *a*-C:H). In the former case, polymers of DMA produced at different pressures may have different structures and are also different from that produced catalytically. In terms of polymer structures, multiple characteristics are of great importance, for example, conjugated chain length, the chain conformations, polymer architecture (cross-linking), tacticity and the crystallinity of the polymer, etc. The Raman spectra of the recovered sample exhibit no lattice modes below 300 cm^{-1} suggesting that polymers synthesized by high-pressure at room temperature are amorphous solids. In the latter case, pressure-induced amorphization may produce amorphous hydrogenated carbon materials, causing those additional IR peaks (e.g., 894 cm^{-1}). The amorphous hydrogenated carbon has been identified as the product of pressure-induced benzene amorphization where the reaction occurred mainly upon decompression.[11] Finally, we found that the recovered solid products containing

poly(DMA) is stable in the air as evidenced by the identical IR absorption spectrum collected from the recovered sample after being exposed in air for a few weeks. This superior chemical stability compared to the air sensitive poly(acetylene) makes poly(DMA) a highly appealing conjugated polymer for practical application.

6.4 Conclusions

In summary, *in situ* high pressure FTIR and Raman spectroscopy were used to investigate the structures and transformations of DMA in a diamond anvil cell up to 24.4 GPa at room temperature. We found that DMA remains in the crystalline phase II and chemically stable up to 12 GPa. Above this pressure, amorphization was initiated and the process was rather sluggish, spanning from 12 GPa to 24.4 GPa. The reactivity from solid DMA can be unambiguously identified during the decompression process with a minimum compression pressure of 14.4 GPa. *In situ* florescence analysis suggests excimer formation occurs at crystal defects, which subsequently induce the chemical reactions. The vibrational spectral analysis suggests the recovered products mainly contain amorphous poly(DMA) with possible additional amorphous hydrogenated carbon. Our findings provide important insight into the production of conjugated polymeric materials under controlled conditions with high efficiency by pure external compression.

6.5 References

(1)   Bini, R.; Schettino, V. *Materials under extreme conditions: molecular crystals at high pressure*; World Scientific, 2013.
(2)   Chelazzi, D.; Ceppatelli, M.; Santoro, M.; Bini, R.; Schettino, V. *Journal of Physical Chemistry B* **2005**, *109*, 21658.
(3)   Yoo, C. S.; Nicol, M. *Journal of Physical Chemistry* **1986**, *90*, 6732.
(4)   Sun, J. M.; Dong, X.; Wang, Y. J.; Li, K.; Zheng, H. Y.; Wang, L. J.; Cody, G. D.; Tulk, C. A.; Molaison, J. J.; Lin, X. H.; Meng, Y. F.; Jin, C. Q.; Mao, H. K. *Angewandte Chemie-International Edition* **2017**, *56*, 6553.
(5)   Trout, C. C.; Badding, J. V. *Journal of Physical Chemistry A* **2000**, *104*, 8142.
(6)   Sakashita, M.; Yamawaki, H.; Aoki, K. *Journal of Physical Chemistry* **1996**, *100*, 9943.
(7)   Aoki, K.; Kakudate, Y.; Yoshida, M.; Usuba, S.; Fujiwara, S. *Journal of Chemical Physics* **1989**, *91*, 778.
(8)   Khazaei, M.; Liang, Y. Y.; Venkataramanan, N. S.; Kawazoe, Y. *Physical Review B* **2012**, *85*.
(9)   Murli, C.; Song, Y. *Journal of Physical Chemistry B* **2010**, *114*, 9744.

(10)   Ciabini, L.; Santoro, M.; Gorelli, F. A.; Bini, R.; Schettino, V.; Raugei, S. *Nature Materials* **2007**, *6*, 39.

(11)   Ciabini, L.; Santoro, M.; Bini, R.; Schettino, V. *Journal of Chemical Physics* **2002**, *116*, 2928.

(12)   Cai, W. Z.; Dunuwille, M.; He, J. G.; Taylor, T. V.; Hinton, J. K.; MacLean, M. C.; Molaison, J. J.; dos Santos, A. M.; Sinogeikin, S.; Deemyad, S. *Journal of Physical Chemistry Letters* **2017**, *8*, 1856.

(13)   Guan, J. W.; Song, Y. *Journal of Chemical Physics* **2016**, *144*.

(14)   Reynolds, J. R. *Conjugated polymers: processing and applications*; CRC press, 2006.

(15)   Pei, Q. B.; Inganas, O. *Synthetic Metals* **1993**, *57*, 3730.

(16)   Cheng, Y.-J.; Yang, S.-H.; Hsu, C.-S. *Chemical reviews* **2009**, *109*, 5868.

(17)   Facchetti, A. *Chemistry of Materials* **2010**, *23*, 733.

(18)   Ceppatelli, M.; Fontana, L.; Citroni, M. *Phase Transitions* **2007**, *80*, 1085.

(19)   Santoro, M.; Ciabini, L.; Bini, R.; Schettino, V. *Journal of Raman Spectroscopy* **2003**, *34*, 557.

(20)   Dziubek, K.; Podsiadlo, M.; Katrusiak, A. *Journal of the American Chemical Society* **2007**, *129*, 12620.

(21)   Bernasconi, M.; Chiarotti, G. L.; Focher, P.; Parrinello, M.; Tosatti, E. *Physical Review Letters* **1997**, *78*, 2008.

(22)   Yost, D. M.; Osborne, D. W.; Garner, C. S. *Journal of the American Chemical Society* **1941**, *63*, 3492.

(23)   Pignataro, E.; Post, B. *Acta Crystallographica* **1955**, *8*, 672.

(24)   Miksic, M. G.; Segerman, E.; Post, B. *Acta Crystallographica* **1959**, *12*, 390.

(25)   Prasad, P. N.; Kopelman, R. *Chemical Physics Letters* **1973**, *20*, 513.

(26)   Butler, I. S.; Newbury, M. L. *Spectrochimica Acta Part a-Molecular and Biomolecular Spectroscopy* **1980**, *36*, 453.

(27)   Grosev, V. M.; Furic, K. *Journal of Molecular Structure* **1999**, *482*, 653.

(28)   Alefeld, B.; Kollmar, A. *Physics Letters A* **1976**, *57*, 289.

(29)   Ibberson, R. M.; Prager, M. *Acta Crystallographica Section B-Structural Science* **1995**, *51*, 71.

(30)   Baonza, V. G.; Montoro, O. R.; Taravillo, M.; Caceres, M.; Nunez, J. *Journal of Chemical Physics* **2004**, *121*, 11156.

(31)   Pasynkiewicz, S.; Oledzka, E.; Pietrzykowski, A. *Journal of Molecular Catalysis a-Chemical* **2004**, *224*, 117.

(32)   Dong, Z. H.; Song, Y. *Journal of Physical Chemistry C* **2010**, *114*, 1782.

(33)   Guan, J. W.; Daljeet, R.; Song, Y. *Canadian Journal of Chemistry* **2017**, *95*, 1212.

(34)   diLauro, C.; Bunker, P. R.; Johns, J. W. C.; McKellar, A. R. W. *Journal of Molecular Spectroscopy* **1997**, *184*, 177.

(35)   Aoki, K.; Usuba, S.; Yoshida, M.; Kakudate, Y.; Tanaka, K.; Fujiwara, S. *Journal of Chemical Physics* **1988**, *89*, 529.

(36)   Fanetti, S.; Citroni, M.; Bini, R. *Journal of Chemical Physics* **2011**, *134*.

(37)   Fanetti, S.; Citroni, M.; Bini, R. *Journal of Physical Chemistry B* **2011**, *115*, 12051.

(38)   Dreger, Z. A.; Lucas, H.; Gupta, Y. M. *Journal of Physical Chemistry B* **2003**, *107*, 9268.

Chapter 7

7 Highly Efficient and Selective Pressure-Assisted Photon-induced Polymerization of Styrene*

7.1 Introduction

The polymerization of styrene monomers has been very well established as the route to produce polystyrene, one of the most important polymeric materials in the world.[1] The annual consumption worldwide of polystyrene was reported ca. 1.15×10^7 ton.[2] Polystyrene has three different tactic polymeric chain structures. Successful commercial applications of amorphous atactic polystyrene (APS, shown in Fig. 7.1) as the most abundant polystyrene material are based on many factors, including its low cost, high clarity, good electrical properties, ability to be foamed, and its ease of polymerization. The discovery of isotactic polystyrene (IPS) and syndiotactic polystyrene (SPS), especially crystalline SPS, brought intense attention to this class of materials because the transition temperature of crystalline SPS ($T_m = 273$ $^{\circ}$C) is much higher than the glass transition temperature of APS ($T_g = 90$ $^{\circ}$C, Fig. 7.1), making it useful for many applications such as electrical and electronics, automotive, appliance, packaging, specialty films and fibers.[1]
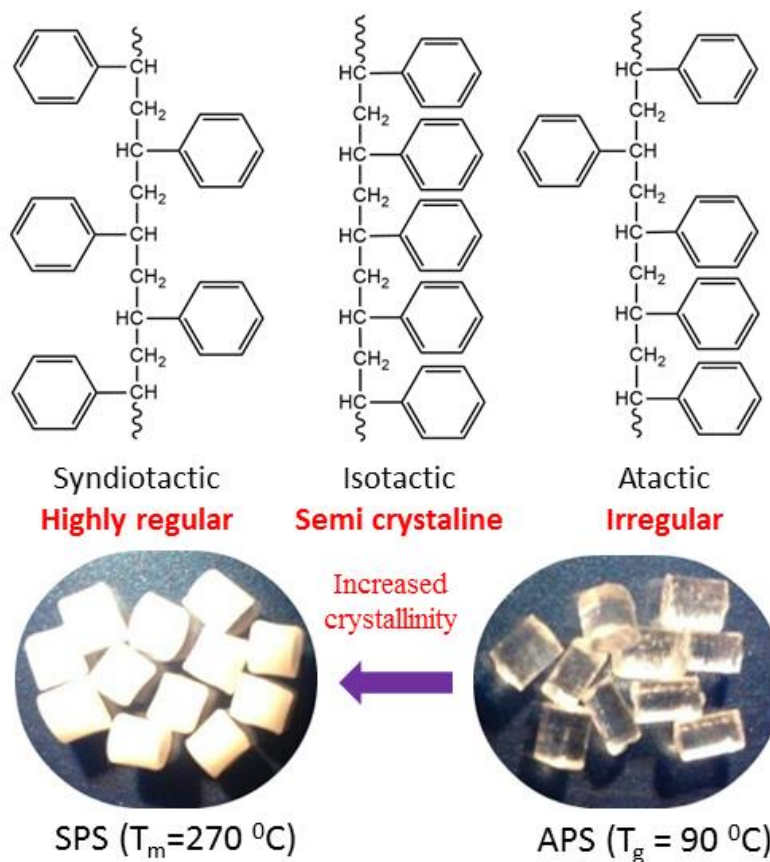
Figure 7.1: Structures and tacticity of polystyrene (top); physical appearances and properties of different polystyrene (bottom). The average size of the granules in both photos is ~3 mm.

Polystyrene can be synthesized from monomeric styrene by radical, cationic, or anionic mechanisms, where solvents, initiators and/or catalysts are required. In recent years, photoinitiated polymerization has received revitalized interest due to its wide range applications in coatings, adhesives, inks, printing plates, and optical waveguides.[3] Numerous cleavage and H-abstraction types of photoinitiators with different absorbance characteristics, quantum efficiencies, and solubilities are available.[4,5] In the case of photoinitiated polymerization of styrene, the cleavage type photoinitiators are preferred because of their low quenching rate of excited triplet states of the photoinitiators by styrene monomer.[6] A recent study by Kathleen et al. used two cleavage type photoinitiators to

explore photoinitiated bulk and emulsion polymerization of styrene.[7] Under UV or visible light radiation, it was found that photoreactions of bulk styrene at ambient conditions took as long as 150 h for the initiator-free bulk polymerization to accomplish 80% conversion. With the best photoinitiator, it still took at least 30 h to obtain a same conversion ratio.

Pressure, as one of three principal thermodynamic variables, has been established to be an effective factor for influencing photoreaction kinetics, as well as for modifying the properties of the final product.[8-21] The reactive species from the photoexcitation of the sample can be particularly aggressive from a chemical point of view and, depending on their lifetime and free mean path, can substantially facilitate the initiation and propagation of a reaction. Furthermore, photoreactions become more efficient when combined with other conditions, such as increasing pressures, because the increasing density of the materials at high pressure results in reduced intermolecular distances that favor the interaction between excited and ground state molecules. The efficiency of these processes has been attested by several reactions occurring in pure condensed unsaturated hydrocarbons initiated by UV or visible irradiations. For instance, studies of ethylene,[22] acetylene[8] and butadiene[10] show that the high reaction threshold pressure required in stress-induced polymerization of these unsaturated compounds can be significantly lowered by introducing laser irradiation.

The pressure threshold for monostyrene to polystyrene conversion was reported to be as high as 15 GPa at room temperature.[23] In this study, the possibility of producing polystyrene from styrene as the monomer using photon-assisted polymerization was examined. Here we report a highly efficient and selective polymerization process characterized by a near-perfect reaction yield, significantly improved reaction rate, and much less drastic pressure conditions observed under the current experimental scheme. Furthermore, since this method is based on physical synthesis (i.e., no solvent, no initiators, and catalysts-free), which represents an interesting perspective for green chemistry, it

makes the production of useful polystyrene in an alternative way very appealing. Overall, pressure as a thermodynamic variable also provides us a window that allows the probing of possible polymerization mechanisms of liquid and solid styrene in-depth. The analyses provide new insights into the understanding of the polymerization process of styrene under these special conditions.

7.2 Experimental Section

A symmetric diamond anvil cell (DAC) equipped with a pair of type II diamonds with a culet size of 600 μm was used in the experiment. The liquid styrene (purity ≥99.9% from Sigma Aldrich) along with a ruby ball was loaded into a hole with a diameter of 100─200 μm drilled on a stainless steel gasket that was pre-indented to a thickness of 30─50 μm. The pressure was determined using the well-established ruby fluorescence method while irradiation of the sample by the the excitation laser was avoided. Multiple loadings were done with different initial loading pressures (e.g., 0.02, 0.1, 0.28, 0.34, 0.67, 1.26, and 2.34 GPa) to explore the pressure effects on photopolymerization reactions.

Upon loading, the high pressure reactions were subsequently triggered by focusing the multi-line UV emission with a peak wavelength at ~ 350 nm of an argon ion laser onto the sample with a beam size of ~ 40 μm in diameter and a power ranging from 35 to 300 mW. The reaction progress was monitored by Fourier transform infrared (FTIR) spectroscopy with IR absorption spectra collected at appropriate time intervals. The reactions were considered to complete when no further spectral changes with time were observed. The IR spectra of commercial polystyrene were collected as a spectral comparison with the IR spectra of the final products. Atactic polystyrene was purchased from Goodfellow Cambridge, Ltd and syndiotactic polystyrene was provided by Idemitsu Kosan, Co. Ltd, Japan.

For IR absorption measurements, a customized IR micro-spectroscopy system consisting of a FTIR spectrometer from Bruker Optics (model Vertex 80v) equipped with a Globar IR light source was used. The detailed instrumentations have been described elsewhere.[24] The system was operated under a vacuum of < 5 mbar, such that the absorption by H_2O and CO_2 was efficiently removed. The variable aperture equipped on the IR microscope allows area-selected IR absorption measurement on different part of the sample or as a whole. This allows IR measurements on only the UV-irradiated areas of samples to exclude unreacted regions due to the UV beam being smaller in size than the entire sample. The reference spectrum, i.e., the absorption of diamond anvils that was collected before styrene samples were loaded, was divided as the background from each measurement. The spectral resolution used was 4 cm^{-1}.

7.3   Results and Discussion

7.3.1 Reaction evolution of liquid styrene loaded at 0.1 GPa upon UV radiation

The reaction evolution with different loading pressures shows similar IR spectral changes with time except for the different reaction completion times. Herein, the reaction process monitored by IR spectra for the sample with an initial loading pressure at 0.1 GPa is selected as a representative as shown in Fig. 7.2. The purity of the sample was first checked by the IR absorbance measurement and the assignment of IR bands of pure styrene was listed in Table S1.[40] As shown by the selected IR spectra in Fig. 7.2(a) and 7.2(b), when the liquid styrene is irradiated by the 350 nm UV laser with a power of ~35 mW, a new IR peak at 2900 cm^{-1} appears at 15 min, indicating that the reaction can be efficiently induced with even low laser power.
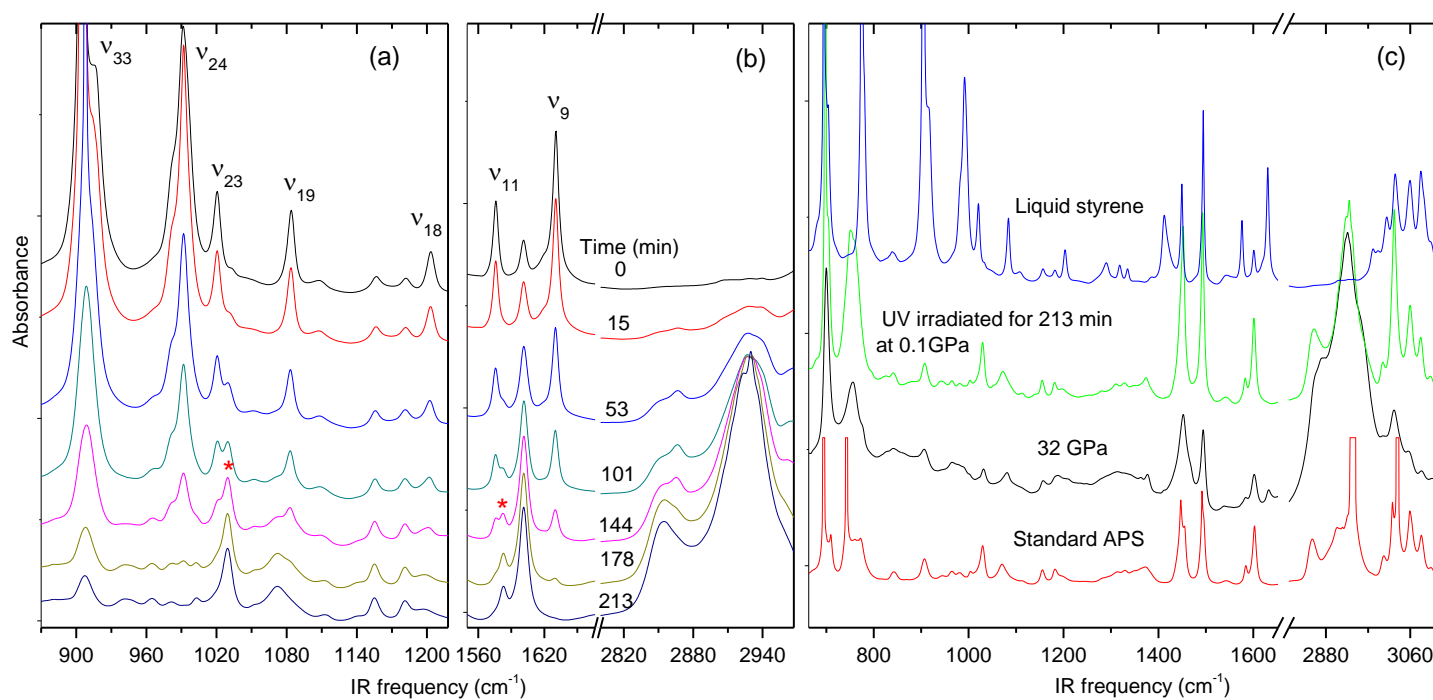
Figure 7.2: Selected FTIR spectra of styrene with an initial loading pressure of 0.1 GPa upon multi-line UV irradiation (with peak UV wavelength of 350 nm and power of 35 mW) collected as a function of time in the spectral region of 870 - 1225 cm^{-1} (a) and 1545-2970 cm^{-1} (b). Comparison of IR spectra for liquid styrene (blue), photoproducts after 213 min UV irradiation (green), pressure-induced products collected at 32 GPa (black) and commercial standard APS (red) collected at ambient condition is shown in panel (c).

Upon further irradiation, several IR bands (e.g. 905 (v_{33}), 991 (v_{24}), 1021 (v_{23}), 1082 (v_{19}), 1204 (v_{18}), 1576 (v_{11}) and 1631 (v_9) cm^{-1}) that belong to styrene monomer are gradually weakened while new peaks (e.g. 1030, 1583 cm^{-1} and those in range of 2800-3000 cm^{-1}) are intensified. Among them, the most significant change is the gradual disappearance of the v_9 mode (assigned as C_e=C_e stretch of the vinyl group) at 1631 cm^{-1}, the most characteristic IR band of the styrene monomer. After 213 min radiation, this band is barely visible, which indicates the near complete consumption of the monomer and thus the completion of the photoreaction. Fig. 7.2(c) shows the full IR spectrum of final products in comparison with that of the commercial APS. Convincingly, the IR spectrum of the final product is consistent with the one collected from the commercial APS. Therefore, the UV photon-induced reactions of liquid styrene with a 0.1 GPa initial loading pressure mainly produce the plastic APS.

According to Gourdain *et al.*, the pure pressure-induced chemical reaction also gives rise to the polymerization of styrene monomers, where the reaction yield was reported to be 85% at 32 GPa.[23] We reproduced the experiment of Gourdain *et al*. by applying pressure only without laser irradiation and depict the IR spectrum of the recovered products from 32 GPa in Fig. 7.2(c). It can be seen that pure pressure induced polymerization can give the same products (i.e., APS) as the photopolymerization. The broad and intense absorption profile in the 2800-3000 cm^{-1} spectral region compared to the standard APS sample is likely due to the amorphous nature of the polystyrenes obtained by a different method rather than the decomposition into benzene, consistent with the observation by Gourdain *et al*. that the phenyl group remains stable at this pressure. However, in contrast to the pure pressure-induced polymerization, the photon-assisted polymerization requires much less drastic pressure conditions and offers nearly 100% polymerization yield (PY).

7.3.2 Pressure selectivity in photon-induced polymerization of styrene

In order to check the pressure effects on the polymerization process, styrene samples were loaded with different initial pressures. As shown in Fig. 7.3(a), the IR spectra of the final polymerization products are collected from the samples with the initial loading pressure at 0.02, 0.13, 0.34, 0.85 GPa, respectively. At 0.1 GPa and room temperature, styrene is in the liquid phase, while it freezes into a solid phase at 0.3 GPa.[23] Thus, above 0.3 GPa, photopolymerization occurs in the solid phase. Polystyrene with different tacticity, which has a significant influence on the physical properties of the polymer, has been chemically synthesised successfully in three types[1,25] (i.e., atactic, isotactic, and syndiotactic as shown in Fig. 7.1). The top two IR spectra depicted in Fig. 7.3(a) represent the crystalline SPS and amorphous APS. By comparison, the formation of SPS in our experiments can be ruled out at any initial loading pressures due to the missing of the characteristic IR peak at 1222 cm^{-1}.[26,27] At the loading pressure of 0.02 GPa, the IR spectrum of the polymerization products shows a shoulder peak at 1052 cm^{-1} (labeled with an asterisk in Fig. 7.3(a)) preceding the major broad IR band at 1075 cm^{-1}, the frequency and profile of which are both characteristic of APS. Close examination of the broad peak at 1075 cm^{-1} by deconvolution reveals two peaks at 1070 and 1083 cm^{-1}. The IR bands at 1052 and 1083 cm^{-1}, which are very characteristic peaks to identify the IPS as compared with the reference spectra in Fig. 7.3(c),[27] suggest the formation of small amount of IPS at low loading pressures. The spectral analysis of the IR profiles at 0.13 and 0.34 GPa gives similar results as 0.02 GPa. In contrast, the IR profile at 0.85 GPa shows no IR signatures of IPS (Fig. 7.3(b)) and thus APS is the sole product at this pressure. These observations strongly suggest pressure selectivity of tacticity during the polymerization process of styrene.
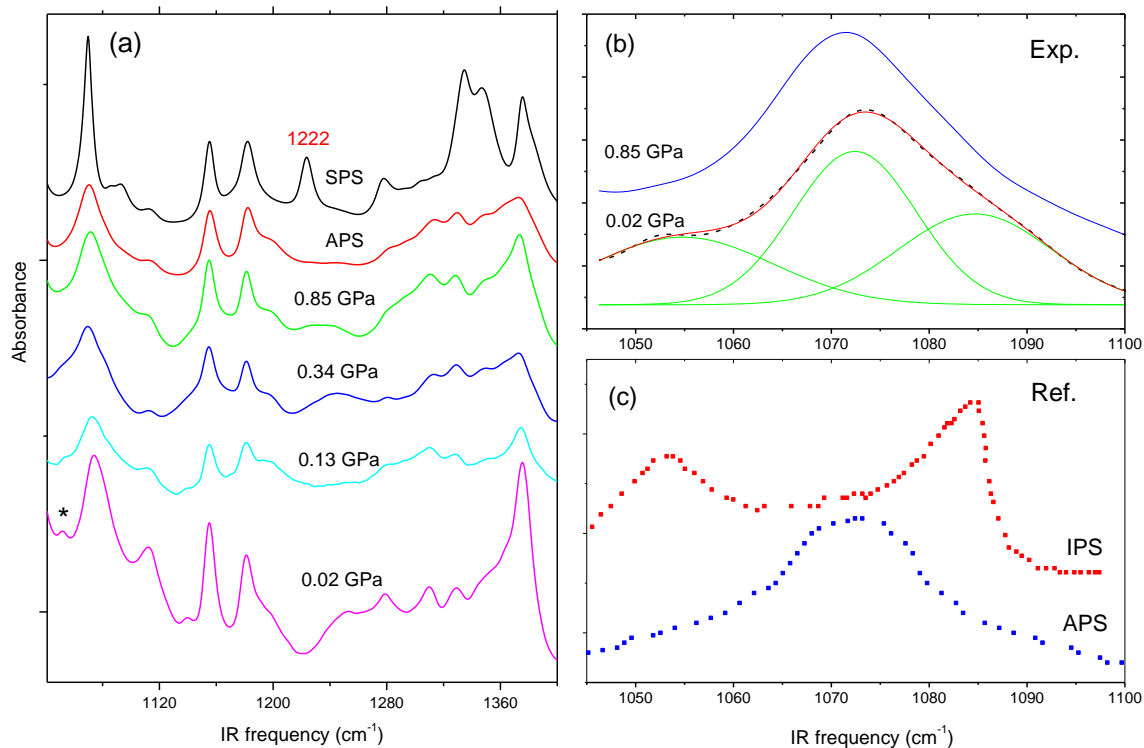
Figure 7.3: (a) Selected FTIR spectra of the final photo-polymerization products recovered from samples with different initial loading pressures (labeled in the figure) and radiation time. The asterisk labels the peak at 1052 cm^{-1}. (b) The comparison of the IR spectra between the recovered samples with initial loading pressure of 0.02 GPa (red) and 0.85 GPa (blue) in the spectral region of 1040-1100 cm^{-1}, with the deconvoluted profile (green solid lines and black dashed line) for the former spectrum shown below. (c) The standard IR spectra of pure IPS and APS in the same spectral region reproduced from ref. 27.

7.3.3 Photon-induced polymerization kinetics

The evolution of the characteristic bands of monomer and polymer can be monitored to keep track of the polymerization progress. In particular, during the polymerization of styrene monomers via the vinyl group, C=C double bonds are broken and C-C single bonds are formed. Consequently, quantitative kinetics information of polymerization reactions

can be obtained from the IR spectral evolution, in particular, the decrease in intensity of vibrational band associated with $C_e=C_e$ vinyl stretching vibration at 1631 cm^{-1}. The PY at the time t, or fraction of polymerized component, can be determined according to

$$PY(t) = 1 - \frac{(I_{C=C})_t}{(I_{C=C})_{t=0}} \qquad (7.1)$$

where $I_{c=c}$ is the integrated intensity of the characteristic bands of styrene at 1631 cm^{-1}. In Fig. 7.4, the PY as a function of radiation time for each sample with different initial loading pressure is plotted. For the sample loaded at 0.02 GPa, a laser power of 300 mW was used due to the very slow reaction rate at low laser power while all the other samples were irradiated by a laser power of 35 mW. With increasing initial loading pressure, obviously, the reaction completes sooner until 0.67 GPa which suggests that the reaction can be accelerated efficiently by increasing the initial loading pressure. Beyond this pressure, such as at 1.26 and 2.34 GPa, however, the reactions seem to be deaccelerated, indicating that 0.67 GPa, a pressure at which styrene exists in solid phase, is a threshold pressure for maximum reaction rate. Acceleration of pressure-induced chemical reactions such as polymerizations or dissociations upon laser irradiation has been reported in literature for samples in both liquid and solid states.[8,12,21,22]
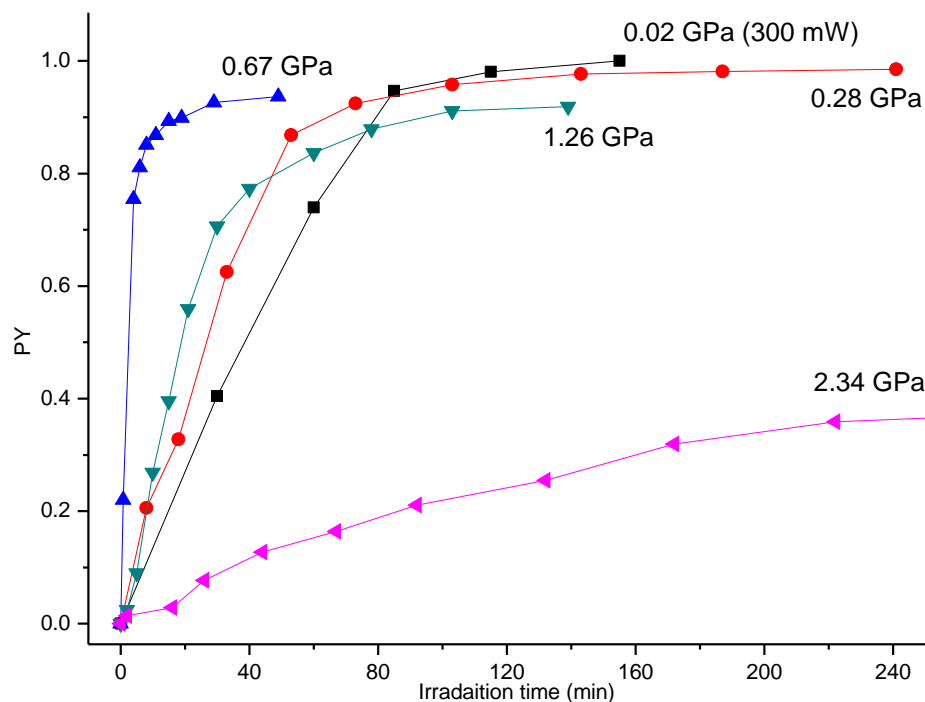
Figure 7.4: The polymerization yield (PY) of styrene samples with different initial loading pressures (labeled for each plot) as a function of UV irradiation time. The laser power of ~35 mW was used for all samples except the one with loading pressure of 0.02 GPa, for which the irradiation power was ~300 mW.

To better understand the roles played by the initial loading pressures, the polymerization kinetics can be further analyzed using the Avrami model[28,29]

$$PY(t) = PY_\infty[1 - \exp(-kt^n)] \qquad (7.2)$$

where $PY(t)$ and PY_∞ are the polymerization yield at time t and at the end of the polymerization process, k is the rate constant, and n is a parameter, whose value depends on the nucleation law and growth geometry. Regression of PY (t) data using Eqn. 7.2 are shown in Fig. S1 of the supporting information,[40] yielding the values of rate constant k, the parameter n as well as the polymerization yield PY_∞ as tabulated in Table S2[40] and plotted in Fig. 7.5. The similar values of parameter n (i.e., in the range of 1.0-1.6) obtained in these

experiments indicate that the growth geometry of the polymer chains is not strongly influenced by the laser irradiation intensity or pressure conditions. Originally, the Avrami equation was proposed to model crystal growth from a liquid phase and has been adapted later to polymerization processes.[8,30,31] According to this model, the values of n are expected to increase with the dimensionality of the process, ranging from 1 to 2 in the case of linear growth. If the one-dimensional growth is facilitated by diffusion, a value of n close to 0.5 would have been expected, as recently reported in the laser-assisted pressure-induced polymerization of solid acetylene[8] and 2-(hydroxyethyl)methacrylate.[20] The n values derived from our experiments close to 1─1.6 thus suggest the linear growth of styrene chains with little influence from the diffusion step. The low-dependence of long-range diffusion in the polymerization process of styrene has important implications such as the relatively long lifetime of the excited states of styrene in the initiation step, which will be discussed below.
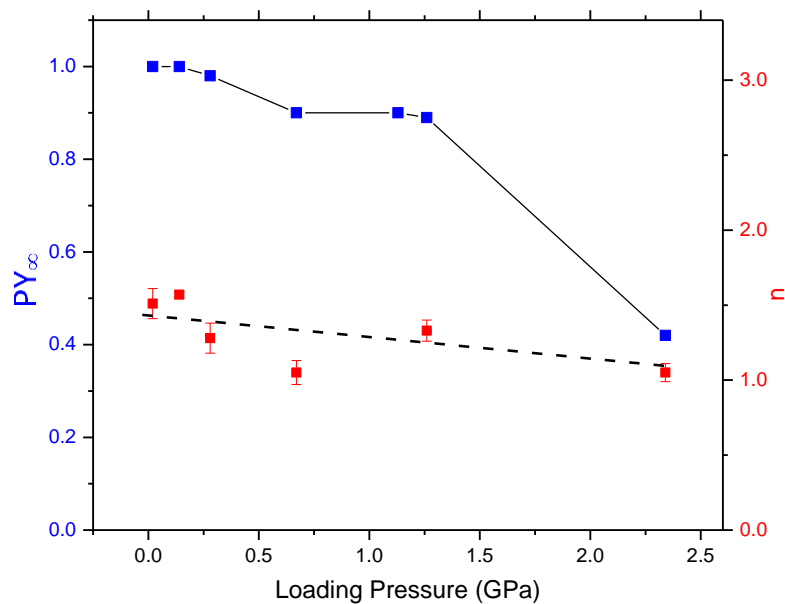

Figure 7.5: Avrami model parameters PY∞ (refer to the left y-axis) and n (refer to the right y-axis) derived from the polymerization kinetics data of styrene at different loading pressures.

The pressure dependence of the rate constant k at constant temperature is expected to be given by

$$\left(\frac{\partial \ln k}{\partial P}\right)_T = -\frac{\Delta V^{\neq}}{RT} \qquad (7.3)$$

where, according to the transition state theory, $\Delta V^{\neq}$ is the activation volume of the polymerization process.[12,32] In Fig. 7.6(a), we plot the ln$k$ values derived from the polymerization reactions as a function of pressure. The dependence of the $\ln k$ values with pressure below 1.4 GPa can be best reproduced using a quadratic equation:

$$\ln k = a + bP + cP^2 \qquad (7.4)$$

with $a =-8.2$, $b =18.6$ GPa^{-1}, and $c =-12.1$ GPa^{-2}. By combining Eqn. 7.3 and 7.4, the activation volume as a function of pressure can be obtained below and plotted in Fig 6b

$$\Delta V^{\neq}/RT = -(b+2cP) \qquad (7.5)$$

The isothermal activation volume is generally independent of the rate constant. The assumption is sometimes made that the logarithm of the rate constant is a linear function of the pressure and hence that the activation volume is also independent of pressure.[32] This is, however, true only in some instances and over small pressure ranges. As shown in Fig. 7.6(b), $\Delta V^{\neq}$ is negative below 0.77 GPa indicating the formation of the transition state from the styrene monomers involves a net contraction in volume and thus the rate constant increases with pressure. In contrast, the $\Delta V^{\neq}$ value is positive above 0.77 GPa giving decreasing rate constant k above this pressure. Therefore, at 0.77 GPa, photon-assisted transformation from styrene monomers to polystyrene can be characterized by a barrierless reaction (i.e., $\Delta V^{\neq}=0$). This result, when considering the effects of the increased density on the reactants and on the transition state, is extremely useful to understand the reaction mechanism. Specifically, the $|\Delta V^{\neq}|$ value can be extrapolated to be 46.0 cm^{3}mol^{-1} at atmospheric pressure, which is much larger than the value (23.5 cm^{3}mol^{-1}) obtained from

the emulsion polymerization studies of styrene under high pressure.[32] It is also much larger than the value (17.9 cm^3mol^{-1}) obtained from photosensitized polymerization of liquid styrene by using 1, 1'-azobiscyclohexane-l, l'-dinitrile as photoinitiator.[33] The differences in these values are possibly associated with the different polymerization mechanisms. Unlike pressure-induced polymerization, photon-assisted polymerization is initiated by the excited monomer instead of those in the ground state. Moreover, the smaller activation volume (e.g., 17.9 cm^3mol^{-1}) suggests that photoinitiator can significantly lower the reaction barrier. However, these polymerization reactions involving the UV radiation or particular photoinitiators at ambient pressure only yield up to 80% and take 30 h long. In our study, we show that this catalytic effect can also be achieved and significantly improved by applying a few hundred atmospheres pressure for the initiator-free photopolymerization, making the production of polystyrene with high yield (e.g., ~ 100% below 0.1 GPa) and fast kinetics (e.g., a few minutes of completion time at ~0.7 GPa) extremely appealing.
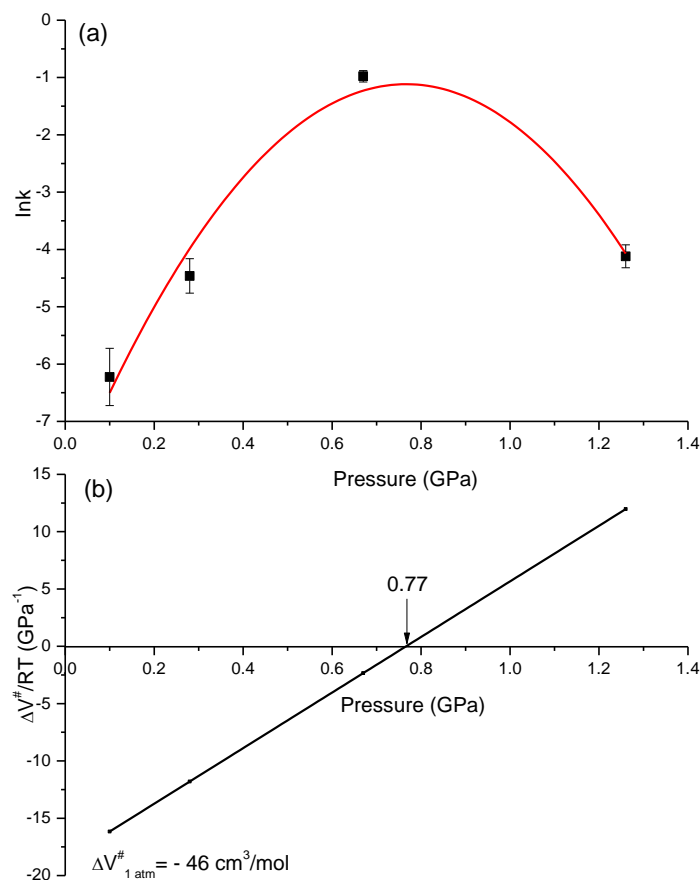
Figure 7.6: Quadratic regression of ln*k* as function of pressure at ambient temperature (i.e., 298 K) (a) and its pressure derivative as a function of pressure at 298 K (b). The intercept with the y-axis allows the determination of ambient pressure activation volume as labeled (see text).

7.3.4 Polymerization pathways

The photon-assisted polymerization process of unsaturated compounds is usually explained by excitation of the monomers to π^* antibonding states.[8,10,11] For styrene, however, the available photochemical data are only limited to the ambient pressure range.[34,35] Based on these data, a schematic energy diagram of styrene is summarized in Fig. 7.7. In the case of UV excitation, the single 350 nm (or 3.5 eV) photon is not sufficient in energy to excite to the first singlet state (S_1) located at 4.43 eV. The lowest triplet state

(T_1) of styrene is located vertically at 3.40 eV above the ground state, which was experimentally determined by electron energy loss spectrum of styrene deposited on a thin film of solid argon at 15 K.[35] The calculation showed that the excited electron of the T_1 state in the π^* orbital results in the elongation of the vinyl C=C double bond, making it a single-bond character. The question is whether the molecule in the ground state can be directly excited to the long-lived T_1 state, a less likely process because of the change in electronic spin state.
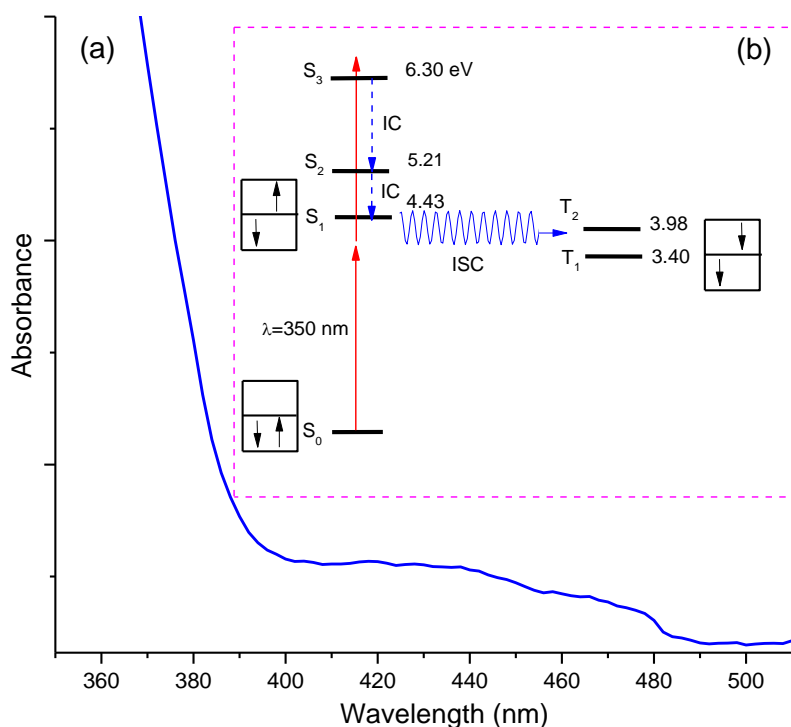

Figure 7.7: (a) UV-Vis absorption spectrum of liquid styrene collected at ambient conditions. (b) The schematic electronic energy levels showing possible electronic transitions of styrene. The electronic spins of the ground state (S_0), the first singlet state (S_1) and the first triplet state (T_1) are shown in the boxes. The possible transitions are denoted by arrows. The energy values in eV are given from Refs 34 and 35.

To address the questions above, we performed a UV-visible absorption measurement of liquid styrene in high wavelength region with the result shown in Fig. 7.7. Clearly, a

broad absorption onset at 480 nm (2.6 eV) is observed, corresponding to transition to the lowest vibrational level of the T_1 state. The second triplet state (T_2) of styrene is located vertically at 3.98 eV which can be accessed mainly via the transitions between the singly excited configurations such as (HOMO-1)→(LUMO+1) and (HOMO-1)→LUMO.[36] Although the energy of the S_1 state is higher than the energy of a single 350 nm photon, two-photon absorption would allow the access to the S_1 state, except that the transition cross section is significantly smaller. Owing to the small energy difference between the S_1 and T_2 states (i.e., 0.25 eV), the possible singlet-triplet intersystem crossing (ISC) can lead to the efficient energy transfer to the triplet state. A triplet configuration where a molecule possesses two electrons that are both orbitally and spin unpaired will necessarily result in diradical intermediates.[37] The diradical pathway has been proposed in photon-assisted polymerization of similar materials.[12] Subsequently, the T_1 excimer can initiate the polymerization reaction when in an appropriate configuration with available neighboring ground-state monomer molecules. Moreover, if the excimers have a long lifetime at the T_1 state, the diffusion process becomes negligible[38] in the propagation process of forming polystyrene, resulting in a larger growth geometry parameter ($n \geq 1$) than if significant diffusion is required (i.e., n close to 0.5) as discussed above.

Next, pressure selectivity in producing different tacticities of polystyrene is of great interest. In the liquid phase, random thermal collisions between the ground-state monomers and excimers would have equal probability of producing SPS and IPS regardless of their thermal stabilities. The lack of SPS is likely to due to its highly ordered crystal structure, which requires monomers to arrange in a well-defined periodic manner at the stage of nucleation. In contrast, the formation of APS tacticity possesses the maximum probability as this structure features random alignment of phenyl groups along the C-C chain.

At higher loading pressures, the reaction rate can be accelerated due to the shortened mean free path, favoring the formation of products. This pressure-facilitated propagation

of the polymerization reaction was observed in the entire liquid phase and even part of the solid phase below 0.77 GPa. However, this is also in competition with steric hindrance with increasing pressure, which causes a reduction of the reaction yield and may ultimately prohibit the reaction. The reaction process in the crystalline phase (i.e., above 0.3 GPa) thus is of interest in terms of topochemistry. Although the crystal structure of styrene above 0.3 GPa is still unknown, it can be inferred from the crystal structure of styrene at ambient pressure determined at a low temperature of 120 K,[39] assuming a normal P-T phase diagram of styrene. In Fig. 7.8, the orthorhombic structure of styrene (Space group: Pbcn, a=15.6757 Å, b=10.4805 Å, c=7.5277 Å, V=1236.72 Å^3, Z=8) at 120 K is shown. On the bc plane, it can be seen that three layers of styrene monomers are stacked in a unit cell with the orientation of the second layer opposite to that of the first and third layer. When an unsaturated vinyl C=C double bond is photoinitiated to form a radical, subsequently, the distance and the relative orientation between the nearest neighboring molecules are the two key properties to determine the polymerization process. On the ab plane (Fig. 7.8), the key intermolecular distances surrounding a C_1=C_5 double bond in the first layer are labeled. For instance, if the C_1=C_5 double bond is activated, the C_5 may attack the nearest C_6 belonging to a styrene molecule in the second layer that is 4.88 Å away. The C_1 has three neighbouring competing vinyl C=C bonds. From the bond distances, the nearest one is coplanar C_2 with a minimum distance 4.04 Å along the diagonal of ab plane. The other two neighbouring atoms C_3, C_4 are located at a distance 4.51, 4.20 Å, respectively. Based on these distances, a possible direction for the growth of the polystyrene chains is along the diagonal of the ab lattice plane. The subsequent relaxation of the products such as via the adjustment of the phenyl rings will lead to the formation of APS primarily. Similarly, compression along the b axis of the unit cell will result in shorter intermolecular distances such as between C_1-C_4, such that a segment of the polymer skeleton in a bonding sequence of -C_6-C_5-C_1-C_4-C_7-C_8- is also favorable for the formation of the APS configuration. This pressure-enhanced intermolecular interaction, even in the solid phase of styrene, provides

an effective driving force that leads to higher reaction rates until 0.77 GPa when the optimal distances are reached as discussed above. Beyond this pressure, severe steric hindrance at higher loading pressure (e.g., 2.34 GPa) would prevent the adjustment of phenyl rings resulting in low reaction rates and low polymerization yields.
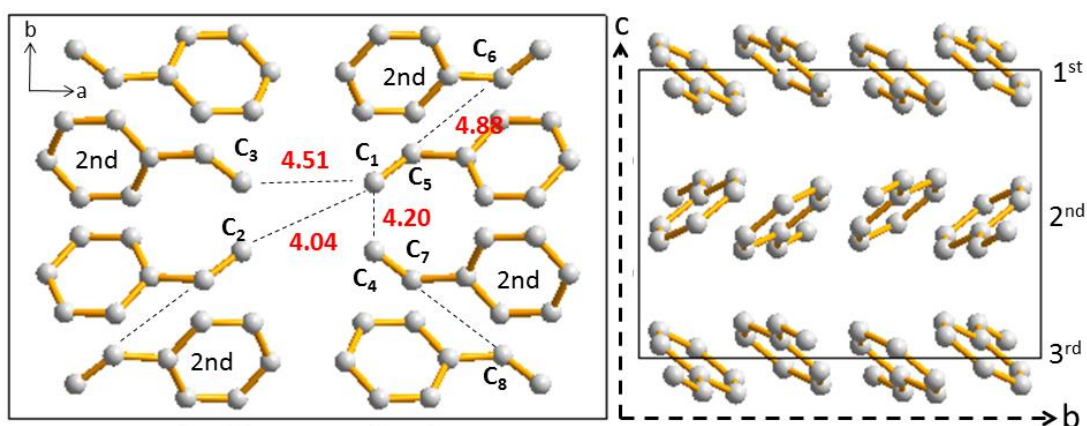

Figure 7.8: The crystal structure of solid styrene at 120 K (Space group: Pbcn, a=15.6757 Å, b=10.4805 Å, c=7.5277 Å, V=1236.72 Å³, Z=8) viewed along the c-axis (left) and a-axis (right). The inter-atomic distances in angstroms for solid styrene are provided from Ref. 33.

Finally, our study shows that pressure-induced photopolymerization of styrene provides practical applications in the production of useful polymers with great tunability and controllability. In particular, the production of amorphous APS or ordered IPS produced photochemically from pure styrene monomer without any photoinitiators could be developed as a new and clean way for producing these important engineering plastic materials. By carefully selecting the favorable pressure, temperature, as well as the radiation energy, the reaction channels producing APS can be tuned and optimized to selectively generate the desired product. More significantly, the detailed kinetics analysis of the present studies provides a window to further understand the roles played by high pressure in photochemical reactions, especially for photo-assisted polymerization reactions in general.

7.4 Conclusions

In summary, pressure-induced photopolymerization of condensed styrene has been studied in a diamond anvil cell. The polymerization reactions were triggered by using 350 nm MLUV laser with different power densities. The photoproducts and reaction evolution of polymerization were characterized by in situ FTIR spectroscopy. In liquid phase, styrene was found to transform to amorphous APS with minor IPS, while APS is the sole product when the monomer is rendered in solid phase with loading pressures above 0.3 GPa. An optimal loading pressure at 298 K under 350 nm irradiation was determined to be 0.77 GPa, where a barrierless reaction proceeded based on the kinetic analysis of pressure-dependent reaction profiles. The kinetic analysis further allows the identification of a linear growth mechanism of the polystyrene chains, which was characterized by the growth geometry parameter ($1<n<1.6$). Topological analysis of the crystalline styrene along the diagonal of the *ab* lattice plane strongly supports this mechanism. Finally, the photoreaction induced by 350 nm laser illumination indicates a triplet state initiated reaction mechanism for photopolymerization of condensed styrene. Overall, our study demonstrated high selectivity and controllability of pressure-assisted photon-induced polymerization reactions with great potential for practical applications.

7.5 References

(1)   Schellenberg, J. *Syndiotactic polystyrene: synthesis, characterization, processing, and applications*; John Wiley & Sons, 2009.
(2)   Maul, J.; Frushour, B. G.; Kontoff, J. R.; Eichenauer, H.; Ott, K. H. *Ullmann's Encyclopedia of Industrial Chemistry* **2000**.
(3)   Yagci, Y.; Jockusch, S.; Turro, N. J. *Macromolecules* **2010**, *43*, 6245.
(4)   Gruber, H. F. *Progress in Polymer Science* **1992**, *17*, 953.
(5)   Hageman, H. J. *Progress in Organic Coatings* **1985**, *13*, 123.
(6)   Kuhlmann, R.; Schnabel, W. *Angewandte Makromolekulare Chemie* **1978**, *70*, 145.
(7)   Kruger, K.; Tauer, K.; Yagci, Y.; Moszner, N. *Macromolecules* **2011**, *44*, 9539.
(8)   Ceppatelli, M.; Santoro, M.; Bini, R.; Schettino, V. *Journal of Chemical Physics* **2000**, *113*, 5991.

(9)   Ciabini, L.; Santoro, M.; Bini, R.; Schettino, V. *Physical Review Letters* **2002**, *88*.

(10)   Citroni, M.; Ceppatelli, M.; Bini, R.; Schettino, V. *Science* **2002**, *295*, 2058.

(11)   Bini, R. *Accounts of Chemical Research* **2004**, *37*, 95.

(12)   Citroni, M.; Ceppatelli, M.; Bini, R.; Schettino, V. *Journal of Physical Chemistry B* **2007**, *111*, 3910.

(13)   Citroni, M.; Bini, R.; Foggi, P.; Schettino, V. *Proceedings of the National Academy of Sciences of the United States of America* **2008**, *105*, 7658.

(14)   Ceppatelli, M.; Bini, R.; Schettino, V. *Journal of Physical Chemistry B* **2009**, *113*, 14640.

(15)   Ceppatelli, M.; Bini, R.; Schettino, V. *Proceedings of the National Academy of Sciences of the United States of America* **2009**, *106*, 11454.

(16)   Ceppatelli, M.; Bini, R.; Schettino, V. *Physical Chemistry Chemical Physics* **2011**, *13*, 1264.

(17)   Ceppatelli, M.; Bini, R.; Caporali, M.; Peruzzini, M. *Angewandte Chemie-International Edition* **2013**, *52*, 2313.

(18)   Ceppatelli, M.; Bini, R. *Macromolecular Rapid Communications* **2014**, *35*, 787.

(19)   Ceppatelli, M.; Pagliai, M.; Bini, R.; Jodl, H. J. *Journal of Physical Chemistry C* **2015**, *119*, 130.

(20)   Evlyukhin, E.; Museur, L.; Traore, M.; Nikitin, S. M.; Zerr, A.; Kanaev, A. *Journal of Physical Chemistry B* **2015**, *119*, 3577.

(21)   Guan, J. W.; Song, Y. *Journal of Physical Chemistry B* **2015**, *119*, 3535.

(22)   Chelazzi, D.; Ceppatelli, M.; Santoro, M.; Bini, R.; Schettino, V. *Nature Materials* **2004**, *3*, 470.

(23)   Gourdain, D.; Chervin, J. C.; Pruzan, P. *Journal of Chemical Physics* **1996**, *105*, 9040.

(24)   Dong, Z. H.; Song, Y. *Journal of Physical Chemistry C* **2010**, *114*, 1782.

(25)   Gowd, E. B.; Tashiro, K.; Ramesh, C. *Progress in Polymer Science* **2009**, *34*, 280.

(26)   Reynolds, N. M.; Stidham, H. D.; Hsu, S. L. *Macromolecules* **1991**, *24*, 3662.

(27)   Reynolds, N. M.; Savage, J. D.; Hsu, S. L. *Macromolecules* **1989**, *22*, 2867.

(28)   Avrami, M. *The Journal of Chemical Physics* **1939**, *7*, 1103.

(29)   Avrami, M. *The Journal of Chemical Physics* **1940**, *8*, 212.

(30)   Yoo, C. S.; Nicol, M. *Journal of Physical Chemistry* **1986**, *90*, 6732.

(31)   Chelazzi, D.; Ceppatelli, M.; Santoro, M.; Bini, R.; Schettino, V. *Journal of Physical Chemistry B* **2005**, *109*, 21658.

(32)   Ogo, Y.; Sano, T. *Colloid and Polymer Science* **1976**, *254*, 470.

(33)   Ogo, Y.; Yokawa, M.; Imoto, T. *Die Makromolekulare Chemie* **1973**, *171*, 123.

(34)   Molina, V.; Smith, B. R.; Merchan, M. *Chemical Physics Letters* **1999**, *309*, 486.

(35)   Swiderek, P.; Fraser, M. J.; Michaud, M.; Sanche, L. *Journal of Chemical Physics* **1994**, *100*, 70.

(36)   Molina, V.; Smith, B. R.; Merchán, M. *Chemical Physics Letters* **1999**, *309*, 486.

(37)   Turro, N. J. *Journal of Chemical Education* **1969**, *46*, 2.

(38)   Suppan, P. *Chemistry and light*; Royal Society of Chemistry, 1994.

(39)   Bond, A. D.; Davies, J. E. *Acta Crystallographica Section E-Structure Reports Online* **2001**, *57*, O1191.

Chapter 8

8 Pressure, Laser, and Physical-States Effects on Polymerization Kinetics of Phenylacetylene Probed by FTIR Spectroscopy

8.1 Introduction

The study of kinetics under high-pressure has become a valuable tool for investigating the mechanism of many organic reactions.[1,2] Previous experimental studies of the effect of pressure on chemical reactions in solution have demonstrated that reactions can be accelerated or retarded depending on the reaction type. Moreover, the relations between reaction kinetics and pressure have been established and described by the thermodynamic and kinetic equations 1.1[3,4]. Equation 1.1 shows that an increase in pressure will favor chemical reactions occurring with a negative ΔV and will accelerate reaction pathways with negative $\Delta V^{\neq}$. Polymerization is one of the reaction types that has negative $\Delta V^{\neq}$ and can be accelerated by high pressure. As the reaction rate is effectively modified, the increased pressure also brings changes to the yield of the reaction product. This effect is evident for those reactions in solution phase, while the reaction rate and yield in the condensed phase not only depends on the magnitude of external pressure but also on the physical state of the system. For instance, at a given temperature, a much higher threshold pressure is required to induce reactions of a molecular system in the crystalline solid than in the liquid.[5,6] So, the geometric constraints in the crystal have a significant impact on the threshold pressure for the reaction. When dealing with reactions in condensed phases (e.g., liquid, crystal, glass), specific concepts such as topochemical postulate and "reaction cavity", are needed to describe the reactivity.[7,8] More recently, the role of the lattice phonons in driving the high-pressure reactivity of crystalline benzene was demonstrated.[9] However, an

association between these concepts and the reaction activation volume remains ambiguous. Exploration of this association is crucial both for understanding the reaction of molecules in different physical states and for successfully designing and tailoring solid-state reactions, for instance, solid-state polymerization reactions.

As polymerization of unsaturated hydrocarbons possesses a negative reaction volume,[1] high pressure is expected to promote the polymeric transformation from the unsaturated monomers. In recent years, pressure-induced polymerization of unsaturated hydrocarbons has received revitalized interest due to the technological importance of polymer products. Some prominent examples are acetylene,[10] ethylene,[11,12] butadiene,[5,6] etc. Some effects of high pressure on these molecules have been revealed. The studies demonstrated that increasing pressure will substantially reduce intermolecular distances and further change the electronic structure of the molecules and broaden the energy levels and reduce or even eliminate the HOMO–LUMO gap.[13] Consequently, the relative stabilities of these molecules are changed and result in polymeric transformations. In most cases, the transformation requires extremely high threshold pressures, e.g., a few tens of gigapascals (GPa). Considering the reduced HOMO-LUMO gap at high pressure, selected optical pumping can be used to assist the activation of molecules in condensed phases. In this regard, experimental studies have shown that optical pumping via visible or ultraviolet (UV) radiation can significantly lower the high threshold pressure.[14,15] In some cases, combined pressure-photon tuning provides very different reaction pathways and selectively results in novel reaction products.[5] Therefore, it is exciting to apply the combined pressure-photon driving power to study the chemical reactivity of molecular systems and make comparisons with those unsaturated systems that have been studied under pure compression alone.

To discover and synthesize important technological materials such as conducting polymers and amorphous compounds, several unsaturated alkyne systems have been

studied under hydrostatic pressures or shock wave compressions.[16-19] Although the pressure conditions to induce phase transitions and polymerizations have been reported, the kinetics, which are strongly associated with pressure and physical states, have not been studied. Among the alkynes, phenylacetylene (PA) is an interesting candidate to research because the effects of pressure and laser radiation on polymerization kinetics in different physical states have not been explored. Also, at high pressures, the threshold pressures and reaction products are controversial in the previous studies. Specifically, Takahashi and coworkers reported oligomerization and polymerization of PA monomers using a customized high-pressure reactor.[20,21] After 300 h at 1.5 GPa and room temperature, liquid polymeric products are obtained with molecular weights from 100 to 48000.[21] In contrast, Santoro et al. found that liquid PA in a DAC is transformed into a solid state as pressure increases to 1.0-1.1 GPa at room temperature.[19] The solid PA is polycrystalline and consists of two polymorphs PAα and PAβ.[22] The polycrystalline PA was found to react and produce an amorphous solid poly(PA) at 8 GPa.[19] Evidently, this threshold pressure is much higher than the value obtained by the previous work, and the physical properties of the synthesized poly(PA)s are also different in the two studies. To better understand the phase transition behavior and reactivity of PA at high pressures, we therefore, carry out further investigations on this system at high pressure. In the first part, we explore the phase transitions of liquid PA at slow and fast compressions. It turns out the compression rate significantly influences the phase transitions of liquid PA. In the second part, as a comparison, laser effects on polymerization of PA in different physical phases are explored. Using *in situ* FTIR spectroscopy, we monitor the polymerization processes quantitatively. The results allow us to understand detailed reaction mechanisms and kinetics in these phases, pressures, and radiation conditions for the first time. The work further provides important implications for optimizing pressure-photon conditions to produce poly(PA)s with desired reaction rate and yield.

8.2　Experimental Section

A symmetric diamond anvil cell (DAC) equipped with a pair of type II diamonds with a culet size of 600 μm was used in the experiment. Liquid PA (purity ≥98% from Sigma Aldrich) along with a ruby ball was loaded into a hole with a diameter of 200 μm drilled on a stainless steel gasket that was pre-indented to a thickness of 30-50 μm. The pressure was determined using the well-established ruby fluorescence method.

To evaluate the photochemical effects, monochromatic light is introduced into the DAC. Upon loading, the reactions in different physical states were subsequently triggered by homogeneously irradiating the sample with the multi-line UV emission with a peak wavelength at ~ 350 nm of an argon ion laser with a selected power density (398 W/cm^2). Multiple loadings were done with the different initial loading pressures (0.05, 0.55, 0.76, 0.95 and 1.38 GPa) to explore the pressure and phase effects on photopolymerization reactions.

Under the extreme conditions, the changes of the PA sample were monitored by optical microscopy and Fourier transform infrared (FTIR) spectroscopy. The IR absorption spectra were collected at appropriate time intervals. A customized IR micro-spectroscopy system that consists of a Fourier transform infrared (FTIR) spectrometer from Bruker Optics (model Vertex 80v) equipped with a Globar IR light source was used. The detailed instrumentations have been described elsewhere.[23] The system was operated under a vacuum of < 5 mbar, such that the absorption by H_2O and CO_2 was efficiently removed. The reference spectrum, i.e., the absorption of the diamond anvil cell that was collected before styrene samples were loaded, was divided as the background from each measurement. The spectral resolution used was 4 cm^{-1}.

8.3   Results and Discussion

8.3.1 Pressure-induced phase transitions from liquid PA to glass-forming liquid or crystalline solid

The compression rate is an important factor in controlling the pressure-induced crystallization of liquid samples,[24] but this factor has been neglected in previous studies of PA samples. In the first attempts of this work, the liquid PA sample (sample 1) is compressed slowly (~25 MPa/s) from 0.08 GPa to 0.95 GPa. The sample 1 remains in the liquid state up to 1.10 GPa. At this pressure, the liquid PA is unstable, which undergoes a slow crystallization process and the process is on the laboratory timescale (e.g., 1 minute at 1.1 GPa as shown in Fig. 8.1). However, in the second trials, with fresh loadings and faster compression rates, the solidification process of the liquid PA sample at 1.1 GPa is postponed or avoided. For instance, the compressed sample (sample 2) remains in a liquid-like state up to 1.46 GPa. At this pressure, the crystallization starts after 8 minutes and the process completes within next few seconds (the crystallization process is captured as shown in Fig. 8.1). Therefore, in the pressure range 1.1-1.46 GPa, the relaxation time of the crystallization is increased as pressure increases. More importantly, in some cases, the solidification process is found to be completely avoided at fast compressions.

Besides the differences evidenced by the microphotographs, the corresponding changes are also revealed by IR spectra. At a pressure close to ambient pressure (0.05 GPa), we measure the IR spectrum of the PA sample with results consistent with values in the previous report.[25] As the pressure increases from 0.05 to 0.95 GPa, IR modes v_{15}, v_{14}, v_{17}, v_{27}, v_6 shift to higher frequencies due to the compression as shown in Fig. 8.2(a). Above 0.95 GPa, at the fast compression where the sample 2 does not crystalize, these IR modes continue blue-shifting (red lines), where the pressure dependency (dv/dp) of the IR frequencies remain linear as shown in Fig. 8.2(b).
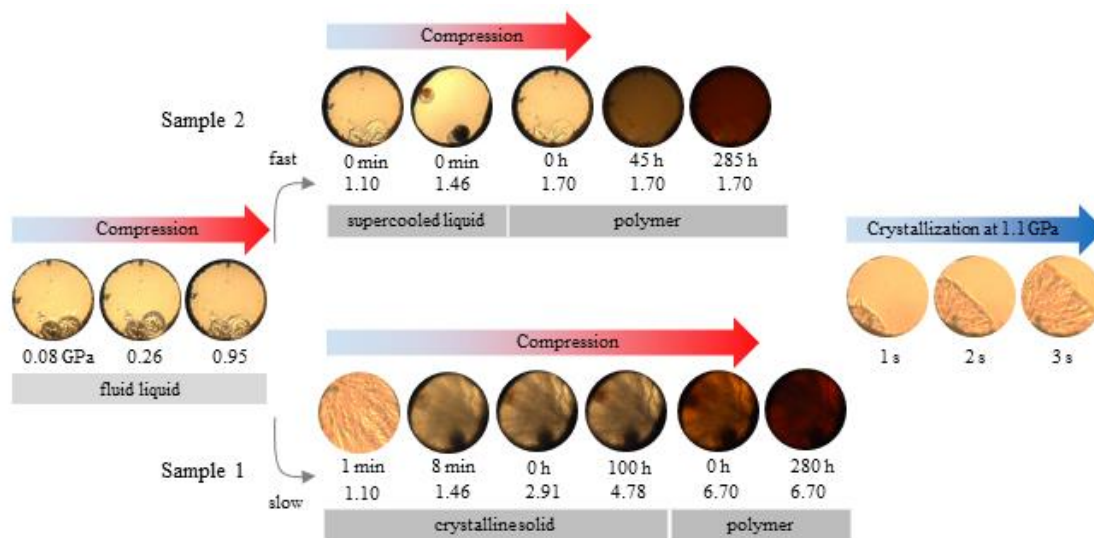
Figure 8.1: Microphotographs (~200 μm in diameter) of phenylacetylene samples upon compression at room temperature. The sample 1 is compressed from 0.08 to 6.70 GPa with a slow compression rate (~ 25 MPa/s) and different ageing time. The sample 1 crystalizes at 1.1 GPa after 1 min and the crystallization process completes within 3 s. The crystallized sample 1 shows an orange color at 6.7 GPa. Sample 2 is compressed from 0.08 to 1.70 GPa with a fast compression rate and no aging time. At 1.70 GPa, the sample 2 shows an orange color after 45 h. In the different pressure ranges and conditions, the four physical states are evidenced and labeled.

Whereas, once the liquid PA (sample 1) crystallizes at 1.1 GPa, both the IR modes v_{15} and v_{14} will split into two IR peaks (blue lines). Meanwhile, the IR modes v_{17}, v_{27} and v_6 are significantly red-shifted. Upon further compression of the crystal from 1.1 to 4.78 GPa, all these IR modes linearly blue-shift (Fig. 8.2(b)). Therefore, the IR results strongly support that there is a liquid-like phase above 1.1 GPa, and the production of which requires a fast compression.
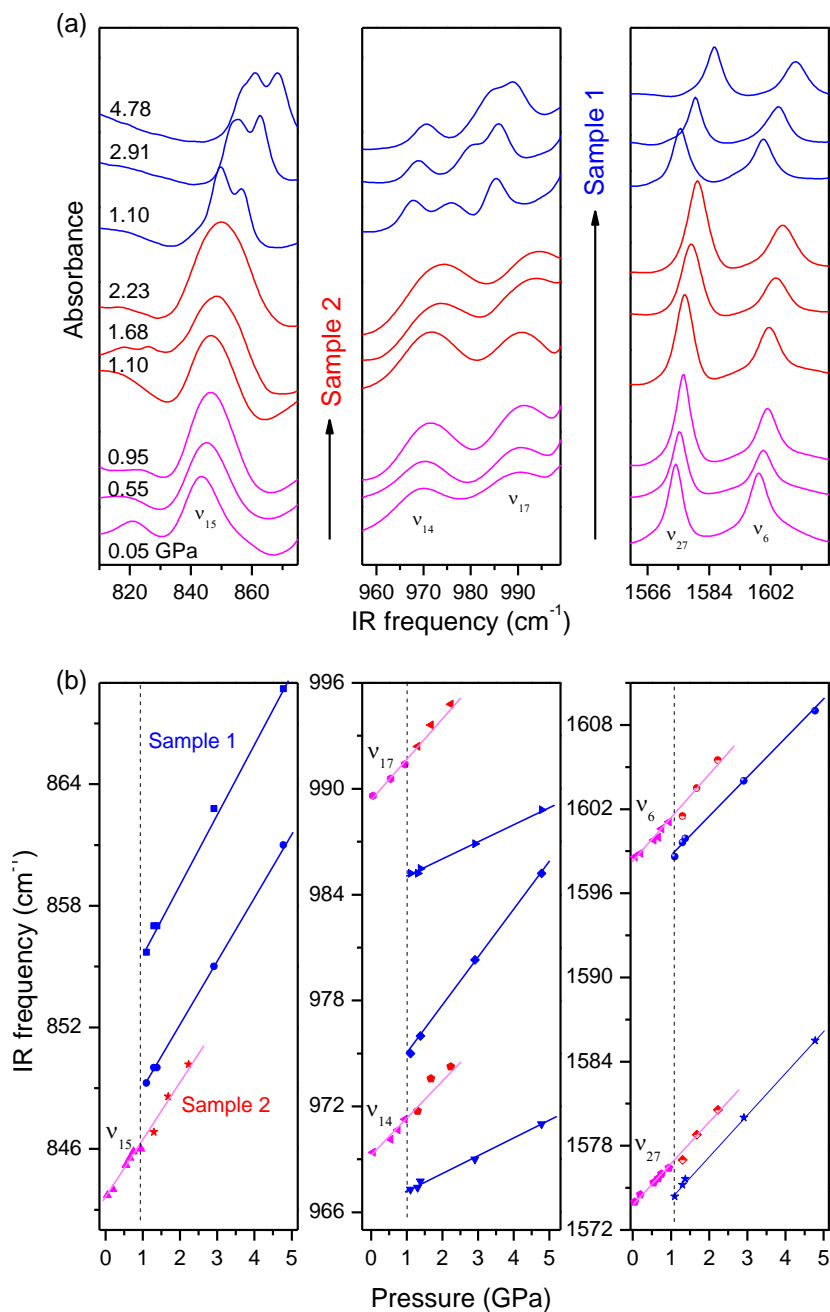
Figure 8.2: (a) Pressure-dependent spectral evolution of the PA in fluid liquid (pink), in glass-forming liquid (red, sample 2), in crystalline solid (blue, sample 1). (b) corresponding pressure-dependencies of the IR frequencies for the fluid, glass-forming liquid, and crystal solid. The IR modes of the crystalized sample 1 and the non-crystalized sample 2 show very different pressure dependencies. The dash lines suggest the phase transition boundary at 1.1 GPa.

At slow compressions, the sample freezes at 1.1 GPa, but the crystallization can be avoided with fast compressions so that the sample remains in a liquid-like state. This phenomenon suggests that the liquid-like state above 1.1 GPa is a metastable state and it is known as the glass-forming liquid state. Although the pressure-induced formation of the glass-forming state of PA was not reported in previous studies under high-pressure, it indeed exists at low temperatures when PA underwent a rapid cooling rate.[26] In this case, upon fast compression across freezing pressure of 1.1 GPa, liquid PA falls into the glass-forming liquid (also known as the supercooled liquid[27]). Under pressure, the metastable glass-forming liquid phase undergoes two competitive physical processes: crystallization and vitrification (glass-transition) (see Fig. 8.3).
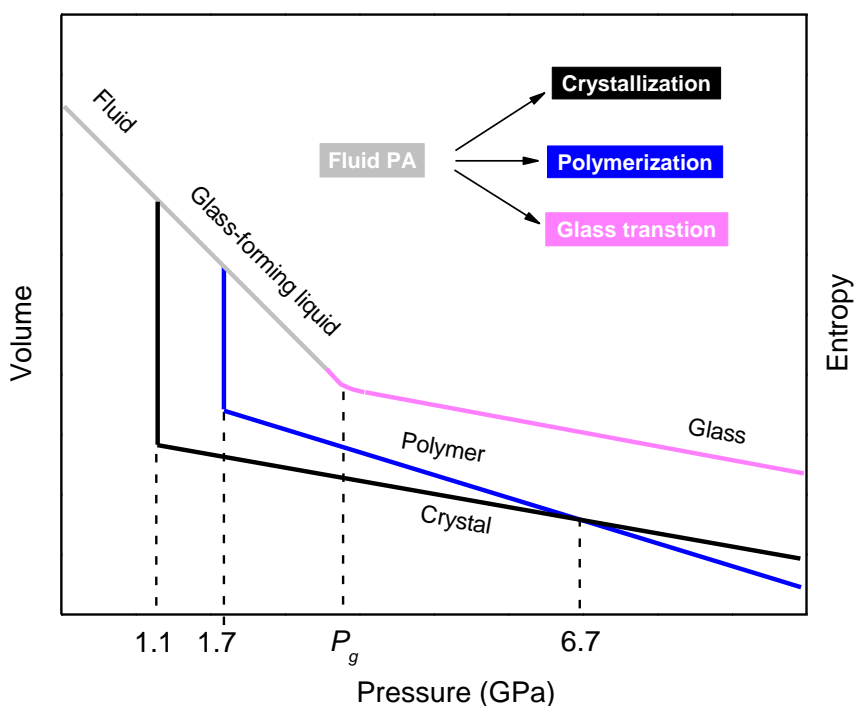
Figure 8.3 Schematic diagram showing the pressure-dependency of liquid PA's volume, entropy at the room temperature. The crystallization and polymerization pressures are labeled. The measurement of the glass-transition pressure P_g can be achieved by a much faster compression rate.

The formation of the glass-forming liquid PA upon fast compression is interesting as it is not the case for many other unsaturated molecules where pressure-induced crystallization is normally observed. The glass-forming liquid PA, therefore, provides a practical example to study the glass transition of non-crystallizing liquids with unsaturated bonds. Although the glass transition of non-crystallizing liquids has been known for millennia, it is still a major scientific challenge in condensed matter physics.[27,28] It is known that under sufficiently fast cooling, many liquids do not crystallize but transfer into a structurally disordered glassy state. In recent years, high pressure has been used to investigate glassy dynamics as it provides insight into the role of different thermodynamic variables in the glass transition.[29,30] So far, pressure-induced vitrification has been found in three classes of materials (van der Waals liquids, polymers, and hydrogen-bonded systems).[31,32] The hydrogen-bonded materials at elevated pressure were found to form glasses quite easily.[24,32] In this case, PA molecules are known to be the prototypic aromatic hydrocarbon exhibiting intermolecular cohesive forces such as $\pi(\text{arene})\cdots\pi(\text{arene})$, $CH\cdots\pi(\text{arene})$ and cooperative $\equiv CH\cdots\pi(C\equiv C)$ weak hydrogen-bonding interactions.[22,33] Therefore, the easy formation of the glass-forming liquid PA could be attributed to these complex intermolecular bonding dynamic processes at varied compression rates.

8.3.2 Pressure effects on polymerization of PA in the glass-forming liquid and the crystalline solid

At different compression rates, we find that the glass-forming liquid PA not only undergoes the two competitive physical processes (i.e., crystallization and vitrification), but also competes with a chemical process, polymerization (see Fig. 8.3). The polymerization will be discussed below. For the first time, competitions between the two physical processes and a chemical reaction under high pressures is found, in contrast with other glass-forming liquids, where only the physical processes are competing. In the

polymerization process, the threshold pressures and kinetics of the polymerization are examined by optical microscopy and FTIR spectroscopy as discussed below.

In the glass-forming liquid: As shown in Fig. 8.1, after fast compression of the fluid liquid to the pressure range 1.1-1.46 GPa, the sample is unstable and could possibly undergo the crystallization. However, after fast compression of the fluid liquid to higher pressures, no crystallization is observed, and instead chemical reactions are seen. For instance, at 1.70 GPa, the color of sample 2 turns from colorless to orange after 45 h and becomes red after 285 h. The color change suggests a pressure-induced reaction of the glass-forming PA at this pressure. More pronounced evidence is provided by in situ IR spectroscopy. The IR spectrum at 285 h (Fig. 8.4) shows that the intensity of IR mode v_{27} (v_{C-C}) decreases while the IR peak at 1603 cm^{-1} becomes a broad and intensive profile. In the C-H stretching region, an IR peak centered 3050 cm^{-1} appears, which is direct evidence for the sp^2 carbon sites.[19] Also, the intensity of the ethynyl C-H mode ($v_{C\equiv C-H}$) at 3030 cm^{-1} is reduced suggesting the reaction involves the C≡C triple bond of PA monomers. These changes clearly show that the polymeric transformation from PA monomers to conjugated poly(PA) can be induced at a very low pressure (e.g., 1.70 GPa). Therefore, the glass-forming liquid state formed by rapid compression effectively reduces the threshold pressure for polymerization in this state to 1.70 GPa. Note that a weak IR profile appears centered at 2930 cm^{-1} which can be assigned to IR vibrations associated with the sp^3 C-H stretch.[19] This may suggest the cross-linking structure of poly(PA), where a small amount of the sp^2 carbons in the polymer chains further react under pressure.
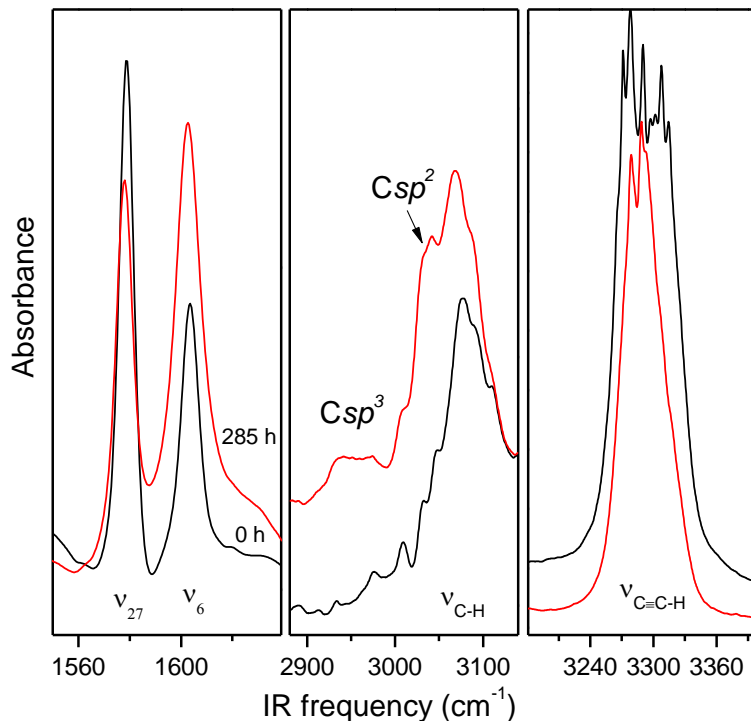
Figure 8.4: Time-dependent spectral evolution of the glass-forming liquid PA at 1.70 GPa as a function of reaction time (0-285 h) in the selected region 1560-1640 cm^{-1}, 2880-3150 cm^{-1} and 3180-3390 cm^{-1}.

Although polymerization is successfully induced at 1.68 GPa, the reaction is very slow. We further examine the effects of higher pressures on the polymerization, especially on the reaction kinetics. The reaction progression is evaluated by monitoring the intensity decrease of the IR peak ν_{27} (Fig. 8.4). The fraction of products can be determined according to

$$Y(t) = 1 - \frac{(I_{C-C})_t}{(I_{C-C})_{t=0}} \qquad (8.1)$$

where I_{C-C} is the integrated intensity of the ν_{27}. In Fig. 8.5(a), the yield as a function of reaction time for the sample reacted at different pressures is plotted. The reactions kinetics at 3.43, 4.75 GPa can be analyzed using the Avrami model:[34,35]

$$PY(t) = PY_\infty[1-\exp(-k(t-t_0)^n)] \qquad (8.2)$$

where PY(t) and PY$_\infty$ are the polymerization yield at time t after the nucleation time t$_0$ and at the end of the polymerization process, k is the rate constant, and n is a parameter whose value depends on the nucleation law and growth geometry. Regression of PY (t) data in the glass-forming liquid using Eq. (8.2) is shown in Fig. 8.4(a), yielding the values of rate constant k, the parameter n, as well as the polymerization yield PY$_\infty$ tabulated in Table 8.1. As pressure increases, the reaction at 4.75 GPa is 12 times faster than the reaction at 3.43 GPa. The reaction at 1. 70 GPa requires 92 h nucleation time and the growth is also very slow. It is evident that the reaction rate increases with increasing pressure (Fig. 8.4(a)). According to Eq. (1.1), the results suggest that the transformation of PA monomers to the polymer has a negative activation volume. More detail along with the other parameters n and PY$_\infty$ in the three cases will be discussed at the end of section 3 in comparison with the corresponding values obtained in the crystalline solid and in the fluid liquid.

In the crystalline solid: The polymerization of PA in the crystalline solid phase are also examined and we particularly emphasize the reaction kinetics. In Fig. 8.1, the crystalline sample 2 turns to orange immediately at 6.7 GPa. This is slightly lower than the reported threshold pressure of 8 GPa at the room temperature. The reaction kinetics at 6.7 GPa and a higher pressure of 10 GPa are measured and shown in Fig. 8.5(b). The parameters obtained for the pressure-induced polymerization in the polycrystalline state are also listed in Table 8.1. It is seen that the polymerization rate at 10 GPa is much faster than the reaction at 6.7 GPa. Thus, even in the crystalline state, the reaction rate is increased under higher pressure. Again, the other parameters, especially n, associated with the nucleation law and growth geometry will be discussed later.
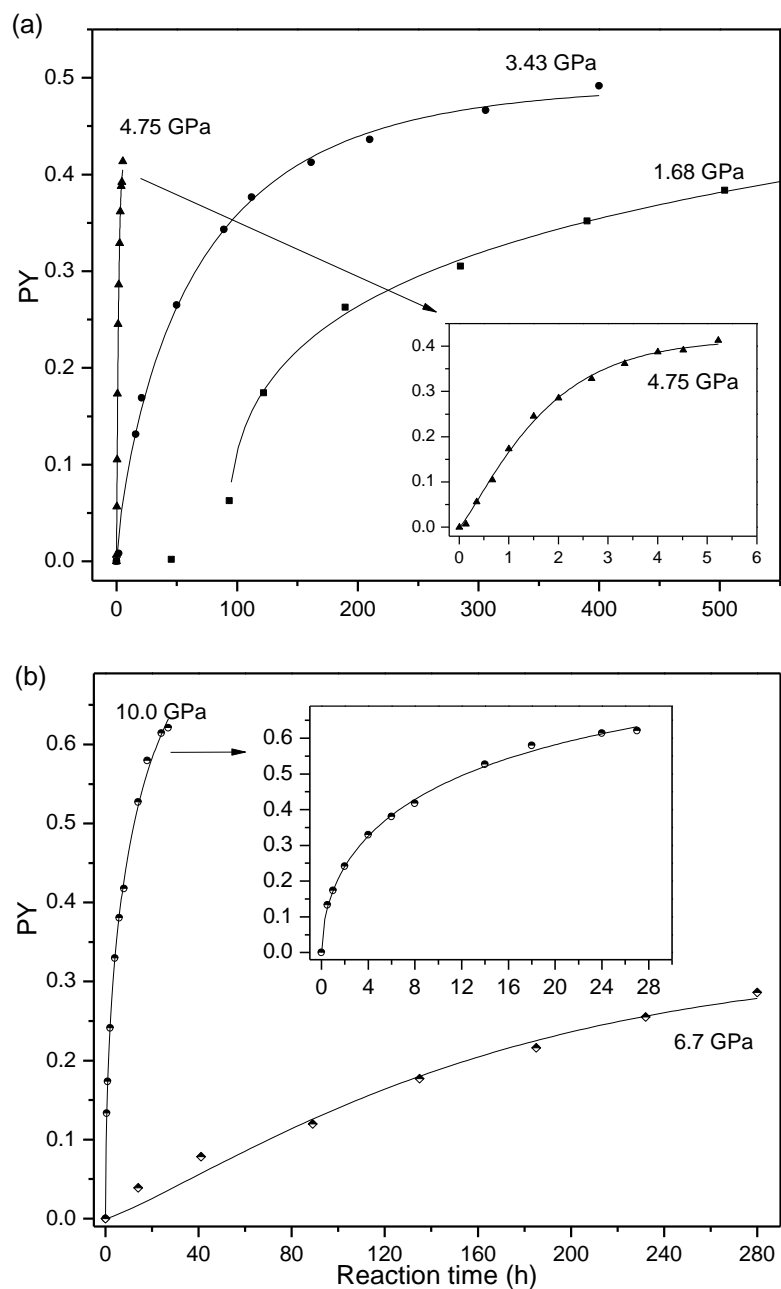
Figure 8.5: The polymerization yield (PY) of (a) the glass-forming PA and (b) the crystalline solid with different pressures (labeled for each plot) as a function of time. The solid lines are fits using the Avrami model. The nucleation time at 1.70 GPa is 92 h and 0 h for reactions at other explored pressures.

8.3.3 Laser effects on polymerization of PA at static pressures

The pressure onset to induce polymerization is at least 1.68 GPa in the glass-forming liquid, and 6.7 GPa in the crystalline solid. Instead, below these pressures, the sample has no chemical reactivity. We attempted to induce the chemical reactions by applying near-UV (ca. 350 nm) laser irradiation. The PA sample is first loaded at five different pressures (0.05, 0.55, 0.76, 0.95 and 1.38 GPa) to examine the effects of physical states and pressure on the photochemical reactivity of PA. Upon irradiation, IR spectral evolution at 0.05, 0.55 and 0.76 GPa show no differences but the varied radiation time. IR spectra of the photoproducts at these pressures have minor differences with the one obtained by pressure-induced polymerization, suggesting minor differences of the microstructure of products. However, these issues are not the topic of current study. Therefore, in analogy with the pressure-induced polymerization, we only present the kinetic information by tracking the spectral evolution of the IR peak v_{27}. As shown in Fig. 8.6(a), the data can also be well analyzed by the Avrami model. The three parameters obtained are listed in Table 8.1 as comparisons. As pressure increases from 0.05 to 0.76 GPa in the fluid liquid, the reaction rate is enhanced. Abnormally, the reaction rate and yield are significantly reduced at higher pressure 0.95 GPa. At this pressure, the sample seemingly remains in the fluid liquid state as it is below the freezing pressure 1.1 GPa. Interestingly, the progression of photoreactions at 0.95 GPa show curves similar to the one induced in the crystalline phases at 1.38 GPa (Fig. 8.6(b)). This suggests that the PA sample at 0.95 GPa has fallen into the glass-forming liquid state, and thus has similar physical behavior to the solid instead of the fluid. A "frozen" nature of the liquid's structure is revealed in the glass-forming liquid state.
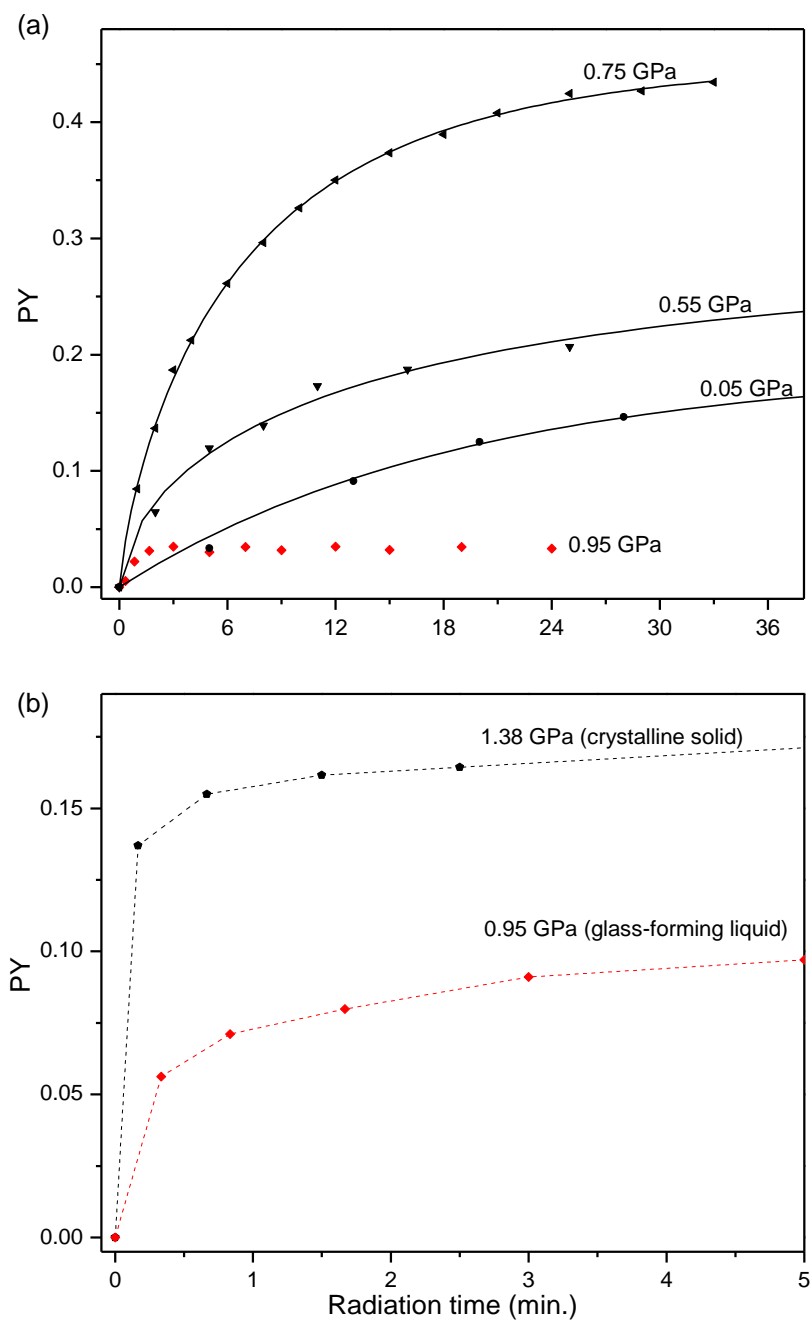
Figure 8.6: The polymerization yield (PY) of (a) fluid PA and (b) crystalline PA with different initial loading pressures (labeled for each plot) as a function of radiation time. The solid lines are fits using the Avrami model.

Table 8.1: Kinetics Parameters of Polymerization of Phenylacetylene Obtained from Least-Square Regression using Avrami Model.

Pressure (GPa)	Reaction rate 10^2k (h^{-1})	lnk	Geometric parameter n	Polymerization yield PY∞
Polymerization in the supercooled liquid				
1.70	0.001 ± 0.00	-2.30 ± 0.00	0.37 ± 0.07	0.74
3.43	3.71 ± 0.55	5.92 ± 0.14	0.77 ± 0.04	0.49
4.75	51.35 ± 2.14	8.54 ± 0.04	1.19 ± 0.06	0.42
Polymerization in the crystalline solid				
6.70	2.1 ± 0.15	5.35 ± 0.07	0.66	0.45
10.00	22.54 ± 2.13	7.72 ± 0.09	0.53 ± 0.03	0.87
Laser-induced polymerization in the fluid liquid				
0.05	275 ± 39	10.22 ± 0.13	0.99 ± 0.12	0.20
0.55	385 ± 90	10.56 ± 0.21	0.82 ± 0.08	0.22
0.75	510 ± 25	10.84 ± 0.05	0.77 ± 0.01	0.45

8.3.4 Effects of pressure, laser, physical-states on the polymerization

The pressure, radiation, and physical-state are decisive factors for the initiation and propagation of the polymerization. As shown in Table 8.1, experimental values of parameter n in the theoretical Avrami model vary in the range of 0.37-1.29. Originally, the Avrami model was developed to model the crystal growth from a liquid phase and was later adapted to polymerization processes.[34,35] According to this model, the values of n are expected to increase with the dimensionality of the process, ranging from 1 to 2 in the case of a linear growth. The n values derived from our experiments close to 0.37–1.19 thus suggest the linear growth of PA chains. If the polymerization process is diffusion-controlled, the value of n close to 0.5 is expected.[35] A diffusion-controlled growth process requires that the formation of product from the transition state is very rapid and thus transport of reactants to reaction site becomes rate determining. In particular, the n number 0.53 obtained at 10 GPa suggests a diffusion-controlled 1D growth process in the crystalline solid.
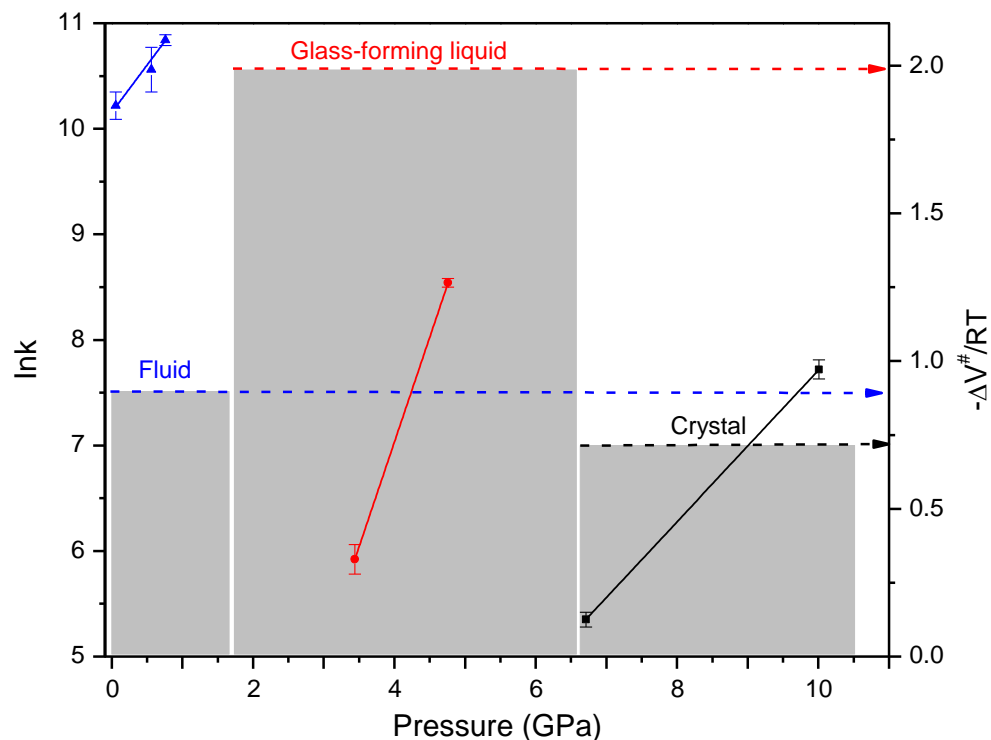
Figure 8.7: Linear regressions of lnk (left axis) as a function of pressure at 298 K for laser-induced reaction in the fluid (blue), pressure-induced reaction in the glass-forming liquid (red) and pressure-induced reaction in the crystal (black). The grey bars and arrows show magnitudes of the derived isothermal activation volumes (right axis).

Photoactivation and physical-state (or phase transition) activation effects on polymerization are further suggested by the relationship of the kinetics with the isothermal activation volume. The activation volume can be derived from Equation (1.1) since we have obtained the reaction rates at varied reaction conditions as listed in Table 8.1. To derive the activation volumes $\Delta V^{\neq}$, the logarithm of the rate constant ln$k$ as a function of pressure is plotted in Fig. 8.7. In the different physical states tuned by pressure, we assume ln$k$ is a linear function of pressure and hence that the isothermal activation volume $\Delta V^{\neq}$ is independent of pressure in the same physical state. Fig. 8.7 firstly shows that the polymerization of the fluid under low pressures and UV radiations gives the highest

reaction rates, which otherwise has no reaction inferring a high activation volume in the fluid phase. Thus, the high activation volume $\Delta V^{\neq}$ is significantly reduced by the photoactivation. Secondly, the figure shows that the $\Delta V^{\neq}$ is decreased by the fluid to glass-forming liquid phase transition, and the crystallization also reduces the activation volume significantly, to a value that is comparable to the one in the photoactivation experiments.

To understand the effect of photoactivation and crystallization on the reduction of the activation volume $\Delta V^{\neq}$, it is necessary to elucidate the nature of the activation volume. Although the activation volume is the difference in partial molal volume between the transition state and the reactant, the volume profile is not simply defined in terms of the reactants, transition state, and products properties. Environmental and medium effects play an important and, at times, dominant role.[1,36] $\Delta V^{\neq}$ often has to be considered as a composite quantity made up essentially of two contributing volumes ($\Delta V^{\neq} = \Delta V_s^{\neq} + \Delta V_m^{\neq}$), the first and intrinsic part $\Delta V_s^{\neq}$ being related to the structural change during the crossing from the initial to transition state and the second $\Delta V_m^{\neq}$ representing the volume change due directly to the modified interaction between the surrounding molecules of medium and the reacting molecules when they form the transition state. In the photo-induced polymerization in fluid PA, the reaction initiated by photoexcited PA would certainly lower the intrinsic activation volume $\Delta V_s^{\neq}$ as when a reactant molecule is brought to the necessary activation energy level (S_1), the excited molecule generally has a reduced bond order, lowered rotational or torsional barriers as well as an increased polarity.[37] This is strongly supported by the finding that the S_1 state of PA is a symmetric, quinoidal structure with an increase in the $C\equiv C$ bond length.[38] While in the fluid phase, environmental effects should be negligible at low pressures (e.g., < 1 GPa). However, after the liquid-to-liquid phase transition, the environmental and medium effects likely become of importance in reducing the activation volume $\Delta V_m^{\neq}$ and thus induce reactions in the glass-forming liquid state. In this phase at pressures >1.70 GPa, as revealed by the experiments above, the glass-forming liquid state has a "frozen" nature in the liquid structure, suggesting a significant increase of viscosity

of the medium after the transition. It has been evident that increasing viscosity of the solvent promotes bond making reactions.[39] As a rule of thumb, the formation of an additional bond in the transition state contributes a negative activation volume of the order of -(10-15) cm^3 mol^{-1}.[39] Therefore, the high viscosity in the glass-forming liquid PA should be responsible for the reduction of the activation volume and thus the initiation of the reaction at the very low threshold pressure.

In the crystal, the actual volumes occupied by the reactants and transition complex differ from the intrinsic part because the packing of the molecules will include voids depending also on the thermal motion. Nevertheless, discussion of the effects of crystallization on the reduction of the activation volume touch the very frontier of this research and thus shall be very conservative. In the solid-state reaction, more factors may be involved and must be considered, e.g., the exact structure of the reactant crystal (molecular orientations, intermolecular distances, intermolecular interactions, electronic distributions and crystal defects), and the role of lattice phonons at a constant temperature. In fact, the collective motions in the crystal such as those represented by the lattice phonons play a very important role that regulates configurations for the reaction to occur.[9] In glassy phases, due to the lack of collective motions, the occurrence of chemical reaction is prevented at very critical P-T conditions. Under these complicated circumstances, the activation volume is expecting to be contributed by many factors, even the transition theory might be not applicable for the reaction in the crystalline phase.

Lastly, our study examines the effects of pressure, laser radiation and physical states on polymerization kinetics of phenylacetylene. The results provide important references in the production of conducting polymers with optimized reaction conditions, where the highest reaction rate and yield can be achieved. Meanwhile, fast compression, in parallel with laser irradiation, can be operated as the other way to obtain the metastable phase and reduce the high threshold pressure of the polymerization, thus shedding light on the feasibility of

industrial scale production of poly(PA). More significantly, the detailed kinetics analysis of the present study provides new insight on understanding the roles played by high pressure, laser irradiation and physical state in polymerization reactions in general.

8.4 Conclusion

In summary, pressure, laser and physical state effects on polymerization kinetics of phenylacetylene have been studied in a diamond anvil cell. Three phases of the sample were examined, e.g., fluid, glass-forming liquid, and crystal solid. The last two phases were obtained by varying the compression rate. At a fast compression above 1.1 GPa, fluid PA was found to transform into a glass-forming liquid phase. In the three physical states, the polymerization reactions were triggered either by high pressures or by using a 350 nm multi-line UV laser. The evolution of polymerization was characterized by *in situ* FTIR spectroscopy.

The results show that the threshold pressures and reaction kinetics strongly depend on pressure, laser, and physical state. The threshold pressures for polymerization in the glass-forming liquid is 1.7 GPa while it increases 6.7 GPa in the crystalline solid. The time-dependent kinetics analysis allows the examination of the polymerization mechanism. At first, a linear growth mechanism of the poly(PA) chains is suggested in all cases, independent of reaction conditions and environment. A diffusion-controlled 1D growth process was found for the pressure-induced polymerization at 10 GPa in the crystalline solid, characterized by the growth geometry parameter ($n = 0.53$). Moreover, the activation volumes were reduced to different extents by laser irradiation or phase transitions. The comparison of these values allows the mechanistic elucidation of laser photoactivation and

environment effects on the polymerization. Finally, high-pressure synthetic applications are expected to be benefited in the light of the above findings and emphasized effects.

8.5 References

(1)   Jenner, G. *Angewandte Chemie-International Edition in English* **1975**, *14*, 137.
(2)   Van Eldik, R.; Klärner, F.-G. *High pressure chemistry*; John Wiley & Sons, 2008.
(3)   Chen, B.; Hoffmann, R.; Cammi, R. *Angewandte Chemie-International Edition* **2017**, *56*, 11126.
(4)   Klarner, F. G.; Wurche, F. *Journal Fur Praktische Chemie-Practical Applications and Applied Chemistry* **2000**, *342*, 609.
(5)   Citroni, M.; Ceppatelli, M.; Bini, R.; Schettino, V. *Science* **2002**, *295*, 2058.
(6)   Citroni, M.; Ceppatelli, M.; Bini, R.; Schettino, V. *High Pressure Research* **2002**, *22*, 507.
(7)   Boldyreva, E. V. *Solid State Ionics* **1997**, *101*, 843.
(8)   Ohashi, Y. *Current Opinion in Solid State & Materials Science* **1996**, *1*, 522.
(9)   Ciabini, L.; Santoro, M.; Gorelli, F. A.; Bini, R.; Schettino, V.; Raugei, S. *Nature Materials* **2007**, *6*, 39.
(10)   Sun, J. M.; Dong, X.; Wang, Y. J.; Li, K.; Zheng, H. Y.; Wang, L. J.; Cody, G. D.; Tulk, C. A.; Molaison, J. J.; Lin, X. H.; Meng, Y. F.; Jin, C. Q.; Mao, H. K. *Angewandte Chemie-International Edition* **2017**, *56*, 6553.
(11)   Scelta, D.; Ceppatelli, M.; Bini, R. *Journal of Chemical Physics* **2016**, *145*.
(12)   Chelazzi, D.; Ceppatelli, M.; Santoro, M.; Bini, R.; Schettino, V. *Journal of Physical Chemistry B* **2005**, *109*, 21658.
(13)   Drickame.Hg; Slichter, C. P.; Frank, C. W. *Proceedings of the National Academy of Sciences of the United States of America* **1972**, *69*, 933.
(14)   Song, Y. In *Applications of Molecular Spectroscopy to Current Research in the Chemical and Biological Sciences*; InTech, 2016.
(15)   Bini, R. *Accounts of Chemical Research* **2004**, *37*, 95.
(16)   Sakashita, M.; Yamawaki, H.; Aoki, K. *Journal of Physical Chemistry* **1996**, *100*, 9943.
(17)   Ceppatelli, M.; Fontana, L.; Citroni, M. *Phase Transitions* **2007**, *80*, 1085.
(18)   Chellappa, R. S.; Dattelbaum, D. M.; Sheffield, S.; Robbins, D. *Shock Compression of Condensed Matter - 2011, Pts 1 and 2* **2012**, *1426*.
(19)   Santoro, M.; Ciabini, L.; Bini, R.; Schettino, V. *Journal of Raman Spectroscopy* **2003**, *34*, 557.
(20)   Kojima, Y.; Matsuoka, T.; Sato, N.; Takahashi, H. *Journal of Polymer Science Part a-Polymer Chemistry* **1995**, *33*, 2935.
(21)   Kojima, J.; Matsuoka, T.; Sato, N.; Takahashi, H. *Journal of Materials Science Letters* **1995**, *14*, 1583.

(22) Dziubek, K.; Podsiadlo, M.; Katrusiak, A. *Journal of the American Chemical Society* **2007**, *129*, 12620.

(23) Dong, Z. H.; Song, Y. *Journal of Physical Chemistry C* **2010**, *114*, 1782.

(24) Brugmans, M. J. P.; Vos, W. L. *Journal of Chemical Physics* **1995**, *103*, 2661.

(25) King, G. W.; So, S. P. *Journal of Molecular Spectroscopy* **1970**, *36*, 468.

(26) Abramczyk, H.; Brozek, B.; Waliszewska, G.; Suwalski, J. P. *Journal of Physical Chemistry B* **2002**, *106*, 1486.

(27) Debenedetti, P. G.; Stillinger, F. H. *Nature* **2001**, *410*, 259.

(28) Kivelson, S. A.; Tarjus, G. *Nature Materials* **2008**, *7*, 831.

(29) Paluch, M.; Grzybowska, K.; Grzybowski, A. *Journal of Physics-Condensed Matter* **2007**, *19*.

(30) Pronin, A. A.; Kondrin, M. V.; Lyapin, A. G.; Brazhkin, V. V.; Volkov, A. A.; Lunkenheimer, P.; Loidl, A. *Physical Review E* **2010**, *81*.

(31) Reiser, A.; Kasper, G.; Hunklinger, S. *Physical Review B* **2005**, *72*.

(32) Pawlus, S.; Paluch, M.; Dzida, M. *Journal of Physical Chemistry Letters* **2010**, *1*, 3249.

(33) Maity, S.; Guin, M.; Singh, P. C.; Patwari, G. N. *Chemphyschem* **2011**, *12*, 26.

(34) Guan, J. W.; Song, Y. *Journal of Chemical Physics* **2016**, *144*.

(35) Ceppatelli, M.; Santoro, M.; Bini, R.; Schettino, V. *Journal of Chemical Physics* **2000**, *113*, 5991.

(36) Schettino, V.; Bini, R. *Chemical Society Reviews* **2007**, *36*, 869.

(37) Guan, J. W.; Daljeet, R.; Song, Y. *Canadian Journal of Chemistry* **2017**, *95*, 1212.

(38) Ribblett, J. W.; Borst, D. R.; Pratt, D. W. *Journal of Chemical Physics* **1999**, *111*, 8454.

(39) Jenner, G. *Mini-Reviews in Organic Chemistry* **2004**, *1*, 9.

Chapter 9

9. Summary and Future Works

In this thesis, we focus on discovering and understanding effects of high pressure on the photochemical reactions of several selected organic hydrocarbon materials. The selected molecular materials, at the ambient pressure, can be divided into the three groups (theme I-III) and undergo three types of photochemical reactions, e.g., photodissociation (theme I), photoisomerization (theme II), and photopolymerization (theme III), respectively.

In theme I, at ambient pressures, laser-induced decomposition (dissociation) of parent molecules in the condensed phase bring multiple products and the associated reaction pathways and mechanisms are rather complicated, and in most cases, incomprehensible. Identification of products based on the overlapped vibrational spectra is very challenging and tedious. Fortunately, dissociative types of photoreactions are not favored at high pressures due to the intrinsic positive activation volume, therefore, increasing pressures are found to efficiently reduce the number of reaction channels, and further facilitate the understanding of the reaction mechanism via kinetics analysis. Based on these known merits, high pressure appears to be a very valuable tool for investigating the mechanism of the dissociative reactions of organic molecules in condensed phases. In particular, future works that focus on the photochemical study of energetic explosives (e.g., high nitrogen containing materials) under static high pressures would be highly interesting because of industrial and military applications of these materials. In addition, for the studies of dissociative reactions in future, performing *ab initio* calculations (if applicable) should be

very helpful in confirming suggested reaction products and further providing some clear interpretation of experimental results.

Under theme II, although the photochemical behavior of cis-stilbene in the gas phase is intensively studied and well understood, it is rarely studied in the condensed phase either at ambient or at high pressures. We examine the pressure effects on the photoisomerization of fluid cis-stilbene. We found that in the fluid phase at the ambient pressure, the cis-trans photoisomerization produces the most stable phase, α-phase of trans-stilbene crystal. At high pressures, pressure firstly tunes the photoisomerization type phase transitions and produces the novel polymorphic trans-stilbene crystals (β and γ phase). Next, higher pressures prohibit the photoisomerization type reaction, and open a new type of reaction, 2+2 photodimerization. The new reaction allows the production of a liquid material. Moreover, mechanism studies via reaction kinetics permit us to clearly demonstrate the relation between the compressibility of the electronic states of the reactant and the selectivity of products. The concrete evidence suggests that the conical intersection between the excited electronic state and the ground state has been destroyed by high pressure. This finding is unprecedented and important as this significant pressure effect is expected to be presented by other photoisomerization systems, e.g., stilbene derivatives, azobenzene derivatives. These materials have crucial applications in optical organic molecular devices and photobiology, therefore, pressure would be an effective parameter in tuning and changing their photo-assisted functionalities. Nevertheless, this outlook requires further systematic studies of these types of materials in the future.

Under theme III, we systematically examine the effects of pressure on the polymeric transformations of three unsaturated hydrocarbons in condensed phases. The efforts are primarily made on the exploring and understanding of the pressure effects on the polymerization kinetics and mechanisms. Due to the constraints of available experimental apparatus, thus, the microstructural determination of the final products recovered from the

tunable pressure-photon conditions faces extreme challenges. In future works, these challenges may overcome by using a large volume compressor, so that the samples produced are in milligram sizes, which allow ordinary characteristic probes of polymers and amorphous solids be applied. Moreover, a fine synthesis of single monomer crystals (avoiding the influence of the crystal defects) would be very helpful to further clarify the mechanisms of solid-state polymeric transformations (e.g., geometric constraints, topochemical, non-topochemical, or lattice phonon assisted) under the combined pressure-photon conditions, which is not possible from the polycrystalline solids.

Appendix I Supporting Materials for Chapter 3
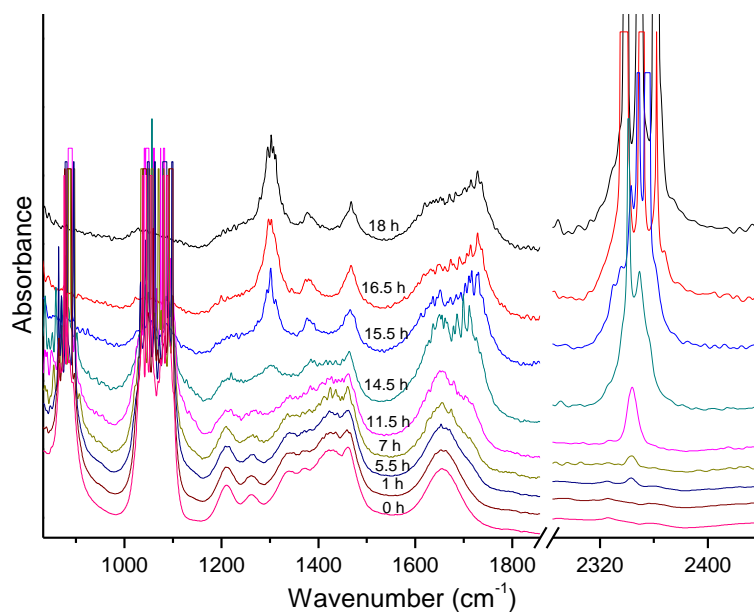
Figure 1S: FTIR spectra of EG with an initial loading pressure of 0.5 GPa upon UV irradiation (with λ of ~ 350 nm and power of ~ 700 mW) collected at different radiation time.
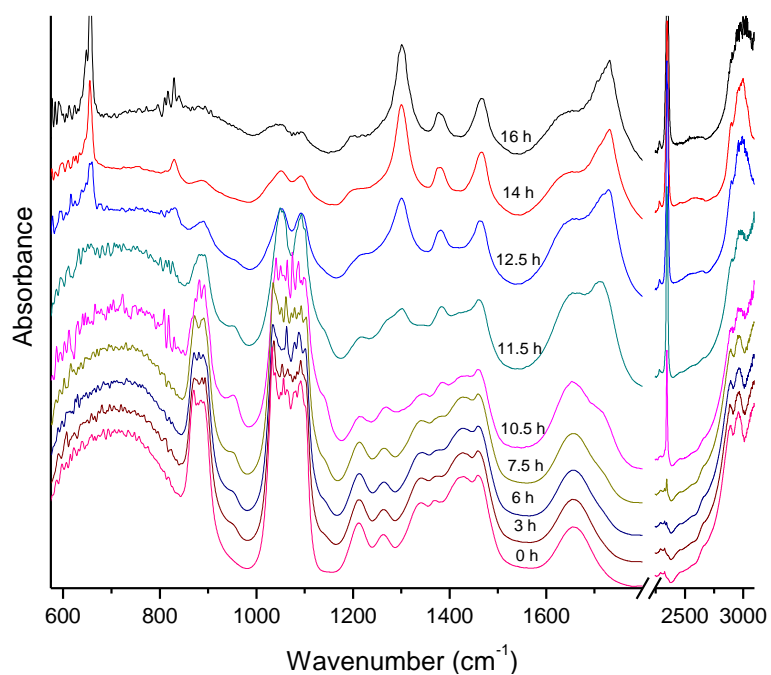
Figure 2S. FTIR spectra of EG with an initial loading pressure of 1.0 GPa upon UV irradiation (with λ of ~350 nm and power of ~700 mW) collected at different radiation time.
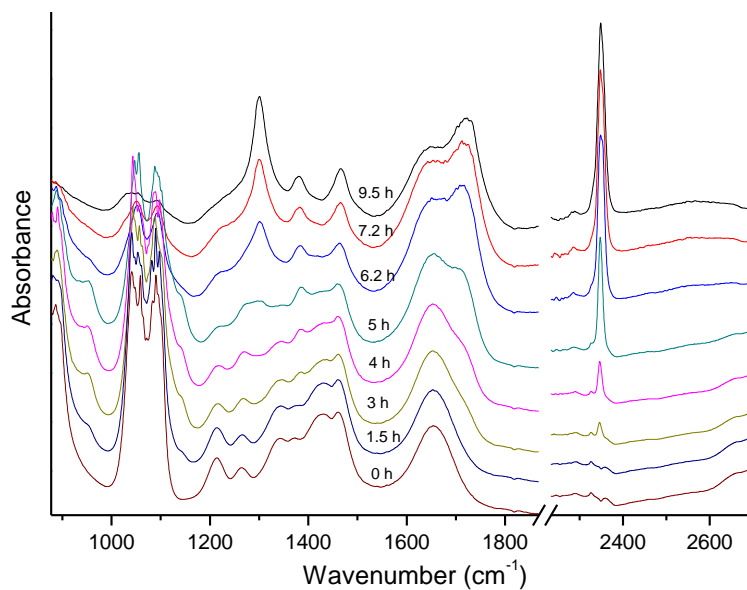
Figure 3S. FTIR spectra of EG with an initial loading pressure of 1.5 GPa upon UV irradiation (with λ of ~350 nm and power of ~700 mW) collected at different radiation time.
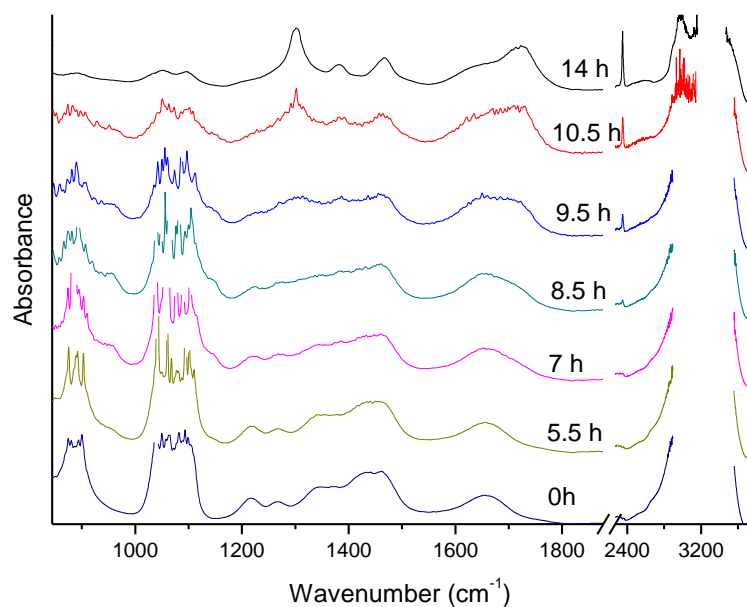
Figure 4S. FTIR spectra of EG with an initial loading pressure of 2.0 GPa upon UV irradiation (with λ of ~350 nm and power of ~700 mW) collected at different radiation time.
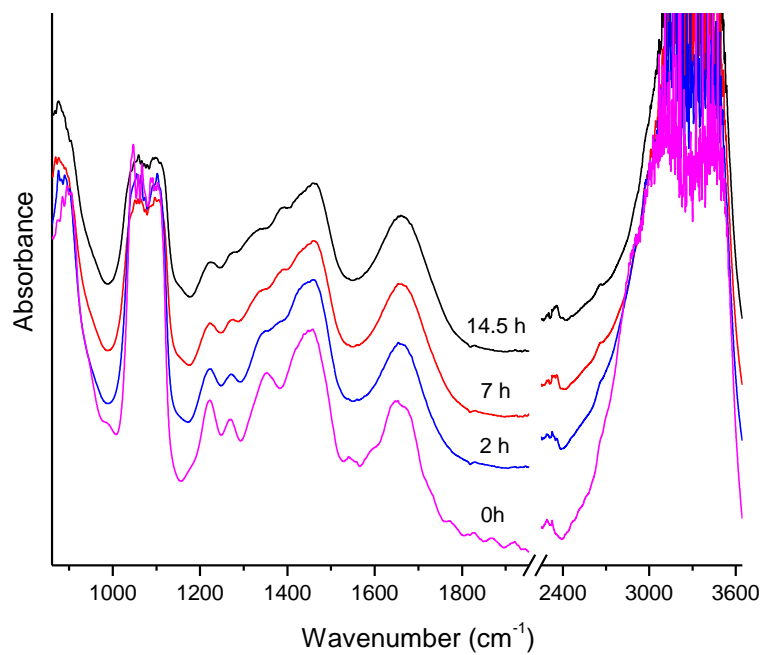
Figure 5S. FTIR spectra of EG with an initial loading pressure of 3.4 GPa upon UV irradiation (with λ of ~350 nm and power of ~700 mW) collected at different radiation time.

Table S1. Observed IR bands of ethylene glycol in liquid phase in comparison with reference values and assignment

This work (cm^{-1})	Reference (cm^{-1})[a, b, c]	Assignments
864	864 m	CC stretch, CO stretch
886	882 s	CH$_2$ rock, CO stretch
1034	1040 vs	CO stretch, CC stretch
1086	1085 vs	CH$_2$ rock, CO stretch (trans)
1207	1200 mb	CH$_2$ twist, CH$_2$ wag
1260	1250 wb	CH$_2$ twist, CH$_2$ wag
1336	1330 s	COH bend, CH$_2$ twist, CH$_2$ wag
1371	1370	COH bend, CH$_2$ twist, CH$_2$ wag
1420	1410 sb	COH bending
1459	1462 s	CH$_2$ scissor
1651	1660	….
2879	2876 vs	CH$_2$ sym
2957	2935 vs	CH$_2$ antisym
3350	3350 vsb	OH stretch

a. b=broad, vs= very strong, s=strong, w=weak, m=medium

b. Sawodny, W.; Niedenzu, K.; Dawson, J., The vibrational spectrum of ethylene glycol. *Spectr. Acta Part A,* **1967,** 23, 799-806.

c. Krishnan, K.; Krishnan, R.; Raman and infrared spectra of ethylene glycol, *Proc. Indian Acad. Sci.,* **1966,** 64, 111-122.

Table S2. Observed characteristic IR frequencies in spectral region of the antisymmetry mode of CO_2 as function of radiation time for EG samples loaded at 0.1, 0.5, 1 and 1.5 GPa.

Loading pressure	0.1 GPa					0.5 GPa					1.0 GPa					1.5 GPa			
Time (h)	11	13.5	14.5	19	22.5	11.5	14.5	15.5	16.5	18	10.5	11.5	12.5	14	16	5	6.2	7.2	9.5
Pressure (GPa)	0.18	0.27	0.6	0.9	0.95	0.83	1.13	1.27	1.43	1.65	1.37	1.66	1.76	1.80	1.86	1.78	1.96	2.1	2.14
				2326	2333														
			2337	2337	2339			2343	2338	2339									
		2337	2343	2349	2346		2341	2349	2351	2350	2345	2345	2345	2345	2345	2347	2347	2347	2347
IR frequency (cm^{-1})	2341					2344													
		2345	2351	2357	2359		2349	2355	2361	2362		2349	2352	2352	2352		2353	2353	2353
															2358				

Appendix II Supporting Materials for Chapter 5
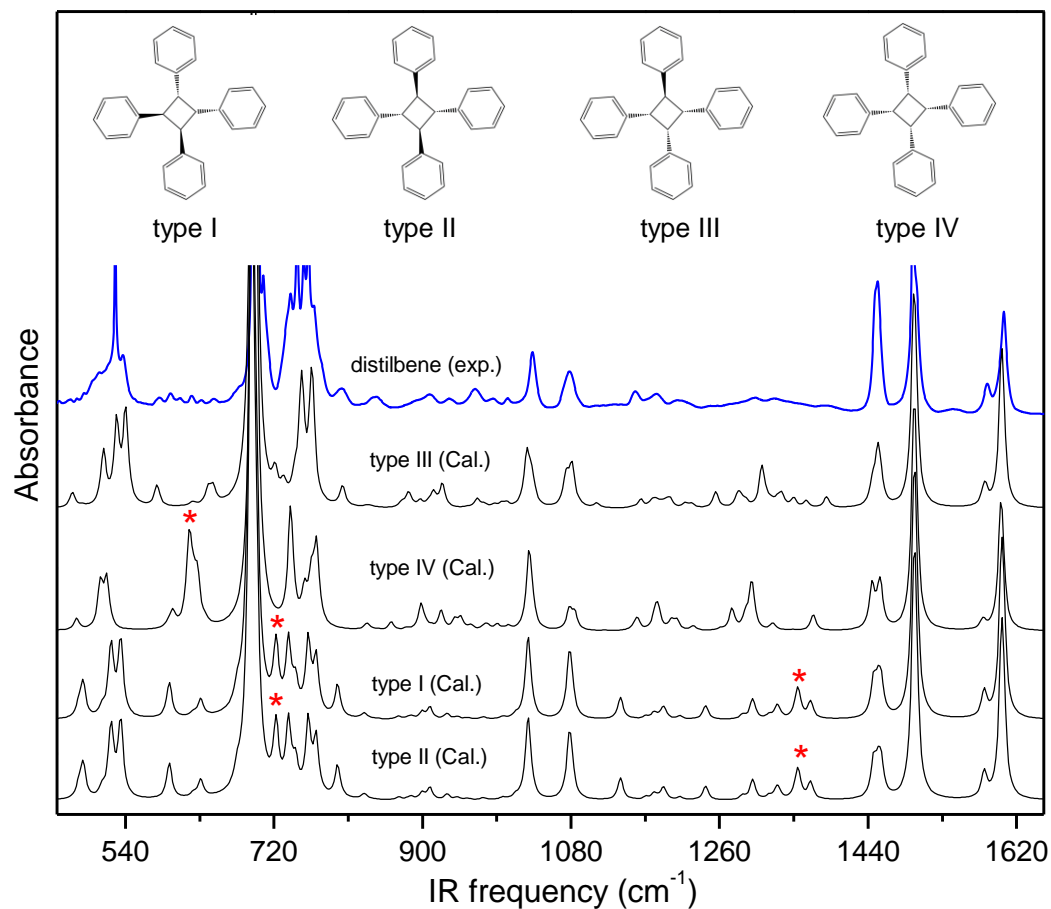
Figure 6S IR spectra of the final photoproduct obtained at 0.80 GPa and the IR spectra of the distilbene-I, II, III, IV calculated at the level of B3LYP/6-311++G(2d, p). The calculated vibrational frequencies are scaled by a factor of 0.976. The asterisks show the major mismatches between the experiments and calculations. The insets show the 4 molecular structures of distilbene.
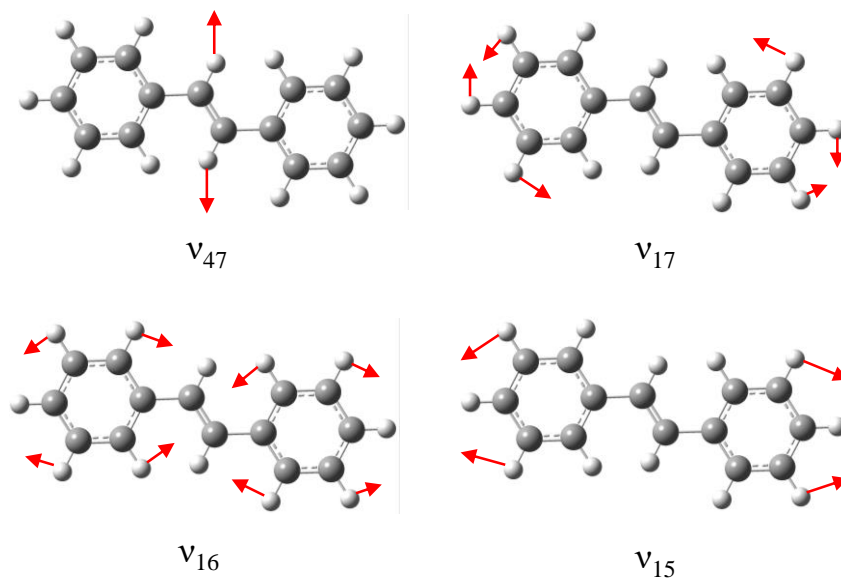
Figure 7S Calculated molecular vibrations of Raman modes ν_{47}, ν_{17}, ν_{16} and ν_{15}.
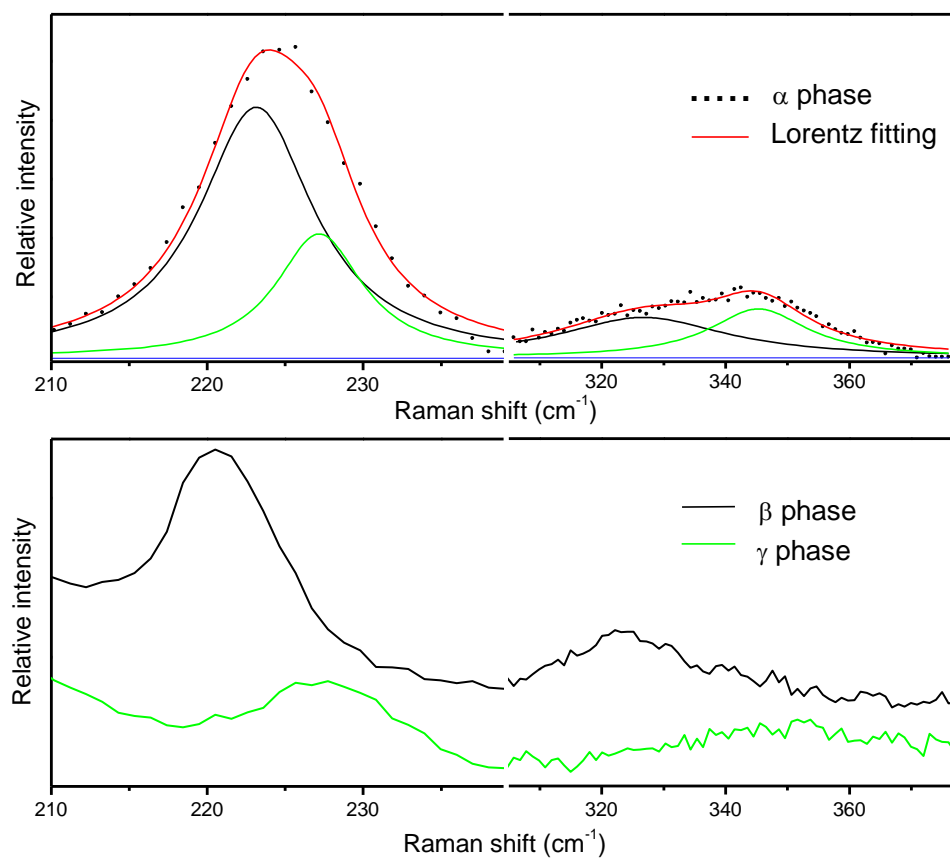
Figure 8S The deconvolution of the measured Raman peaks at 225, 340 cm^{-1} of α phase. The fitted peaks are well consistent with the measured Raman peaks of β and γ phase.
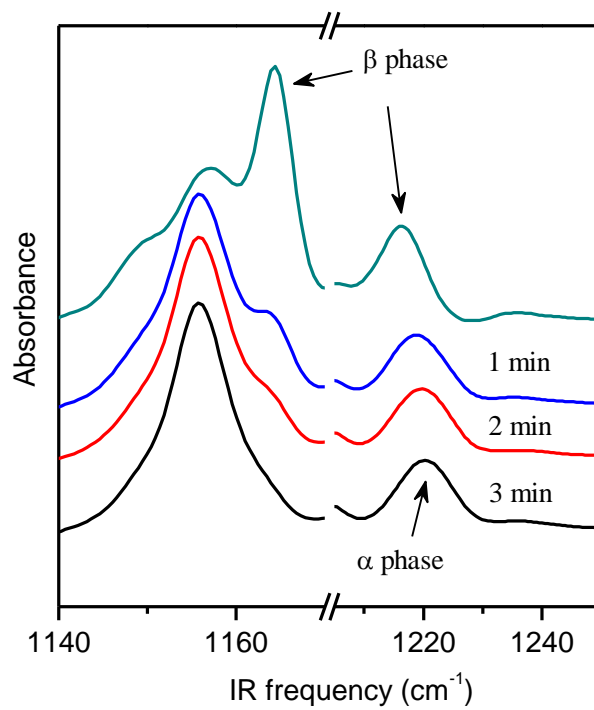
Figure 9S Thermal-induced (300 K) phase transition from β phase to α phase at 0.11 GPa measured by IR spectra.

Appendix III Supporting Materials for Chapter 7

Table S1. Assignment of the IR active modes of styrene (cm^{-1})

Exp.	IR modes	Ref.[a]	Description [b]
621	ν_{26}	621	C_eH rock
696	ν_{37}	697	Benzene wag
775	ν_{25}	776	Vinyl rock
840	ν_{35}	841	Vinyl wag
905	ν_{33}	908	C_bH wag
916	ν_{34}		C_bH wag
991	ν_{24}	991	C_bH rock
1021	ν_{23}	1020	C_bH rock
1084	ν_{21}	1082	C_bH rock
1108	$\nu_{33}+\nu_{41}$	1108	Combination
1157	ν_{20}	1156	C_bH rock
1182	ν_{19}	1182	Benzene asym. def.
1204	ν_{18}	1202	Benzene asym. def.
1290	ν_{17}	1290	Benzene trigonal def.
1319	ν_{16}	1317	C_eH stretch
1335	ν_{15}	1334	C_eH stretch
1412	ν_{14}	1412	C_eH stretch
1449	ν_{13}	1449	C_bH stretch
1494	ν_{12}	1494	C_eH stretch
1543	$\nu_{35}+\nu_{37}$		Combination
1576	ν_{11}	1576	$C_e=C_e$ stretch
1602	ν_{10}	1601	$C_e=C_e$ stretch
1631	ν_9	1630	$C_e=C_e$ stretch
1691	$\nu_{33}+\nu_{36}$		Combination
2981	ν_8	2980	$(C\text{-}C)_e$ stretch
2991	$2\nu_{12}$		Overtone
3010	ν_7	3008	Vinyl stretch
3028	ν_6	3027	$(C\text{-}C)_b$ stretch
3060	ν_4	3060	$(C\text{-}C)_b$ stretch
3082	ν_3		$(C\text{-}C)_b$ stretch
3104	ν_1		$(C\text{-}C)_b$ stretch

a. J. M. Roldan, M. F. Gomez, A. Navarro, Chem. Phys. Lett. **372**, 255 (2003).
b. The subscripts b and e denote the atom on the phenyl and vinyl groups respectively.

Table S2. Kinetics Parameters of Polymerization of Styrene Obtained from Least-Square Regression using Avrami Model

Pressure (GPa)	Laser power (mW)	k (h^{-1})$\times 10^{-2}$	$\ln k$	n	PY_∞
0.02	300	0.3 ± 0.2	-5.8 ± 0.5	1.5 ± 0.1	1.00
0.10	35	0.2 ± 0.1	-6.2 ± 0.5	1.4 ± 0.1	1.00
0.10	100	0.31 ± 0.03	-5.78 ± 0.09	1.57 ± 0.02	1.00
0.28	35	1.2 ± 0.4	-4.5 ± 0.3	1.3 ± 0.1	0.98
0.67	35	38 ± 4	-1.0 ± 0.1	1.05 ± 0.08	0.90
1.26	35	1.6 ± 0.3	-4.1 ± 0.2	1.33 ± 0.07	0.89
2.34	35	0.6 ± 0.2	-5.1 ± 0.3	1.05 ± 0.06	0.42
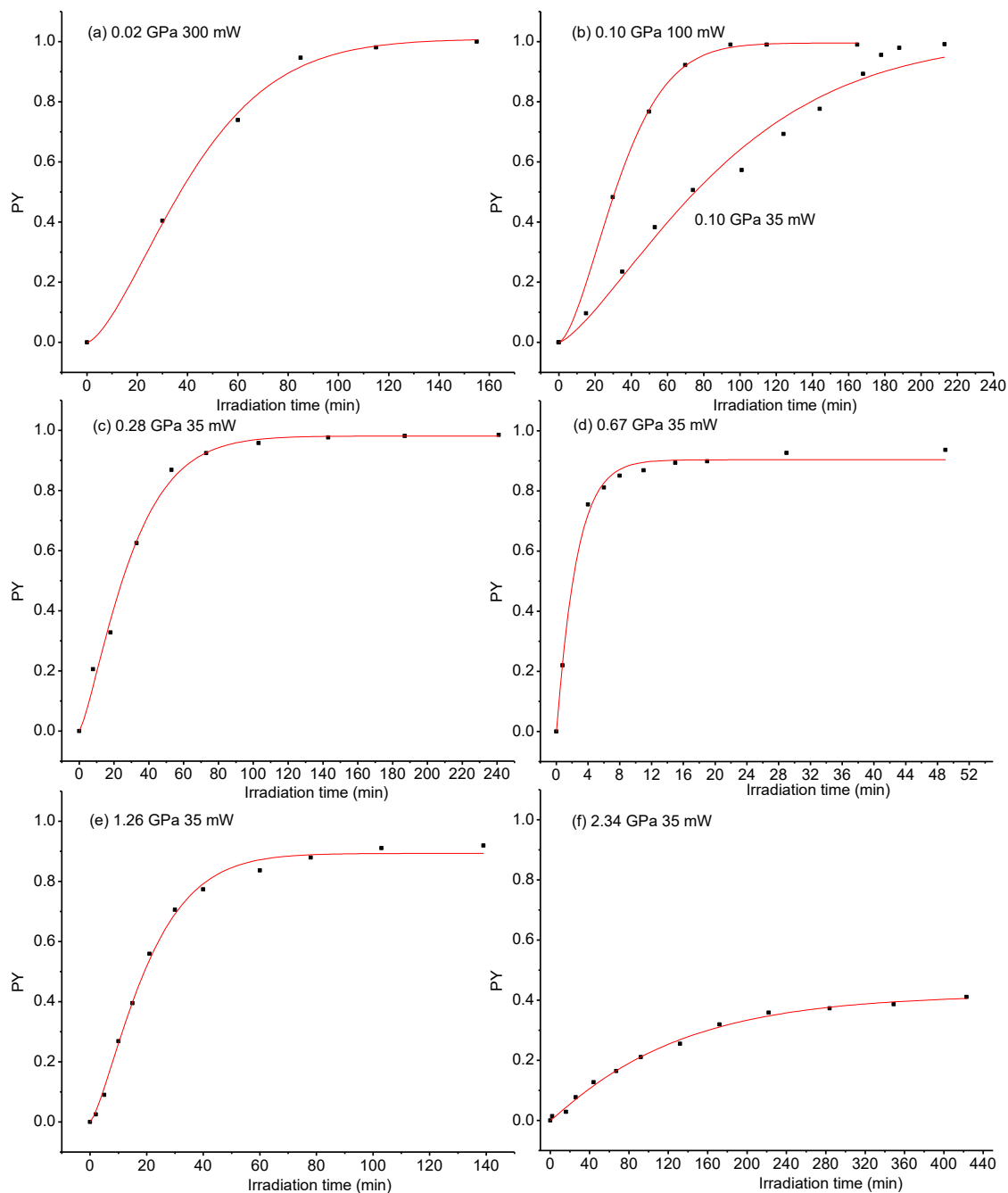
Figure S1. Polymerization kinetics of styrene characterized by polymerization yield (PY) as a function of time for samples loaded under different initial pressures and varying laser irradiation power at wavelength of 350 nm. The solid lines are fits using Avrami model (see the text).

Appendix IV Copyright Permissions

License Number	4336790345041
License date	Apr 26, 2018
Licensed Content Publisher	John Wiley and Sons
Licensed Content Publication	Angewandte Chemie International Edition
Licensed Content Title	High-Pressure Chemistry of Red Phosphorus and Water under Near-UV Irradiation
Licensed Content Author	Matteo Ceppatelli, Roberto Bini, Maria Caporali, et al
Licensed Content Date	Jan 11, 2013
Licensed Content Volume	52
Licensed Content Issue	8
Licensed Content Pages	5
Type of use	Dissertation/Thesis
Requestor type	University/Academic
Format	Print and electronic
Portion	Figure/table
Number of figures/tables	1
Original Wiley figure/table number(s)	Graphic abstract
Will you be translating?	No
Title of your thesis / dissertation	Effects of High Pressure on Photochemical Reactivity of Organic Molecular Materials Probed by Vibrational spectroscopy
Expected completion date	Sep 2018
Expected size (number of pages)	200

This Agreement between Mr. Jiwen Guan ("You") and Springer Nature ("Springer Nature") consists of your license details and the terms and conditions provided by Springer Nature and Copyright Clearance Center.

License Number	4336790833217
License date	Apr 26, 2018
Licensed Content Publisher	Springer Nature
Licensed Content Publication	Nature Communications
Licensed Content Title	High-pressure synthesis of a polyethylene/zeolite nano-composite material
Licensed Content Author	Mario Santoro, Federico A. Gorelli, Roberto Bini, Julien Haines, Arie van der Lee
Licensed Content Date	Mar 5, 2013
Licensed Content Volume	4
Type of Use	Thesis/Dissertation
Requestor type	non-commercial (non-profit)
Format	print and electronic
Portion	figures/tables/illustrations
Number of figures/tables/illustrations	1
High-res required	no
Will you be translating?	no
Circulation/distribution	<501
Author of this Springer Nature content	no
Title	Effects of High Pressure on Photochemical Reactivity of Organic Molecular Materials Probed by Vibrational spectroscopy
Instructor name	n/a
Institution name	n/a
Expected presentation date	Sep 2018

Copyright
Clearance
Center

RightsLink®

Home | Account Info | Help | ✉

ACS Publications
Most Trusted. Most Cited. Most Read.

Title: Pressure-Induced Polymerization of Diiodobutadiyne in Assembled Cocrystals

Author: Christopher Wilhelm, Stephen A. Boyd, Samrat Chawda, et al

Publication: Journal of the American Chemical Society

Publisher: American Chemical Society

Date: Apr 1, 2008

Copyright © 2008, American Chemical Society

PERMISSION/LICENSE IS GRANTED FOR YOUR ORDER AT NO CHARGE

This type of permission/license, instead of the standard Terms & Conditions, is sent to you because no fee is being charged for your order. Please note the following:

- Permission is granted for your request in both print and electronic formats, and translations.
- If figures and/or tables were requested, they may be adapted or used in part.
- Please print this page for your records and send a copy of it to your publisher/graduate school.
- Appropriate credit for the requested material should be given as follows: "Reprinted (adapted) with permission from (COMPLETE REFERENCE CITATION). Copyright (YEAR) American Chemical Society." Insert appropriate information in place of the capitalized words.
- One-time permission is granted only for the use specified in your request. No additional uses are granted (such as derivative works or other editions). For any other uses, please submit a new request.

If credit is given to another source for the material you requested, permission must be obtained from that source.

BACK | CLOSE WINDOW

Copyright Clearance Center

RightsLink®

Home   Account Info   Help

ACS Publications
Most Trusted. Most Cited. Most Read.

Title: Photoinduced Reactivity of Liquid Ethanol at High Pressure

Author: Matteo Ceppatelli, Samuele Fanetti, Margherita Citroni, et al

Publication: The Journal of Physical Chemistry B

Publisher: American Chemical Society

Date: Dec 1, 2010

Copyright © 2010, American Chemical Society

PERMISSION/LICENSE IS GRANTED FOR YOUR ORDER AT NO CHARGE

BACK   CLOSE WINDOW

Copyright Clearance Center

RightsLink®

Home | Account Info | Help

ACS Publications
Most Trusted. Most Cited. Most Read.

Title: Transformations of Cold-Compressed Multiwalled Boron Nitride Nanotubes Probed by Infrared Spectroscopy

Author: Zhaohui Dong, Yang Song

Publication: The Journal of Physical Chemistry C

Publisher: American Chemical Society

Date: Feb 1, 2010

Copyright © 2010, American Chemical Society

PERMISSION/LICENSE IS GRANTED FOR YOUR ORDER AT NO CHARGE

BACK | CLOSE WINDOW

Copyright Clearance Center

RightsLink®

Home   Create Account   Help

ACS Publications
Most Trusted. Most Cited. Most Read.

Title: Pressure Selected Reactivity and Kinetics Deduced from Photoinduced Dissociation of Ethylene Glycol

Author: Jiwen Guan, Yang Song

Publication: The Journal of Physical Chemistry B

Publisher: American Chemical Society

Date: Feb 1, 2015

Copyright © 2015, American Chemical Society

PERMISSION/LICENSE IS GRANTED FOR YOUR ORDER AT NO CHARGE

BACK   CLOSE WINDOW

AIP PUBLISHING LLC LICENSE
TERMS AND CONDITIONS

Feb 24, 2018

This Agreement between Mr. Jiwen Guan ("You") and AIP Publishing LLC ("AIP Publishing LLC") consists of your license details and the terms and conditions provided by AIP Publishing LLC and Copyright Clearance Center.

License Number	4295510004661
License date	Feb 24, 2018
Licensed Content Publisher	AIP Publishing LLC
Licensed Content Publication	Journal of Chemical Physics
Licensed Content Title	Highly efficient and selective pressure-assisted photon-induced polymerization of styrene
Licensed Content Author	Jiwen Guan, Yang Song
Licensed Content Date	Jun 7, 2016
Licensed Content Volume	144
Licensed Content Issue	21
Type of Use	Thesis/Dissertation
Requestor type	Author (original article)
Format	Print and electronic
Portion	Excerpt (> 800 words)
Will you be translating?	No
Title of your thesis / dissertation	Effects of High Pressure on Photochemical Reactivity of Organic Molecular Materials Probed by Vibrational spectroscopy
Expected completion date	Sep 2018
Estimated size (number of pages)	200

NRC RESEARCH PRESS LICENSE
TERMS AND CONDITIONS

Feb 24, 2018

This Agreement between Mr. Jiwen Guan ("You") and NRC Research Press ("NRC Research Press") consists of your license details and the terms and conditions provided by NRC Research Press and Copyright Clearance Center.

License Number	4295500831534
License date	Feb 24, 2018
Licensed Content Publisher	NRC Research Press
Licensed Content Publication	Canadian Journal of Chemistry
Licensed Content Title	Pressure-selected reactivity between 2-butyne and water induced by two-photon excitation
Licensed Content Author	Jiwen Guan, Roshan Daljeet, Yang Song
Licensed Content Date	Nov 1, 2017
Licensed Content Volume	95
Licensed Content Issue	11
Type of Use	Thesis/Dissertation
Requestor type	Author (original work)
Format	Print and electronic
Portion	Full article
Order reference number	
Title of your thesis / dissertation	Effects of High Pressure on Photochemical Reactivity of Organic Molecular Materials Probed by Vibrational spectroscopy
Expected completion date	Sep 2018
Estimated size(pages)	200

General Terms & Conditions

Permission is granted upon the requester's compliance with the following terms and conditions:

https://s100.copyright.com/AppDispatchServlet

1. A credit line will be prominently placed in your product(s) and include: for books the author, book title, editor, copyright holder, year of publication; for journals the author, title of article, title of journal, volume number, issue number, and the inclusive pages. The credit line must include the following wording: "© 2008 Canadian Science Publishing or its licensors. Reproduced with permission," except when an author of an original article published in 2009 or later is reproducing his/her own work.

2. The requester warrants that the material shall not be used in any manner that may be derogatory to the title, content, or authors of the material or to Canadian Science Publishing, including but not limited to an association with conduct that is fraudulent or otherwise illegal.

3. Permission is granted for the term (for Books/CDs-Shelf Life; for Internet/Intranet-In perpetuity; for all other forms of print-the life of the title) and purpose specified in your request. Once term has expired, permission to renew must be made in writing.

4. Permission granted is nonexclusive, and is valid throughout the world in English and the languages specified in your original request. A new permission must be requested for revisions of the publication under current consideration.

5. Canadian Science Publishing cannot supply the requester with the original artwork or a "clean copy."

6. If the Canadian Science Publishing material is to be translated, the following lines must be included: The authors, editors, and Canadian Science Publishing are not responsible for errors or omissions in translations.

Curriculum Vitae

Name: Jiwen Guan

Post-secondary The University of Western Ontario
Education and London, Ontario, Canada
Degrees: 2015-2018, PhD in Physics

       The University of Western Ontario
       London, Ontario, Canada
       2013-2015, Project-based MSc in Physics

       South China Normal University
       Guangzhou, Guangdong, China
       2010-2013, MSc in Optics

       Yangtze University
       Jingzhou, Hubei, China
       2006-2010, BSc in Physics

Related Work Teaching Assistant/Research Assistant
Experience: The University of Western Ontario
       2013-2018

Selected Publications (Peer-Reviewed Journal Articles):

1. **J. Guan**, P. Wang, X. Chen, X. Jing, Y. Song, "Pressure, Laser and Physical-states Effects on Polymerization Kinetics of Phenylacetylene Probed by FTIR Spectroscopy" **2018** (in preparation).

2. **J. Guan**, X. Chen, Y. Song, "Photochemical Liquid-to-Crystal, Crystal-to-Crystal versus Liquid-to-Liquid Phase Transitions of Stilbene at High Pressure: From Product Selectivity to Electronic State Compressibility" **2018** (in preparation).

3. **J. Guan**, R. Daljeet, Y. Song, "Pressure-induced Polymerization of Solid Dimethyl Acetylene Probed by in situ FTIR and Raman Spectroscopy" *Journal of Physics: Condensed Matter*, **2018**, 30, 224004.

4. **J. Guan**, R. Daljeet, Y. Song, "Pressure-selected Reactivity between 2-Butyne and Water Induced by Two-photon Excitation" *Canadian Journal of Chemistry*, **2017**, 95, 1212.

5. P. Wang, **J. Guan**, D. T. K. Galeschuk, Y. Yao, C. F. He, S. Jiang, S. Zhang, Y. Liu, M. Jin, C. Q. Jin and Y. Song, "Pressure-Induced Polymorphic, Optical, and Electronic Transitions of Formamidinium Lead Iodide Perovskite" *Journal of Physical Chemistry Letters,* **2017**, 8, 2119.

6. **J. Guan**, Y. Song, "Highly Efficient and Selective Pressure-Assisted Photon-induced Polymerization of Styrene" *Journal of Chemical Physics*, **2016**, 144, 214904.

7. **J. Guan**, Y. Song, "Pressure Selected Reactivity and Kinetics Deduced from Photoinduced Dissociation of Ethylene Glycol" *Journal of Physical Chemistry B,* **2015**, 119, 3535.

Academic Conferences & Visits (2013-2018)

1. **2016** The 32nd Symposium on Chemical Physics, Waterloo, Canada (Oral talk).
2. **2016** Argonne National Laboratory, Chicago, USA (Experiments).
3. **2015** The 98th Canadian Chemistry Conference and Exhibition, Ottawa, Canada (Poster).